FILTERING AEROMAGNETIC DATA
TO REDUCE THE MASKING EFFECT OF NEAR-SURFACE BASALT

by

David Hugh Inkster B.E., B.A., B.Sc.

This thesis is submitted in partial fulfilment of the
Bachelor of Science, Honours degree, (Geophysics)

Department of Geology and Geophysics
The University of Adelaide

NOVEMBER 1995

Map References:
Clermont SF55-11
Clarke River SE55-13

Table of Contents

THE KANGERONG DATASET:

List of Figures

Maps

Diagrams and Charts

Images: Miclere

List of Figures (continued)

Images: Kangerong

Images: Appendices

Abstract

This project investigated two areas in northern Queensland where Tertiary basalt covers igneous and metamorphic rocks considered prospective for gold. The moderate to high magnetic susceptibility of the basalt, combined with variations in its thickness, give a high degree of variability to the aeromagnetic data which impedes interpretation of deeper structures.

Low-pass filters of the Butterworth, averaging-window and median-window types were used initially, because the near-surface signals tends to be higher in spatial frequency. Upward continuation was also used. All were able to remove high frequencies but none showed a clear superiority at simultaneously resolving detail. The best results eventually were obtained from a differencing method in which the high-frequency signals were first emphasised by downward continuation and then subtracted from the original signal. This enabled identification of several features which had not been visible in either the original, or low-pass-filtered data.

The differencing method is shown to be equivalent to subtracting the first vertical derivative (multiplied by a scaling factor) from the total magnetic intensity.

The generality of this approach was then tested by applying it to another dataset with different sampling and geological parameters. The resolution available in the second case is limited by the 400m flight line spacing, instead of the 200m of the first dataset. The results were less successful but there is evidence that the approach is still valid.

Acknowledgments

I thank my supervisor, Dr. Peter Brooker, for his assistance and support throughout this project. I also owe thanks to Dr. Richard Hillis for useful and constructive comments, and to Stephen Markham for his advice and help.

I must acknowledge the enormous support given by Normandy Exploration Limited, who originated the concept of this project, supplied the datasets, the computing facilities and office space in which to work (and tea, coffee and biscuits to keep me going!). In particular I thank Dr. Michael Sexton, Geraldine Teakle, Graham Boyd, Tom Weis, Robert Stuart, Andrew Foley and Dr. Bretan Clifford, who were all generous with their time and knowledge whenever the need arose.

Mention must also be made of the use of the Geosolutions™ software used for nearly all the filtering, processing and data manipulation needed. The availability and usefulness of this software enabled me to concentrate on the *what* and *why* of the processes, and take the *how* for granted.

Chapter 1

Introduction

1.1 Aims

The aeromagnetic data for this project is from two exploration tenements in northeastern Queensland where Tertiary basalt covers the underlying metamorphic and igneous rocks considered prospective for gold. The imaged data is difficult to interpret due to the signal from the near-surface basalt. The aim was to remove the basalt signal whilst retaining as much resolution as possible in the final image. In pursuing this aim it was hoped to develop a process which might have general application in removing unwanted near-surface signals.

1.2 Background

The tenement known as Miclere encompasses the goldfield of that name which was worked earlier this century, and is located north of the town of Clermont (refer fig. 1.1). The other, known as Kangerong, is close to Charters Towers and the currently productive gold mine at Mount Leyshon. These areas may be prospective for Mount Leyshon style deposits, where breccia-hosted gold occurs in a diatreme of Permian age (Paull *et al* 1990); or, in the case of Miclere, within the Anakie metamorphics which underlie much of that area.

The terrain in both areas is very flat, with little outcrop, so initial exploration reliance is placed on geophysical methods with drilling and geochemical analyses as a follow-up. The basalt flows are a complication in this process because they have variable thickness due to the prior topography, and moderate but variable magnetic susceptibility, which ranges from 100 x 10^{-5} to 2500 x 10^{-5} SI units (refer to appendix G). As a result the total magnetic intensity image contains a significant component representing these basalt variations. The presence of this component, comprising mainly higher frequencies, increases the difficulty in recognising and delineating geological structures. Figure 1.2 exemplifies this. It is the image of the Miclere Total Magnetic Intensity, and shows the irregular 'surface texture' indicative of the basalt covering most of the lease. Only small areas at the western side of the lease appear free of basalt, as indicated by the smoother appearance of the image.

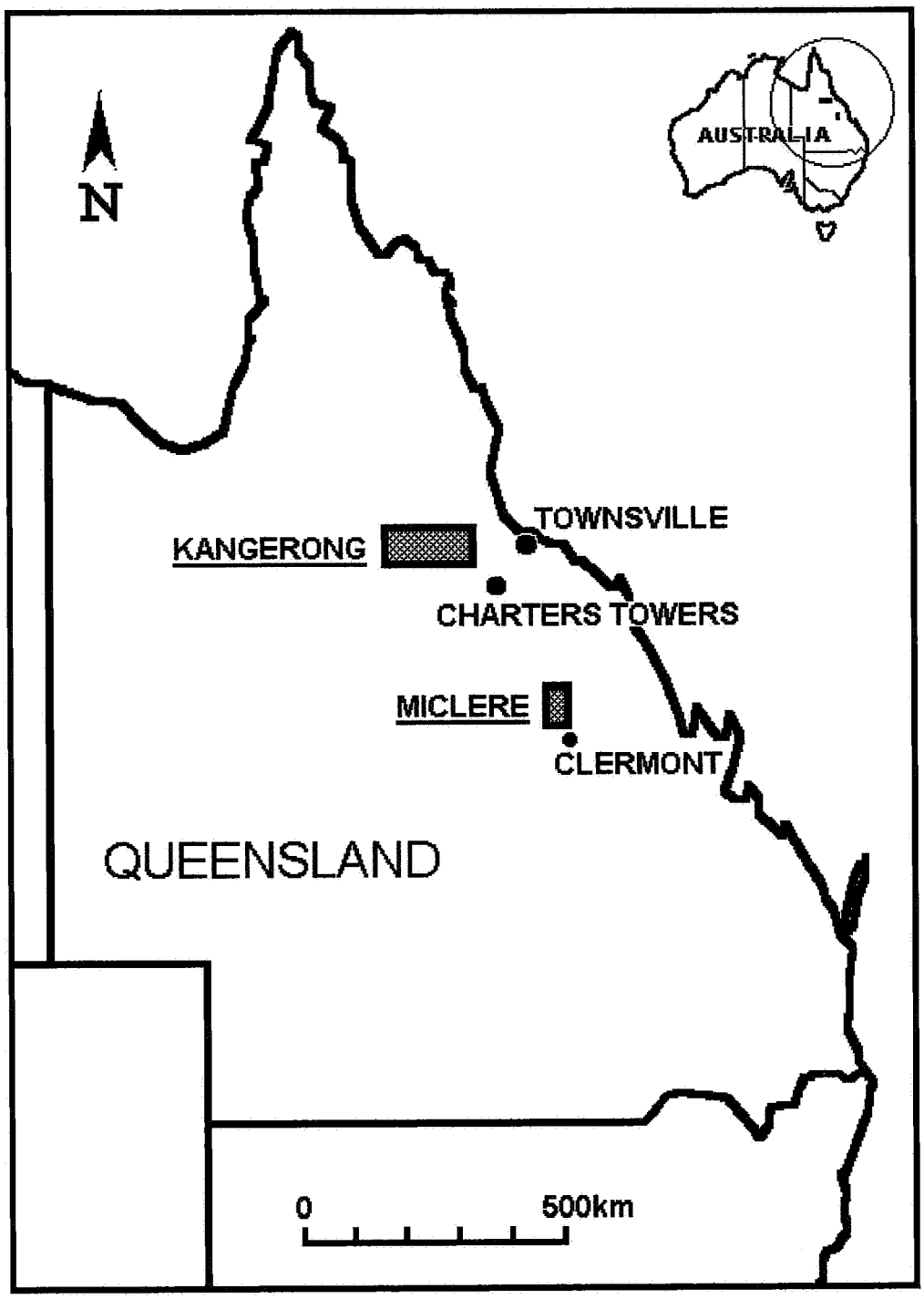

Fig. 1.1: Location of the Miclere and Kangerong exploration leases

fig. 1.2 Total Magnetic Intensity Range 50760 to 52890 nT

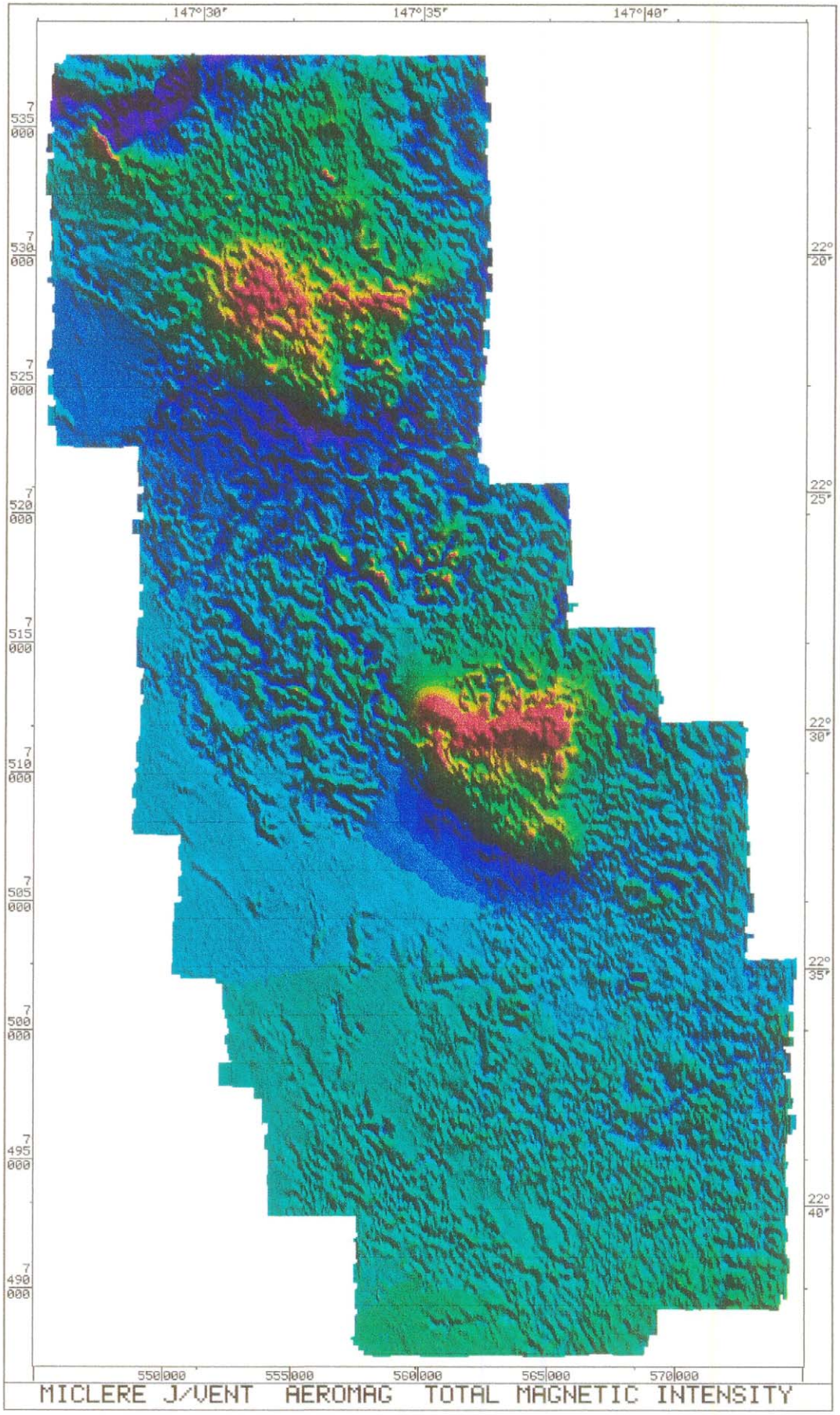

1.3 Filters and Enhancement Processes

The basalt signal is dominated by high frequencies. Due to the proximity of the basalt to the magnetometer its variability, as mentioned above, is reflected in the record rather than being smoothed by the effect of distance. A form of low-pass filtering appeared appropriate for the removal of this unwanted signal. A number of such filters were investigated, as was upward continuation. Delineation of structures using vertical derivatives and Automatic Gain Control (AGC), separately and in combination with low-pass filters, were other approaches tried.

Forward modelling the basalt was considered. If successful, this would enable the basalt signal to be stripped from the TMI signal. However, the random susceptibility and thickness variations of the basalt mitigate against this approach. Nevertheless the idea led to the process I have called differencing, in which the high frequency signal is emphasized by downward continuation, and then subtracted from the TMI signal. This process shows considerable promise.

1.4 Interpretation of Results

The results of all the filters and processes are presented as images, so that judgment as to the best of several alternatives is subjective. This judgment is made more difficult because the frequency spectra of the desired signal and the basalt signal undoubtedly overlap, so that any low-pass filter must be a compromise between retaining the desired signal, and retaining too much of the basalt signal component.
This compromise means that the final choice of cutoff wavelength for any process would be an arbitrary and subjective one. Although the effects of extreme cutoffs are apparent, there is no objective 'best' choice in this regard to the author's knowledge. One guideline consistently applied, however, was that the final choice should still have a trace of the basalt signal, as an indication that the data had not been over-smoothed.

1.5 Presentation of the Images

To standardise the presentation and thus permit valid comparisons, all the colour images employ the same format. Shading is provided by artificial illumination from 20° elevation and 40° azimuth. There are 16 colour bands in a linear stretch across the range of values pertaining to each image. Accordingly, the values represented by a particular colour will in general differ from one image to another. This presents no practical difficulty as the

absolute values are less important than relative values in the interpretation of this type of image. The red end of the colour spectrum represents the highest values of the imaged data; violet represents the lowest values.

The software permits a non-linear colour stretch, and this is useful for enhancement of particular features. This is best done on an image-by-image basis, because in general it is not possible to predetermine which portion of the colour spectrum will need enhancement. Selective application of any process will render invalid any comparison of images, and therefore it was decided at the beginning not to use non-linear stretches.

1.6 Structure of this Thesis

Chapter 2 gives a general outline of the data and data handling. Chapters 3 through 5 detail operations on the Miclere dataset, with chapter 6 summarising and discussing the results. The more promising operations are then applied to the Kangerong dataset with results detailed in chapter 7. Chapter 8 discusses these results; conclusions are presented in chapter 9.

Chapter 2

Data Acquisition, Format and Appraisal

2.1 Data Acquisition

The data from the Miclere tenement was acquired at a 200 metre line spacing, with tie lines every 2000 metres. Flight line direction was East-West, with a sample interval of 6 metres. Sensor height was 70 metres.
The Kangerong data has a 400 metre line spacing and 4000 metre tie line separation. Flight line direction was North-South, the sample interval was 7 metres, and the sensor height 60 metres.
The contractor used a caesium-vapour magnetometer, stinger mounted, for both datasets,and supplied the data corrected for IGRF, diurnal and flight path variations. The data had been levelled to remove inconsistencies between adjacent flight lines, and the contract included radiometric data and fiducials, which were not used in this study.

2.2 Selection of a Working Subset

As I was doing all of the processing at the premises of Normandy Exploration, it was convenient to use their Geosolutions™ software. Only the AGC operations required that I write code. To reduce computing time and memory requirements, the filters and processes were applied initially to a subset of the Miclere tenement. This 'working subset' was chosen because it contained all four basement types (refer fig 2.1); because it was reasonably well known geologically, with 33 logged drillholes (refer appendix G for log data of all Miclere drillholes); and because it was suitably sized for an A4 sheet, at the common mapping scale of 1 to 50000. Fig. 2.2 shows the TMI image of this subset which encompasses most of the Northern intrusive body, one of two prominent magnetic highs evident in fig. 1.2.

2.3 Consideration of Forward Modelling

The possibility of forward modelling the basalt, and then stripping its signal from the total, appears impractical. Examination of drill log data shows a wide and apparently random variation in magnetic susceptibility (refer appendix G). Combined with

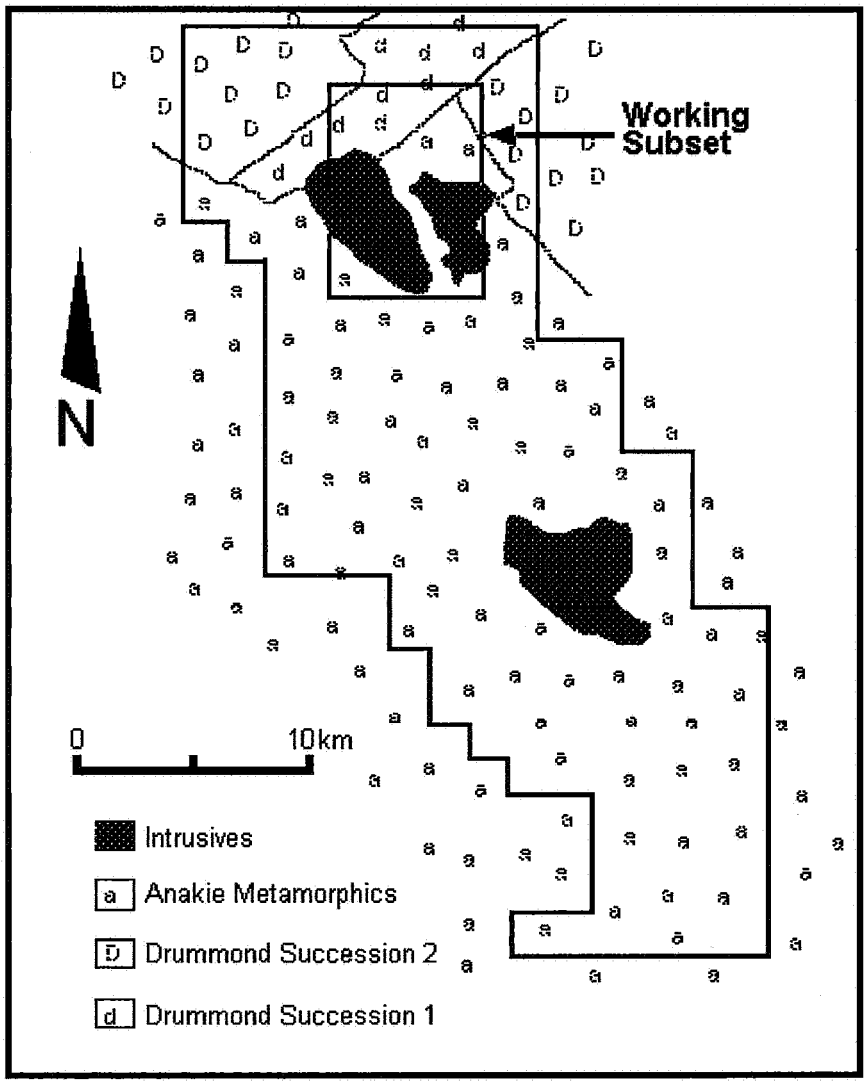

fig. 2.1 Basement geology of the Miclere Tenement (courtesy Normandy Exploration Limited)

fig. 2.2 Working Subset: Total Magnetic Intensity, range 50764 to 52887 nT

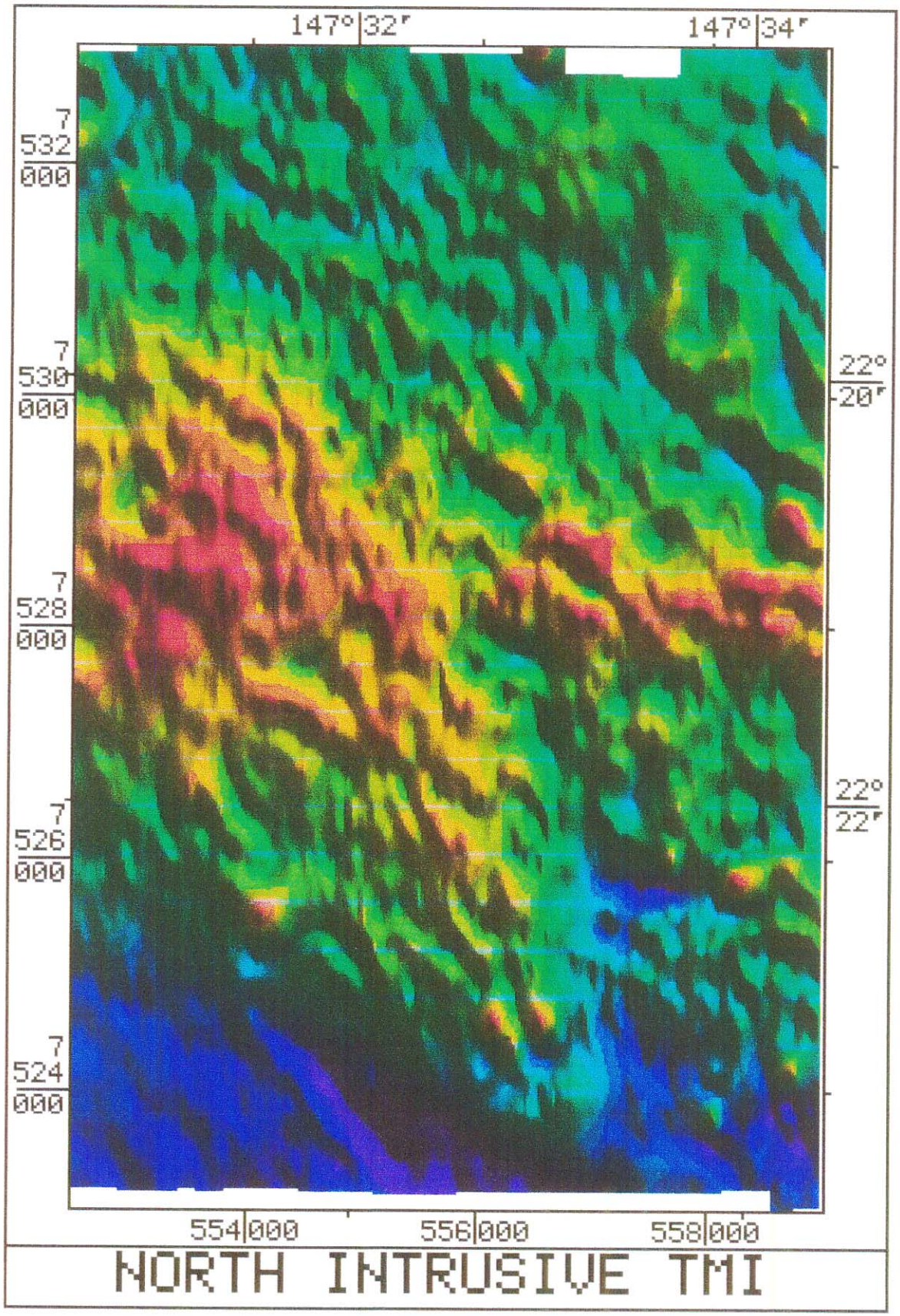

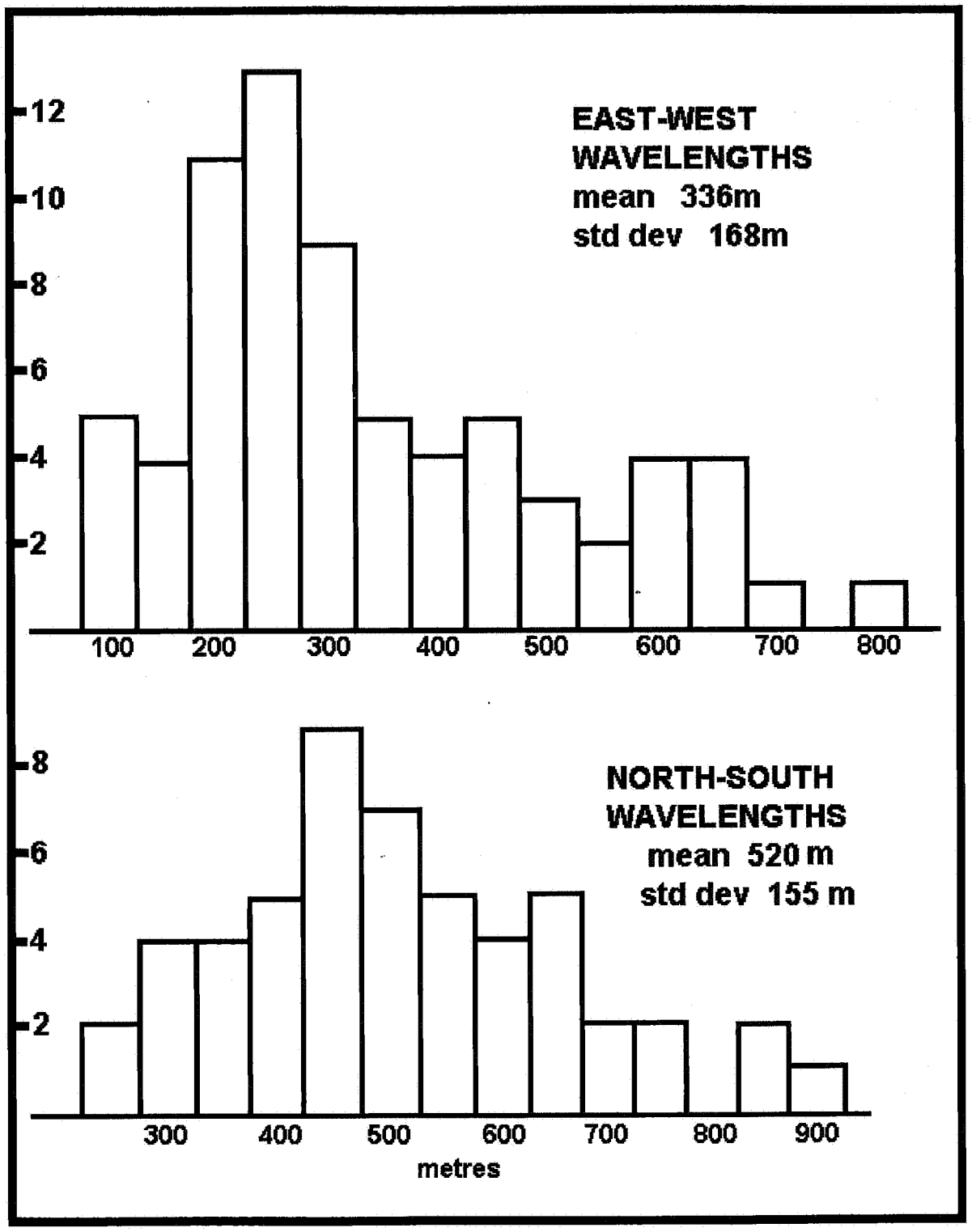

fig. 2.3 Wavelength Analysis Histograms

thickness variations evident from the drill logs, (presumably reflecting the palaeotopography), these factors make construction of a model extremely difficult, although it may be feasible for small subsets, on a scale of less than one kilometre.

2.4 Wavelength Analysis

A quick appraisal of the frequency content of the data was conducted by measuring the spatial distance between successive highs along arbitrarily selected lines, in two sets at 90 degrees. The east-west lines selected were the 7532000; 7530000; 7528000; and 7526000 grid lines. The north-south selections were the 554000; 556000; and 558000 grid lines. The whole span of the working subset was used in each case. This approach only registers the highest frequencies or shortest wavelengths, and this is reflected in the skew of the histograms (refer fig. 2.3). The histograms also confirm the anisotropy suggested by the TMI image. This anisotropy is probably a consequence of the palaeotopography, and will vary with the locality. Indeed, a quick check of the south of the Miclere area gave a value 20% lower for the north-south mean.
The result is very useful, however, as the upper end of the frequency spectrum appears to consist mainly of unwanted basalt signal. This provided a first indication of filter cutoff wavelength: a value of 600 to 700 metres appeared necessary for low-pass filtering.

2.5 Choice of Line or Grid Operations

The initial choice was based on a visual comparison of low-pass Butterworth filtered data, both line-filtered and grid-filtered (refer figs. 2.4 to 2.7). The gridding was done at 25m intervals in both cases. No differences could be detected, so grid filtering was used as it was more convenient due to the structure of the software. Line filters of cutoff wavelength greater than 1000m produced an artificial lineation in the image due to the effect of filtering along the flight lines but not across them. Grid filtering could overcome this by filtering twice, the second time at 90° to the first.
Having started with grid filters and operations, they were then used throughout as it removed one source of variation. With hindsight, it appears that the Miclere flightline spacing was such that the good data density meant no loss of resolution after gridding.
By using gridded data throughout, I avoided the problems which may have arisen had I

fig. 2.4 Line Filtered, 200m cutoff, Butterworth filter, E-W flightlines. Range 50764 to 52886 nT

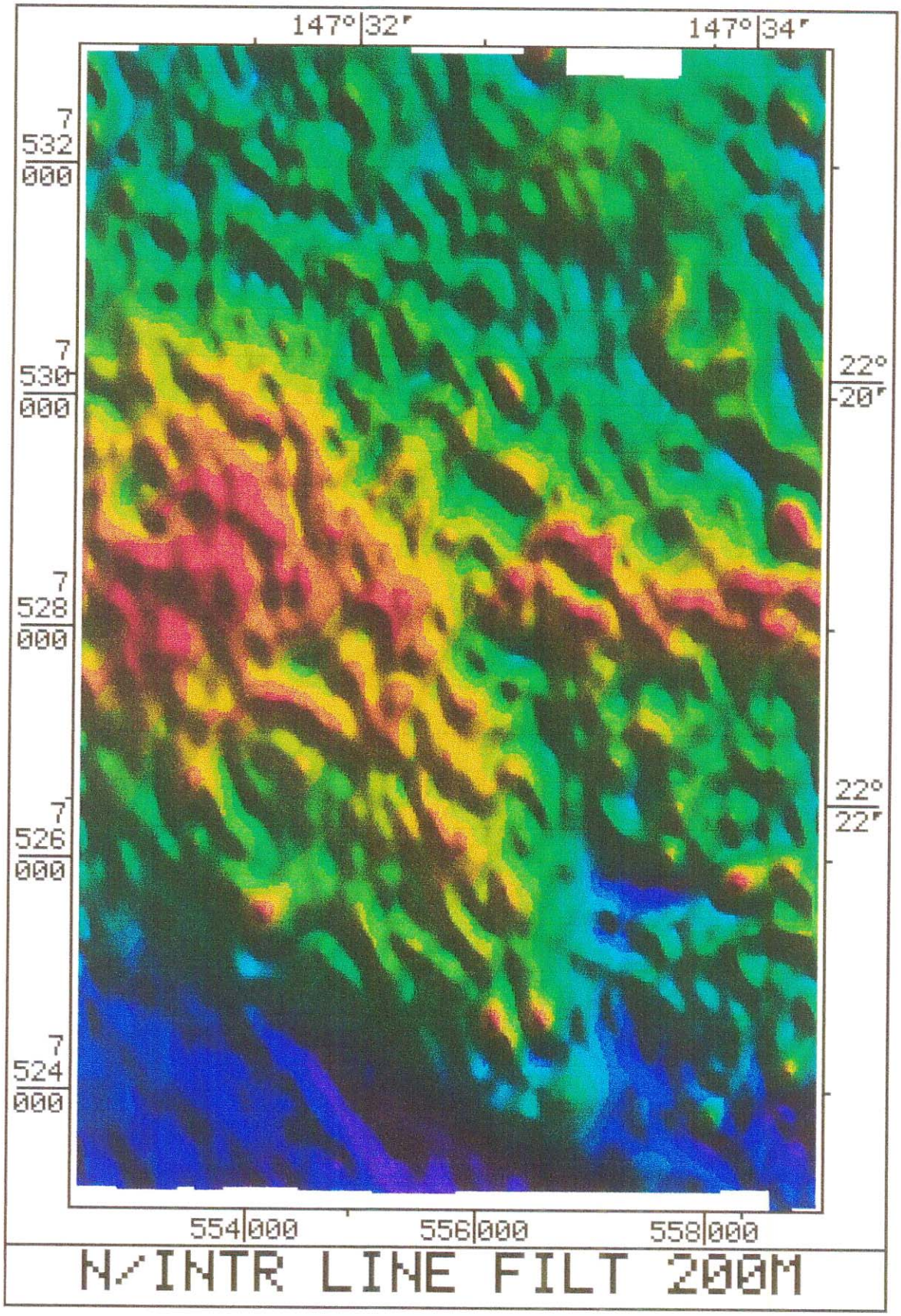

fig. 2.5 Grid Filtered, 200m cutoff, Butterworth filter, E-W flightlines.
Range 50764 to 52886 nT

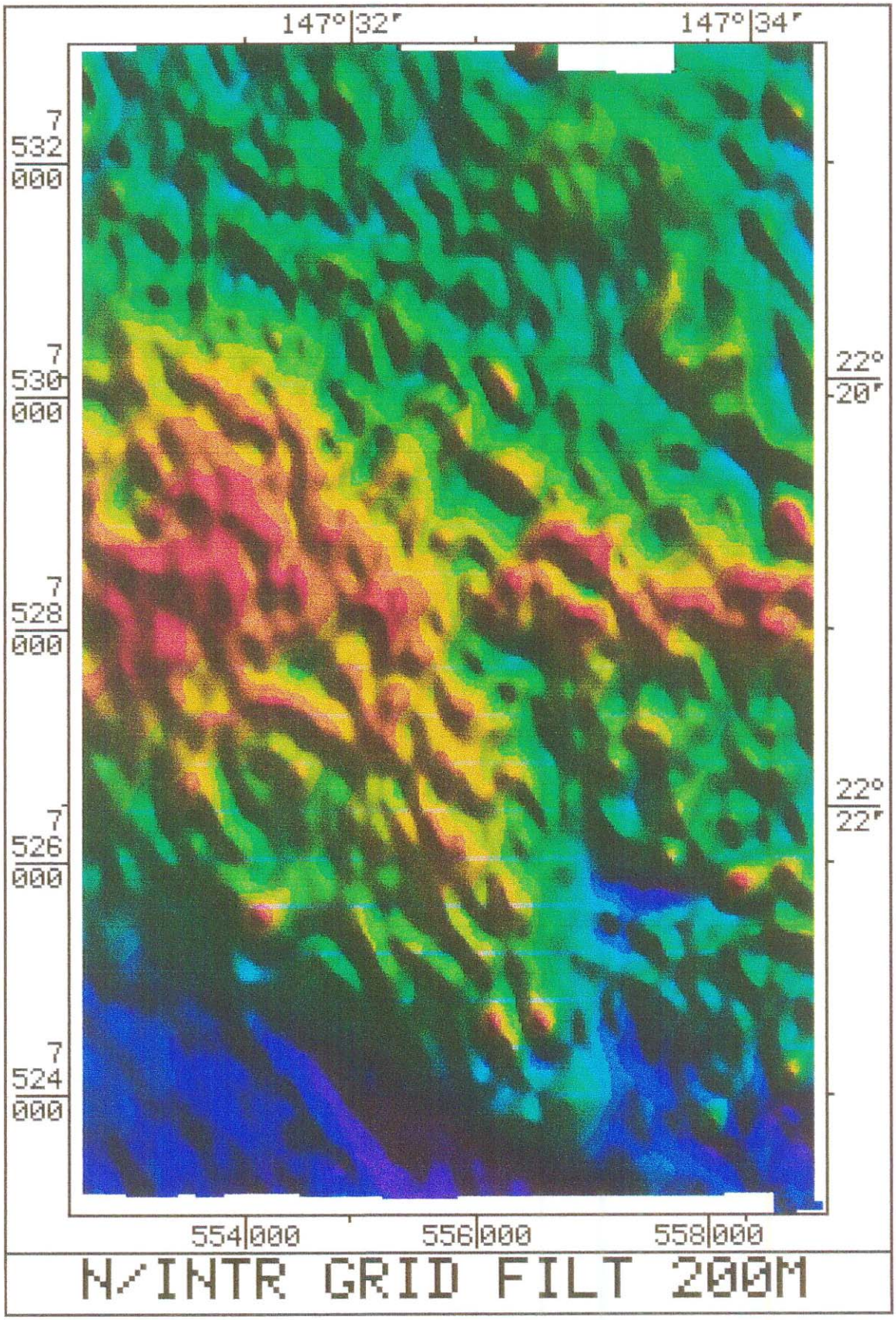

fig. 2.6 Line Filtered, 800m cutoff, Butterworth filter, E-W flightlines. Range 50825 to 52286 nT

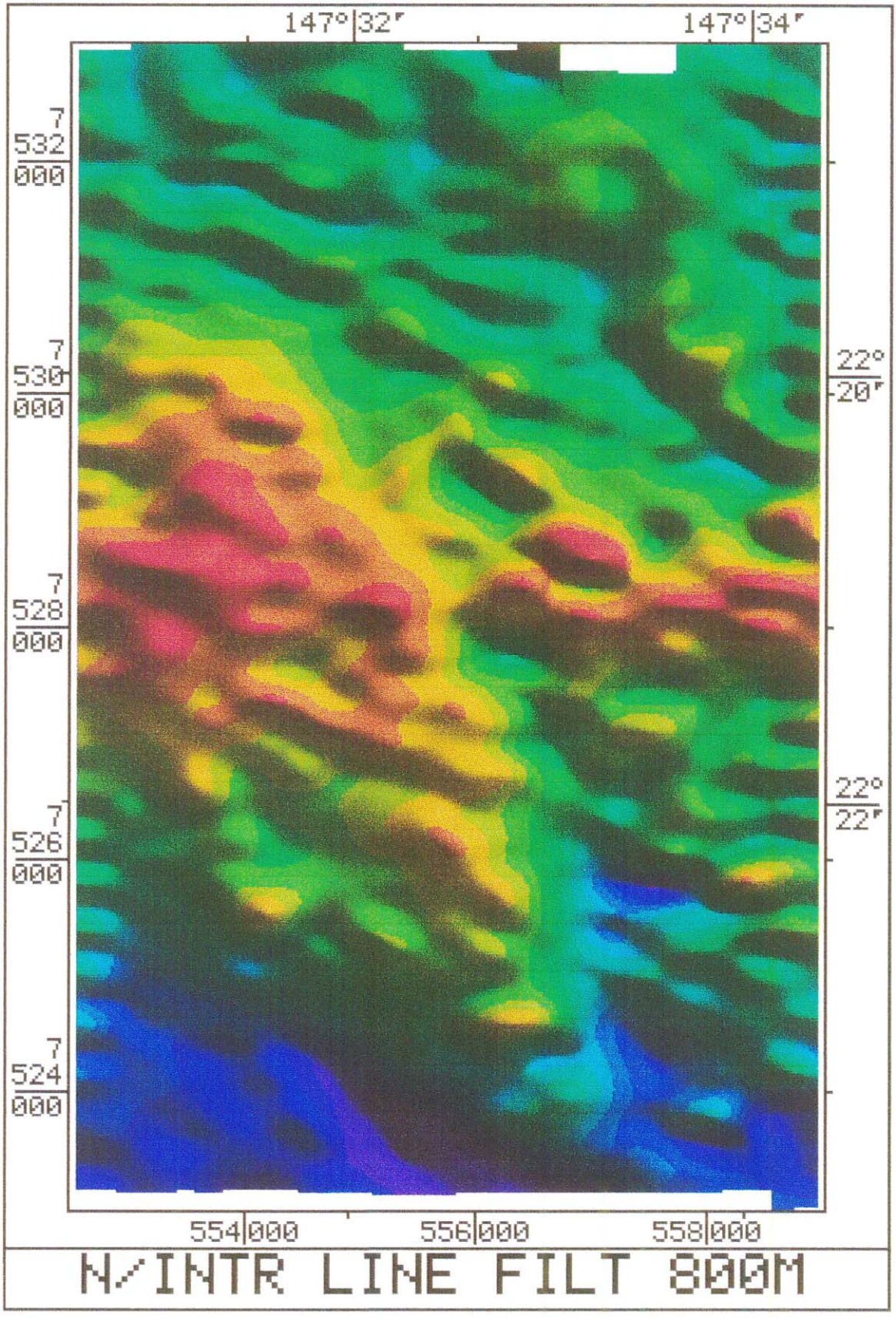

fig. 2.7 Grid Filtered, 800m cutoff, Butterworth filter.
Range 50819 to 52283 nT

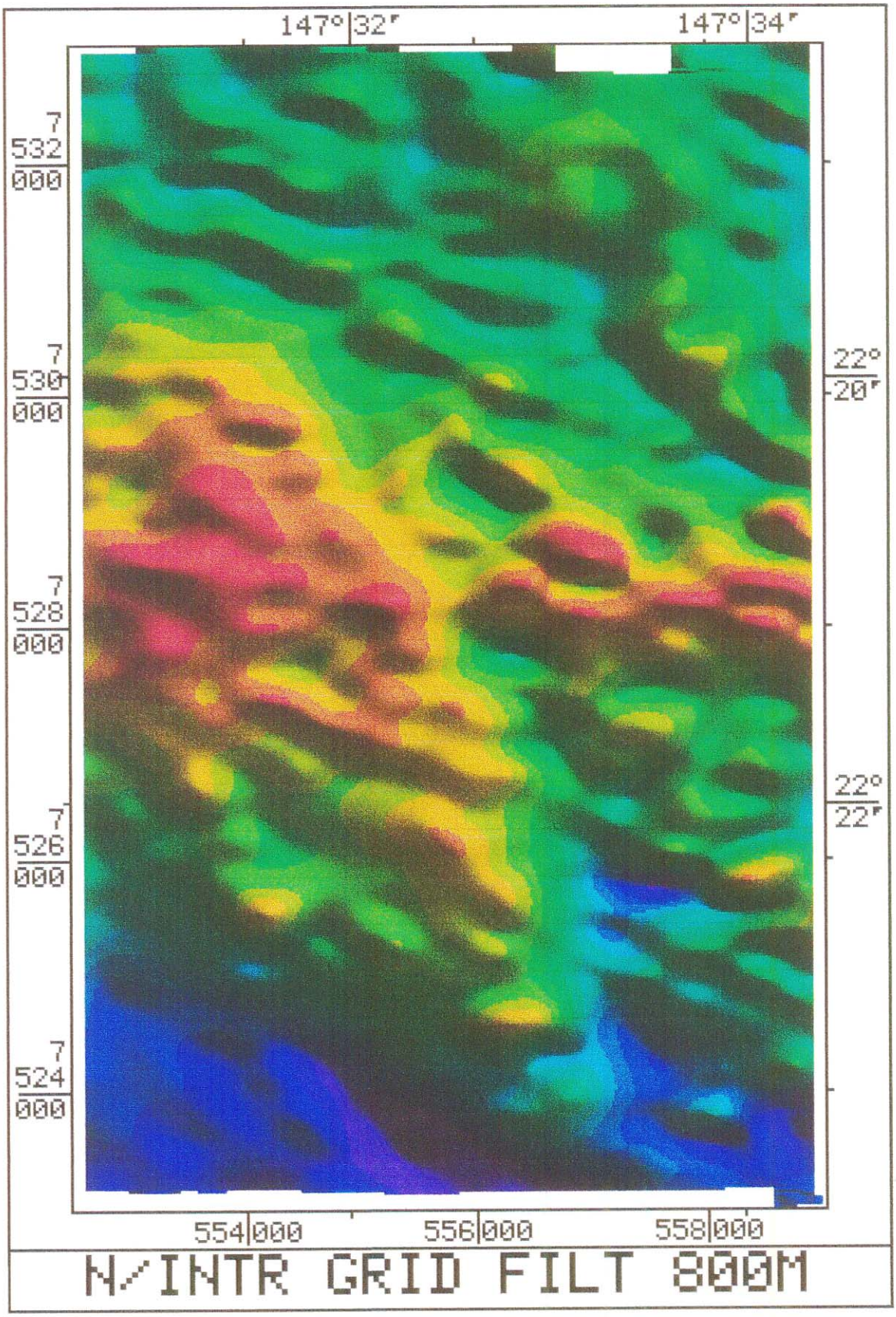

tried subtracting or adding datasets obtained via separate gridding operations. If a dataset gridded after line operations were to be added to one gridded first then subjected to operations, there is an increased risk of artifacts resulting from the inconsistencies between the two gridding operations.

2.6 Choice of Gridding Algorithm

The available Geosolutions™ software had two gridding algorithms, a minimum curvature spline and a bicubic spline. The latter was used exclusively. Not only was it considerably faster, but it was also more accurate, as indicated by a comparison test using the IGRF values associated with the data. In this test the IGRF values were gridded (refer appendix F.1) and the vertical derivatives obtained: in the minimum curvature case the minute differences allowed the derivative to pick out the flight and tie lines (fig. F.2). The bicubic spline showed no such differences (fig F.3). In both diagrams the range of values is the same, 0.078 nanoTeslas/metre, which is much less than the data range for the same area, at 7.05 nT/m. Here the dark pixels represent noise, which in fig. F.3 is more random and less problematical than that in fig. F.2.

2.7 Reduction to the Pole

Reduction To the Pole was not used in the evaluation of different processes. Despite its routine application as an aid to the physical location of structures and orebodies, it is not intended as an improvement for signal to noise ratio, and its use, or non-use, will not affect the validity of the processes applied.

Chapter 3

Low Pass Filters

3.1 Butterworth Filters

Butterworth filters are described as maximally flat in their passband response, due to the derivatives of the filter function all being zero for $\omega = 0$. The flat passband means that they have little tendency to introduce artifacts into the data. Fig. 3.1 shows the amplitude characteristics of a third-order Butterworth filter, with a third-order Chebyshev for comparison. The disadvantage of the pass-band ripple of the latter more than offsets its marginally steeper cutoff (Kuo, 1962).

Butterworth filters had already been tried on the Miclere dataset, with limited success, by Normandy personnel (M. Sexton, personal communication). They would therefore be used as the starting point and benchmark by which other filters and processes would be judged.

The Geosolutions™ software uses a third order recursive Butterworth filter (Blair and Spathis 1980) so as not to introduce phase shifts: an important consideration in this project because flight lines are in alternating directions. An effect of using a recursive filter is to steepen the cutoff, and Blair and Spathis (1980, p20) indicate that a third-order recursive is similar to a fifth-order non-recursive filter.

Filters with cutoff wavelengths much greater than the flightline spacing were required to effectively remove the unwanted signal. At these cutoffs it was necessary to grid-filter in two dimensions to avoid the directionality inherent in a one-dimensional filter (the grid filter software normally only filters up the columns of the grid). This double filtering has the effect of further steepening the overall filter cutoff.

The method of selection of the most appropriate cutoff was to use a panel of outputs, from a range of different cutoff values. The value that gave the visually optimum result was chosen. The panel is presented as appendix A; it is interesting to examine the results in the light of section 2.4, in which a filter cutoff of 600 to 700m was predicted as the minimum. In the panel, the 800m cutoff is the first image which appears reasonably 'clean'. The selected optimum cutoff was 1000m, and the result of this filter is fig. 3.2 (p18).

3.2 Averaging Window Filters

Averaging window filters use a moving 'window' to scan the data grid; the data value at the centre of the window is replaced by the average of all the data values in the

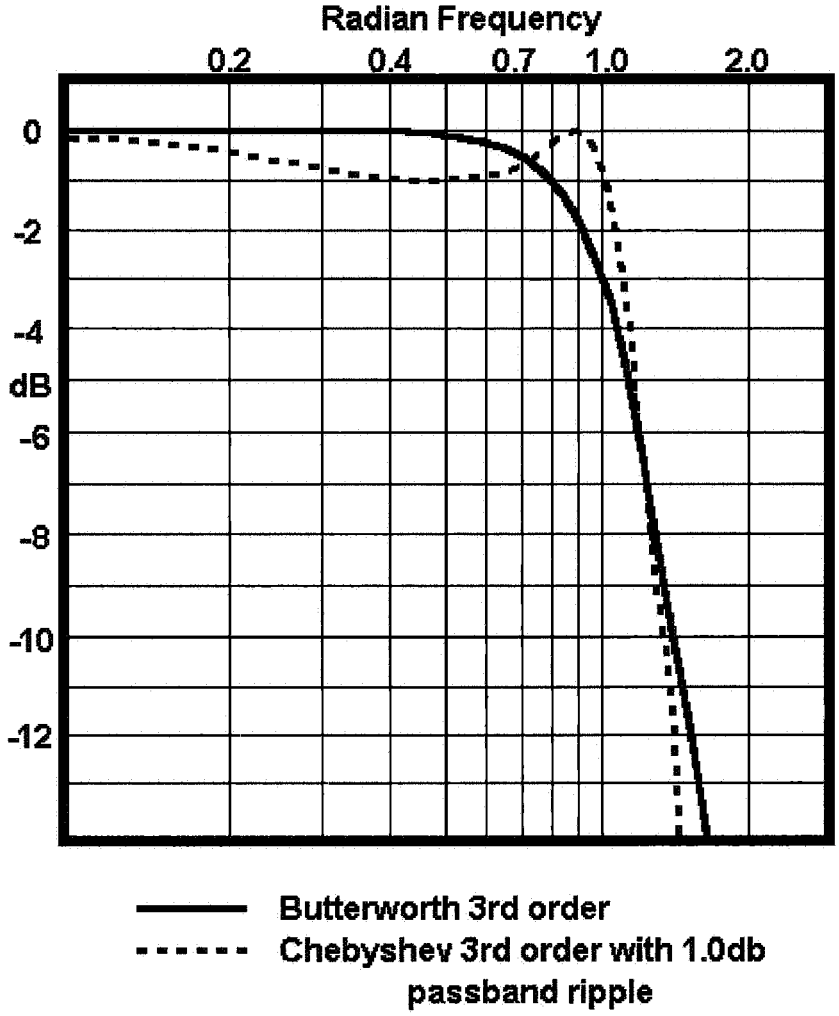

fig. 3.1 Amplitude response of Butterworth and Chebyshev filters (after Kuo, 1962)

fig. 3.2 Grid Filtered; 1000m cutoff, Butterworth filter; N-S on first pass, E-W on second pass. Range 50830 to 52029 nT.

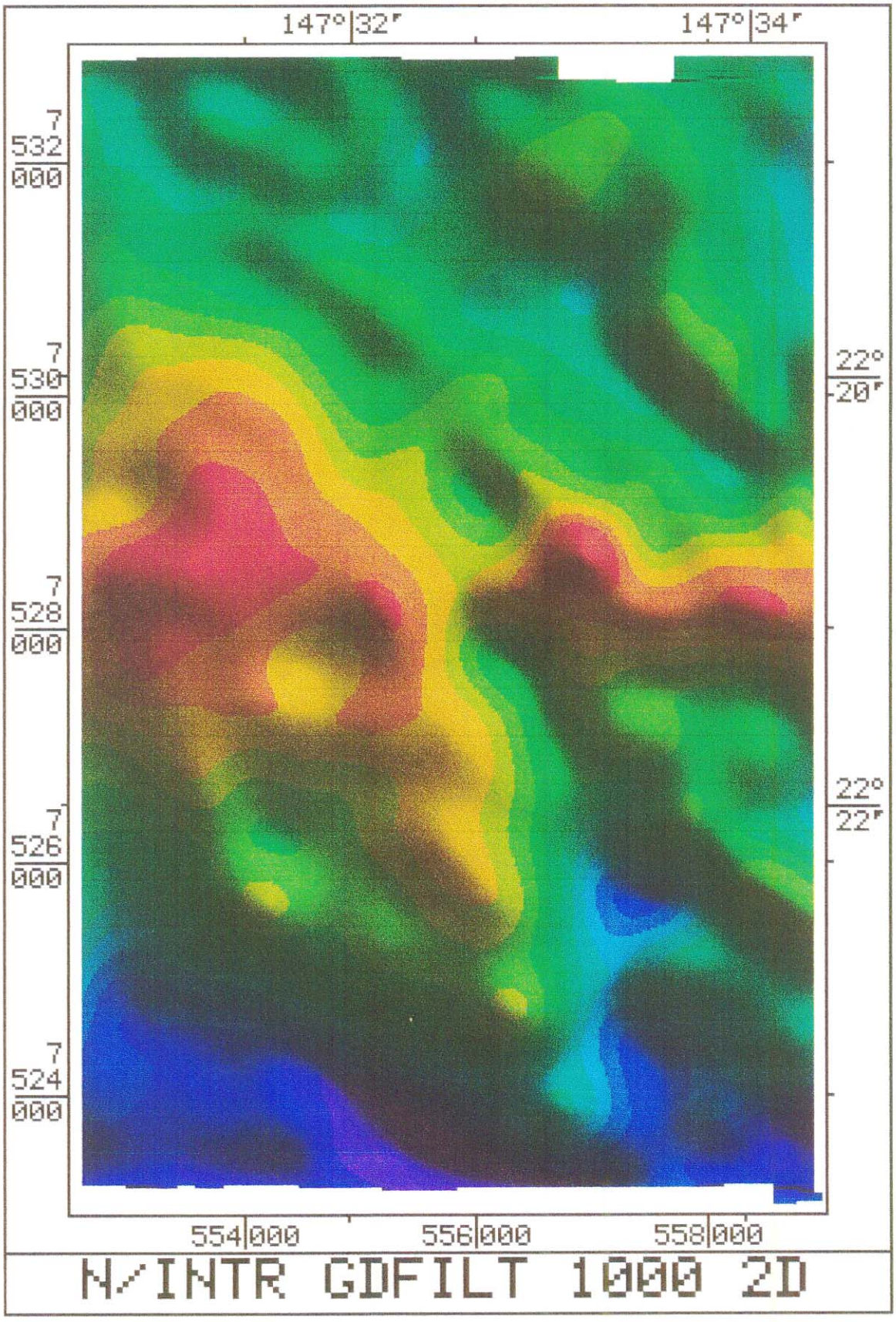

fig. 3.3 Averaging Window Filter, 25x25 grid points (25m grid)
Range 50878 to 51895 nT

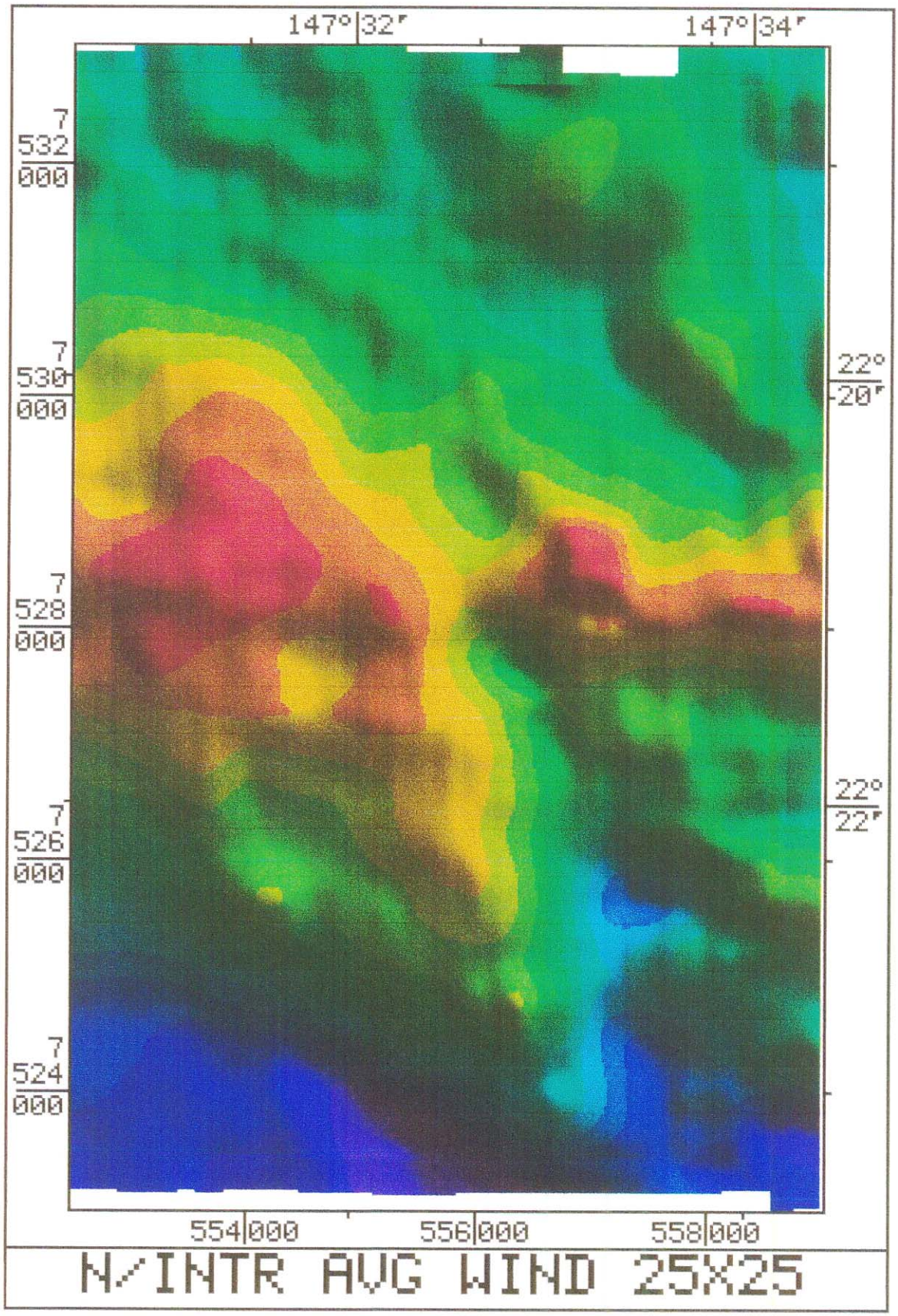

window. The cutoff wavelength is thus determined by the dimensions of the window expressed in grid points, and by the gridding dimension. For example, a window of three grid units has a cutoff value of 2.4 grid units. The cutoff wavelength can thus be seen to approximate the window dimension. It is not necessary for the window to be square, and where the data is anisotropic, it may be advantageous to dimension the sides independently to suit the properties of the data.
In this project, investigations with rectangular windows were conducted, but without useful result. The anisotropy of the data as shown in fig. 2.3 appeared to diminish with increasing wavelength, and was indistinguishable beyond 800m. Appendix B contains the panel of results; fig. 3.3 shows the image resulting from the 25x25 window, judged the most appropriate.

3.3 Median Window Filters

Median filters are recommended by Stanley *et al* (1992) for exploration beneath magnetically noisy cover. Their operation resembles the averaging window, except that the median value of all the cells within the window, rather than the mean, gives the value to the central cell. This selection process makes it a non-linear filter and the transfer function is not a straightforward mathematical expression. Intuitively the cutoff wavelength will closely approximate that of the same size averaging window, for with truly random data the mean and the median coincide. Thus the window dimension is an approximation of the cutoff wavelength. Stanley *et al* (1992) recommend a window dimension greater than twice the desired stripping depth. Basalt thickness of the order of 150m (appendix G) thus suggests a 300m window, or 13x13 in 25m gridpoints. Even at 17x17 (appendix C) there is some residual basalt signal. Of the five window sizes the subjective 'best' is 25x25, as shown in fig. 3.4.

fig. 3.4 **Median Window Filter, 25x25 grid points (25m grid). Range 50881 to 51898 nT**

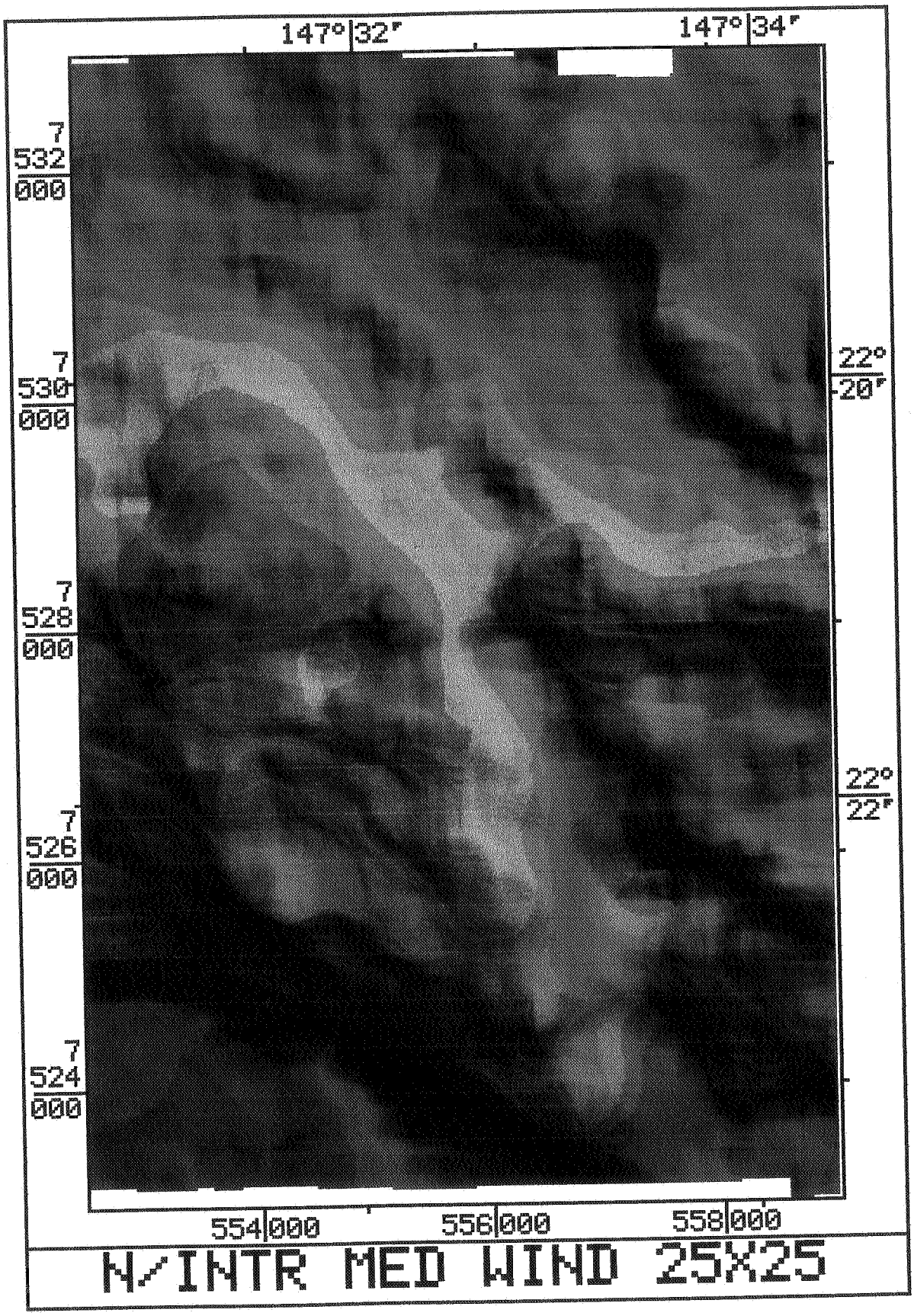

Chapter 4

Frequency Domain Processes

4.1 Upward Continuation

Upward continuation is the mathematical equivalent of re-collecting the data at a greater elevation. It is easily accomplished in the frequency domain via the following relationship:

$$A_z = A_0 . e^{-z\sqrt{(\mu^2 + \nu^2)}}$$

where A_0 is the measured amplitude, A_z is the amplitude at a height z above the measuring level, and μ and ν are the spatial frequencies in the x and y (horizontal) directions.

Use of fast Fourier transform and inverse transform software speeds the process. As the relationship above indicates, the high frequencies undergo more attenuation than the low frequencies. Upward continuation can thus perform a similar task to a low-pass filter.

In this context the high frequencies - in this case the basalt signal, predominantly - are greatly attenuated by upward continuation. The attenuation is greater for larger values of upward continuation. Appendix D shows the results of upward continuation at several different heights. Fig. 4.1 shows the selected result, for upward continuation by 180m.

4.2 First and Second Vertical Derivatives

Derivatives are recommended as a means of picking edges and structural boundaries, (Mudge, 1991 and Rajagopalan and Milligan, 1995). In this context they were tried but with poor results (appendix E.). Another subset, based on the south intrusive, gave reasonable definition of the south-west boundaries of that intrusive. Application of the first derivative process to filtered data gave more presentable results, suggesting that the high frequencies are responsible for the poor definition. This demonstrates that the priority must be to remove as much as possible of the high frequency signal before using the vertical derivative processes.

fig. 4.1 Upward Continuation by 180m. Range 50955 to 51921 nT.

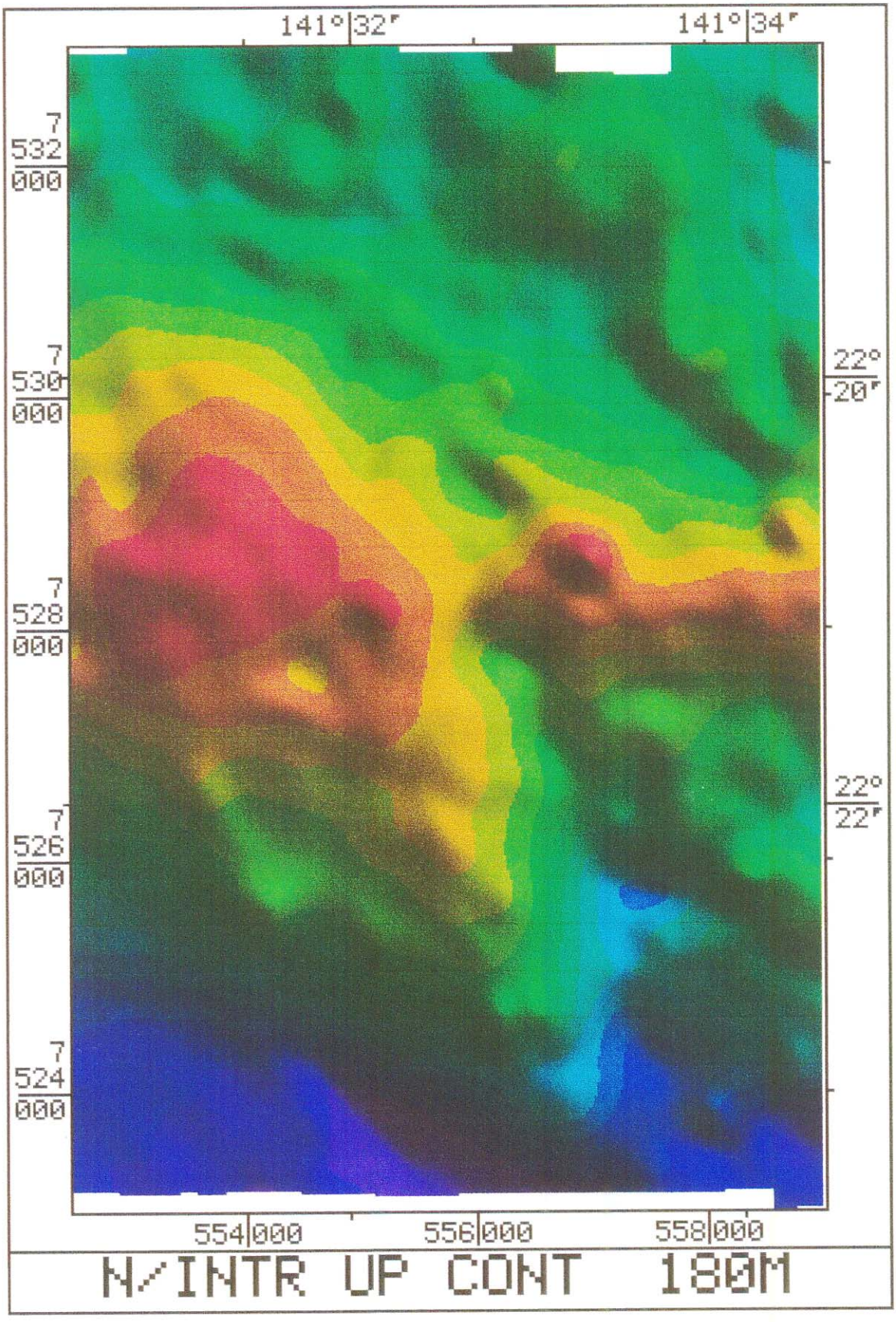

4.3 Downward Continuation then Subtraction (Differencing)

Downward continuation will have the opposite effect to upward continuation; the same formula can be used, but with care. The theory relies on a field without sources and the process can be unstable or generate meaningless results if downward continuation encounters a source such as noise. Noise appears as a source in the plane of the data, so potential sources of noise such as flightline mismatch (poorly levelled data) and Fourier series truncation error must be filtered.

Downward continuation by 40, 20 and 10 metres are presented in appendix E. They show increasing high frequency content with increasing depth, illustrating the reason for the interest in downward continuation. If the unwanted signal can be emphasized then subtracted from the original, the result may prove useful as an alternative to low-pass filtering.

Initial trials of this approach used downward continuations of 50 and 30 metres. The noise in the data, as mentioned above, meant that subtracting a noisy result from the original gave another noisy result. It was not until I used a Hanning window to attenuate the Fourier truncation noise, and started trying a more modest continuation (20m) with its corresponding reduction in noise, that I was able to resolve features inaccessible via the previous methods.

Fig. 4.2 shows what I considered the 'breakthrough' image, with the crater-like feature just right of centre. This item had previously appeared as a peak in all images. Subsequent optimisation of parameters (fig. 4.3), cleanup filtering (fig. 4.4) and greyscale image (fig. 4.5) showed not one but several such features. Initially it seemed that the features may be processing artifacts; however, as will be seen in chapter 6, this is most unlikely to be the case.

fig. 4.2 Differencing Process: Downward continuation by 20m, multiplied by 0.8, then subtracted from the TMI data. Range 10182 to 10405 nT.

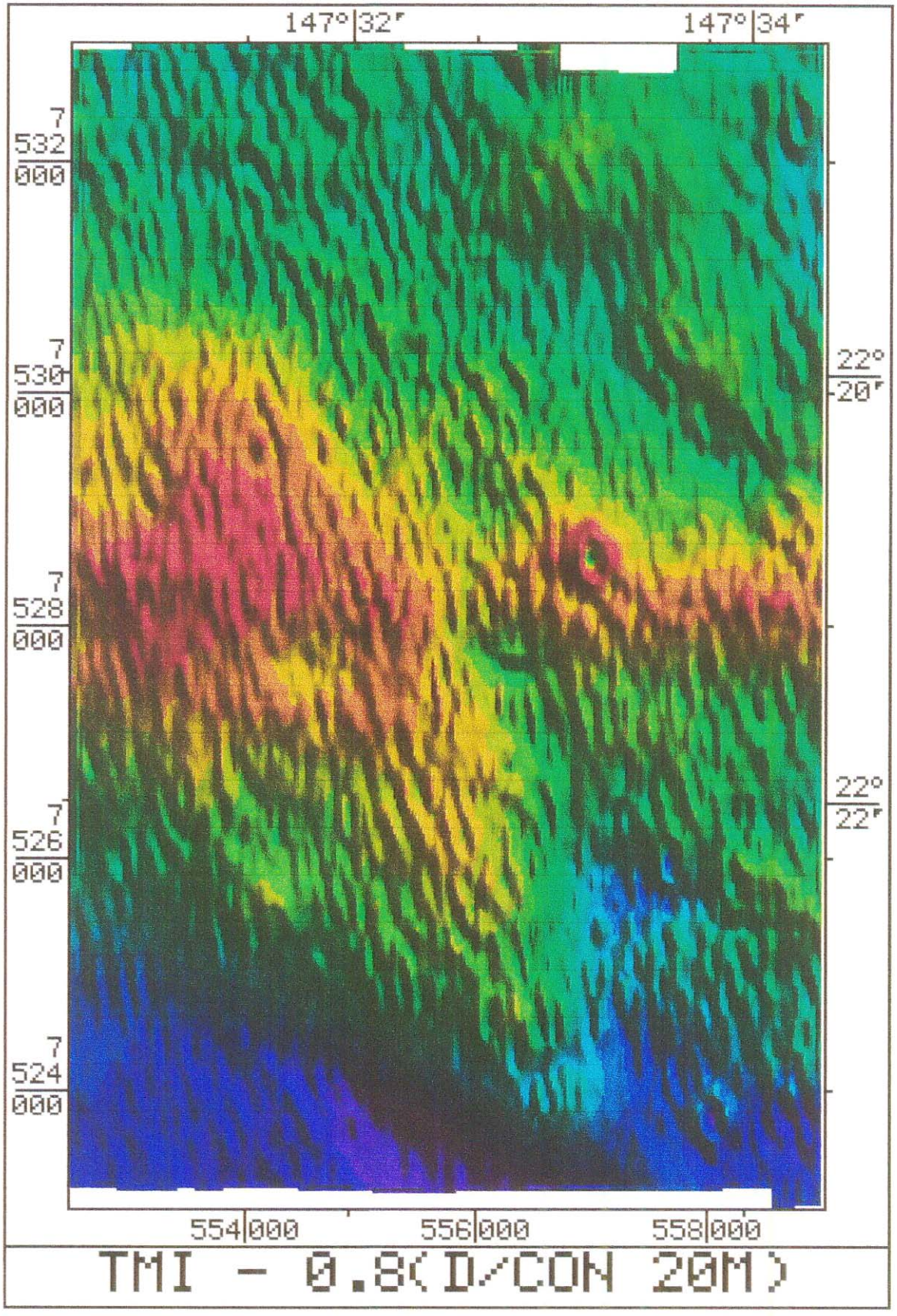

fig. 4.3 Differencing Process: Downward continuation by 10m, multiplied by 0.9, then subtracted from the TMI data. (Optimised parameters) Range 5086 to 5212 nT.

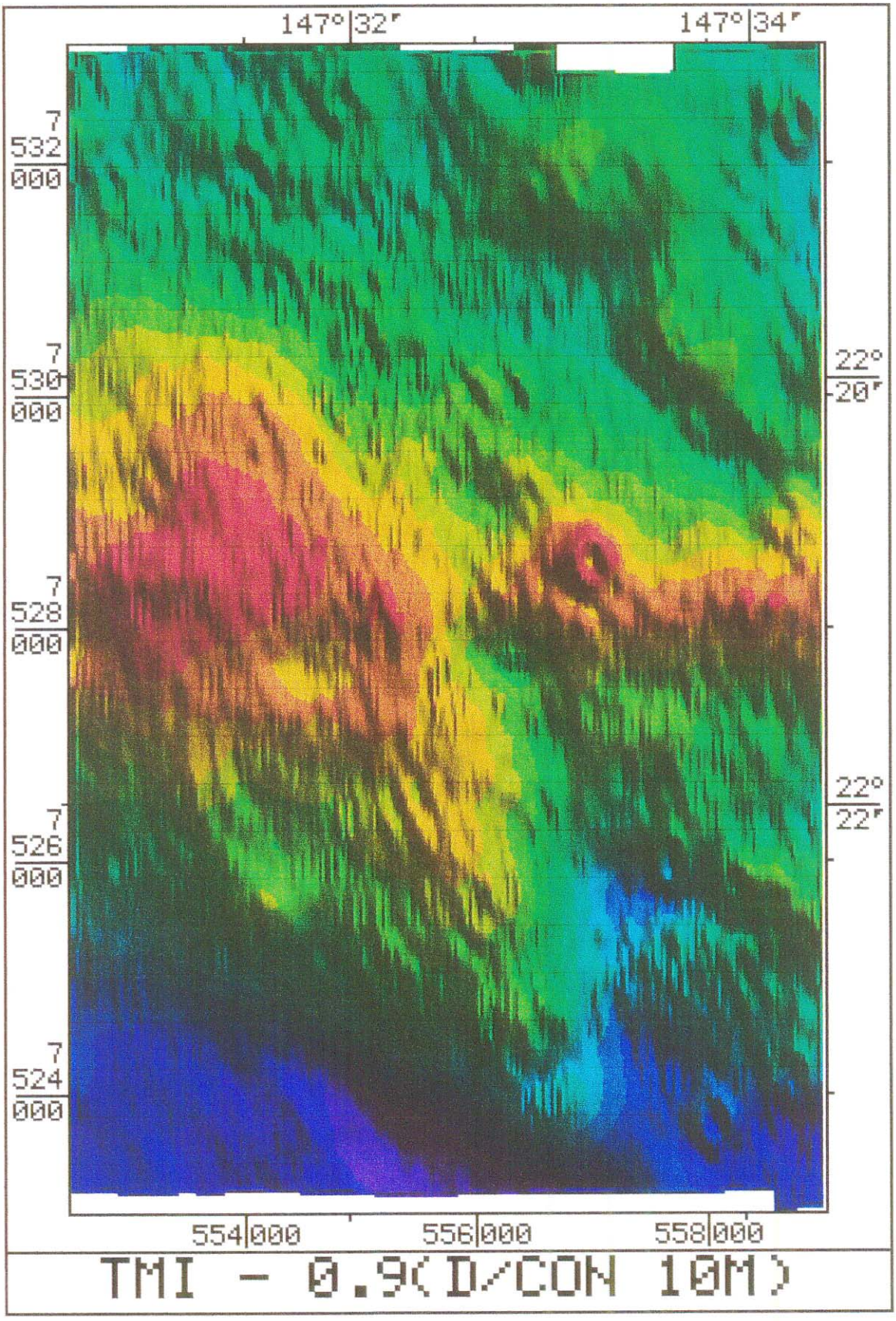

fig. 4.4 Previous image (fig. 4.3) with a Butterworth grid filter of 300m cutoff applied as a 'cleanup filter' to remove high frequency noise.

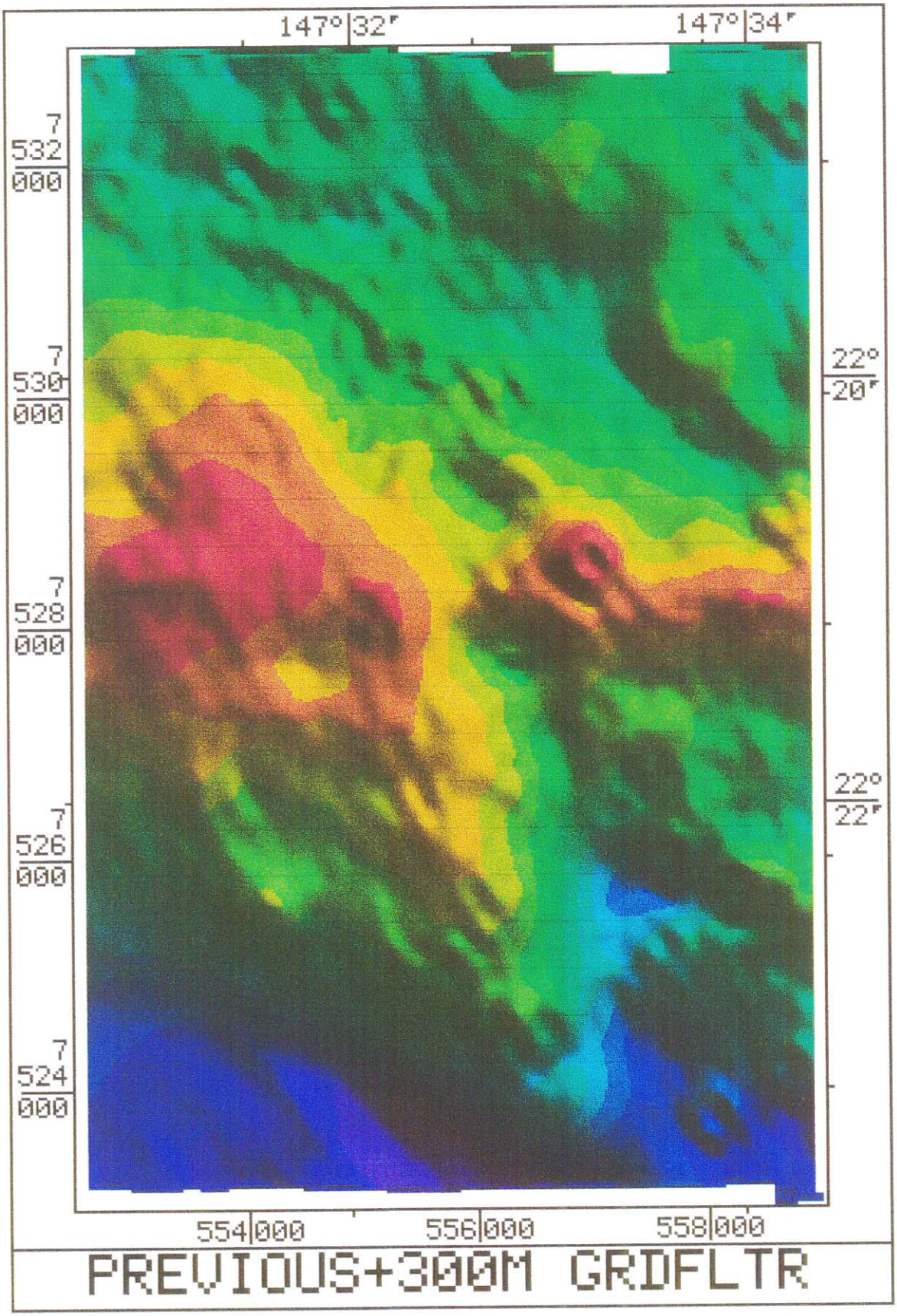

fig. 4.5 **Greyscale version of fig. 4.4. The grey image can clarify features, such as the 'craters' in the lower right of the image, which are less distinct in the colour image**

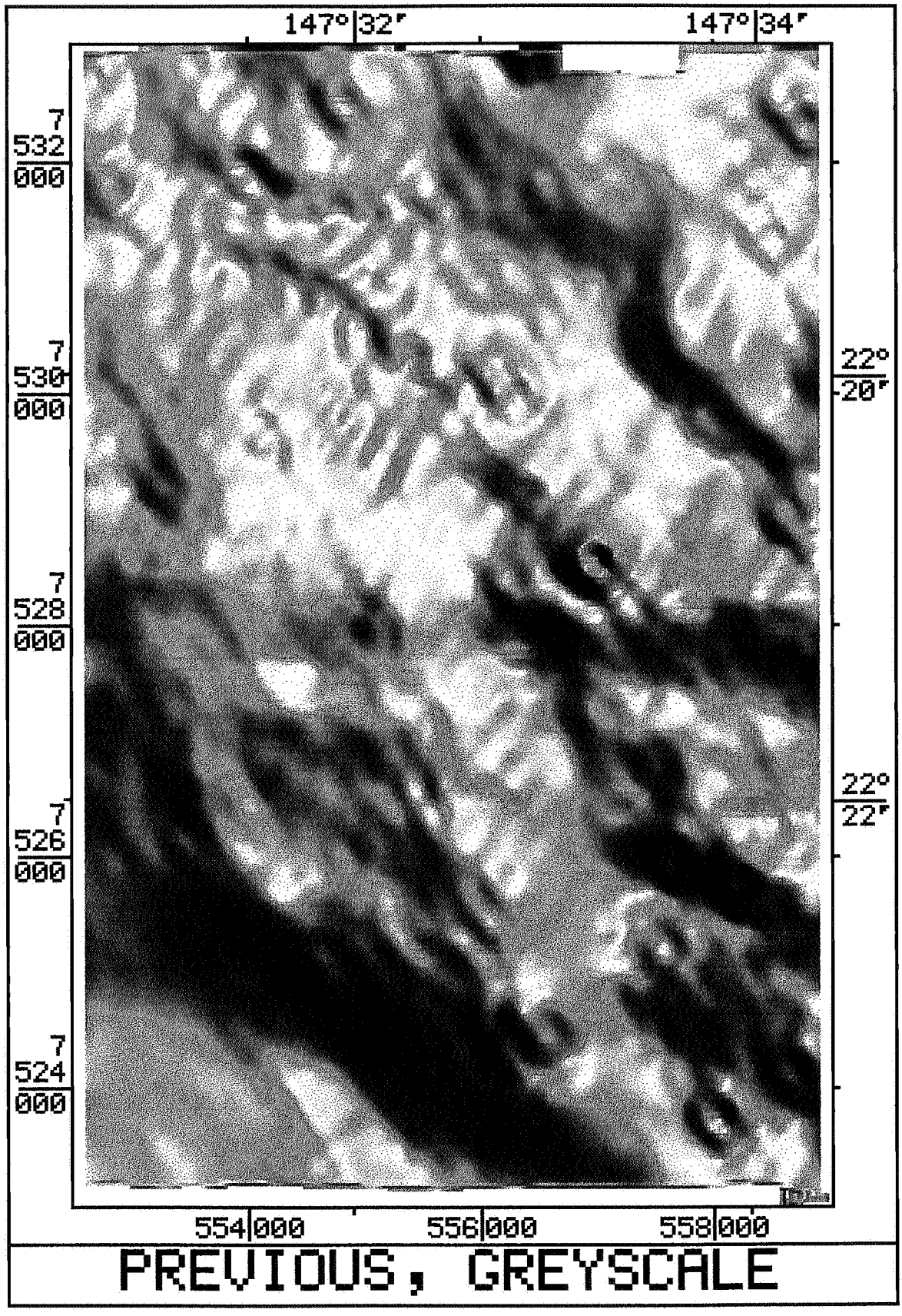

Chapter 5

Automatic Gain Control

5.1 AGC on Vertical Derivatives

Automatic Gain Control has been used by Rajagopalan (1987) and Rajagopalan and Milligan (1995) as an aid to delineation of deeper structures. In this project, as in the cited papers, a root-mean-square (RMS) gain function was used. A range of window sizes from 3x3 up to 25x25 were tried. Rajagopalan and Milligan (1995) recommend window length (= half window size) to be equal to the wavelength to be suppressed. For a wavelength of 300m this implies a window size of 600m or 25 at 25m grid points. The results were unintelligible when derivatives of unfiltered TMI were used, but if the first derivative of filtered TMI was used as the basis, a reasonable image resulted (fig. 5.1).

5.2 AGC on Low-Pass Filtered Data

AGC, again with a RMS gain function, was initially used on unfiltered TMI data with unexpected effectiveness (fig. 5.2). It appeared to sharply delineate the boundary of the intrusive body. The basalt signal detracted from the clarity of the boundary, and this led to its trial on low-pass filtered data (1000m cutoff), (fig. 5.3). The potential of this process for delineation of bodies or structures is clear. In these two images a window size of 3x3 was used, but the result was not window size sensitive, with a 11x11 window giving a similarly well-defined boundary, and additional information on structures. With a 25x25 window (fig. 5.4) the boundary definition is an improvement on the non-AGC image (fig. 3.2), and the structural information appears significantly greater than in the 3x3 window of fig. 5.3.

It appears that, as with the vertical derivatives, useful application of AGC is reliant on effective removal of most of the high frequencies.

fig. 5.1 Automatic Gain Control using a 3x3 window and Root Mean Square gain function, on First Vertical Derivative data which has undergone 180m upward continuation to reduce the high frequency content.

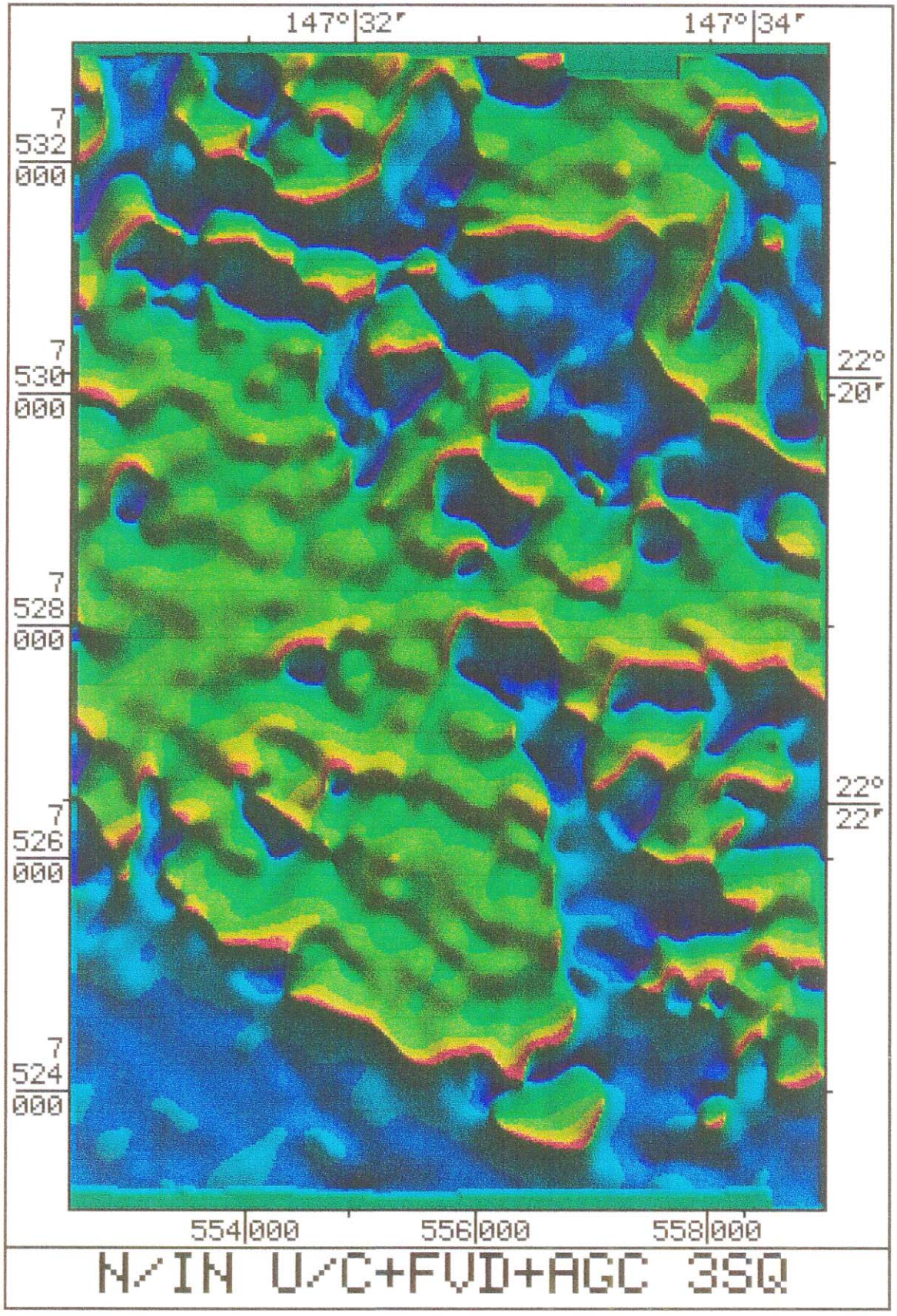

Chapter 6

Summary and Discussion of the Miclere Results

6.1 Differencing versus the Low-Pass Filter Results

The results from Butterworth low-pass filtering, averaging window filtering, median filtering, and upward continuation appeared comparable inasmuch as none appeared able - at least for the selected subset - to resolve features that the others could not. The median filter, recommended by Stanley *et al* (1992) for its ability to remove the noise due to lateritic soils, did not appear exceptional in this case. The reason must lie in the differing physical configurations of these noise-source layers. In the case of the lateritic layer, the noise source is the pebbles of maghemite, which are remanently magnetised with a random orientation. This randomness gives a 'white noise' character to the signal, which extends high into the frequency spectrum. The basalt noise signal is due to the relatively high susceptibility values, not randomness of a remanent field. The basalt signal is a problem because of its variability, due to variations in both susceptibility and thickness. The wavelength of these variations is determined to a large degree by the palaeotopography, and is of the order of 300 metres. This is similar to the resolution required for prospective structures, and filtering is therefore not easily accomplished.

By comparison, the differencing technique did succeed in resolving features unresolved by other filters. There was some concern that the first discovery, the crater-like 'feature of interest' of fig. 4.2, may be an artifact of processing. These concerns were reduced when other similar features were found (refer fig. 4.5, the greyscale image) and vanished when the process was applied to the entire Miclere dataset (fig. 6.1 in colour, fig. 6.2 in greyscale). In fig. 6.2 a row of five of these features can be seen in a straight line trending N350°, through the central northern part of the image. This line coincides with a visible structural lineation, and suggests intrusive bodies along a line of crustal weakness. This view is shared by the Area Geologist, (B. Clifford, pers. comm.) who considers them likely to be basalt plugs. As such, some must have been subject to mineralisation, or been the cause of local alteration, given the evidence of elevated magnetic intensity levels. In particular, the feature which first caught my attention in fig. 4.2 has a magnetic intensity level higher than any other feature on the Miclere lease. This is a strong indication of iron mineralisation.

fig.6.1 Differencing applied to the whole Miclere dataset.

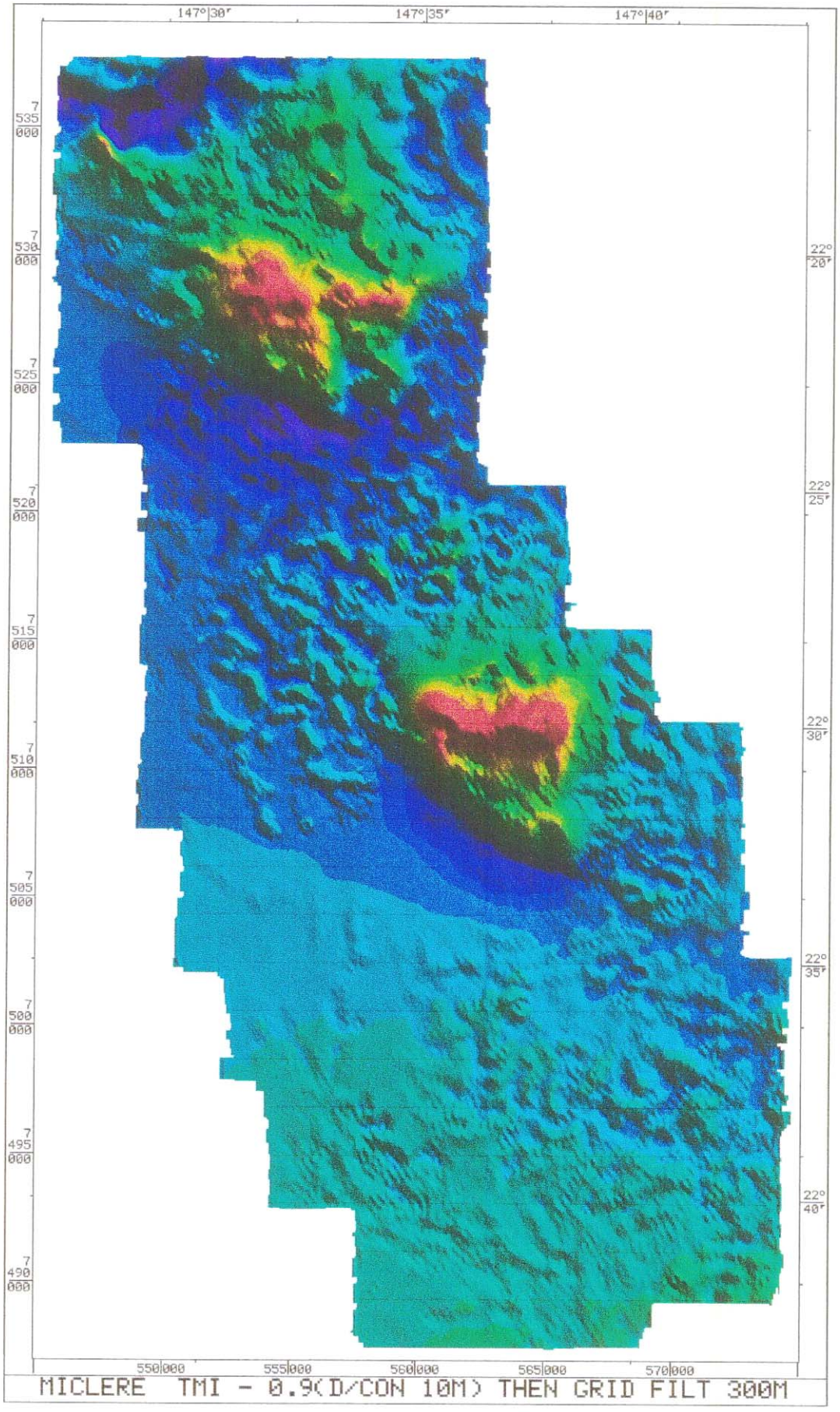

fig. 6.2 Differencing applied to the whole Miclere dataset: greyscale

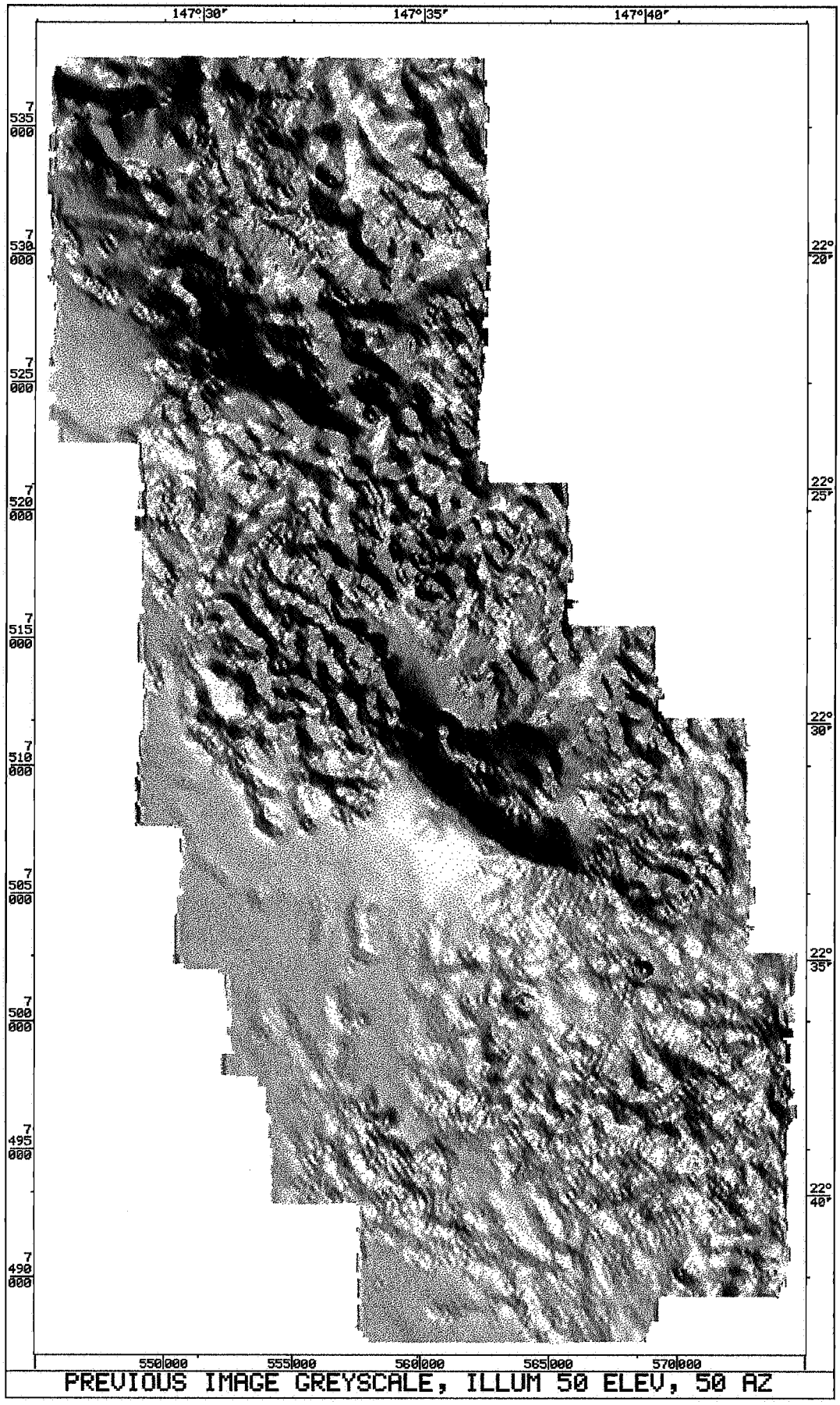

6.2 Reasons for the Effectiveness of Differencing

Before going further, this process I have called differencing should be examined to see why it worked in this case, and whether it is likely to work in other instances. In particular, how does differencing differ from upward continuation? Another point of interest is that, with ever shallower downward continuations and a subtraction coefficient approaching unity, the process appears similar to a first vertical derivative. How does it differ?

Taking the first point, this is addressed by fig. 6.3, where noise and signal, in highly simplified spectral representations, are processed by the differencing method. In this case downward continuation of 30m is used rather than 10m as the effect with the latter would be so slight as to be difficult to see. Although the spectra are stylised, the ordinates of the curves are accurately calculated. The end result is thus a fair representation of the operation of this process. The subtraction coefficient of 0.55 was selected to optimise the result in this particular instance, as would be done in practice with each different dataset.

The result shows a considerable reduction in noise amplitude beyond the middle of this spectrum, with some loss of high frequency signal the penalty. Overall, the signal spectrum has undergone little distortion, and a shallower continuation would reduce this even further.

The negative-going high-frequency 'tail' of the curve is of no consequence, as it can be removed by a suitable low-pass cleanup filter. In this project, such a negative tail was never encountered with the optimum values of subtraction coefficient, but there was still considerable high frequency noise. This made a cleanup filter a useful operation, as figs. 4.3 and 4.4 have shown.

Comparison with upward continuation is addressed in fig. 6.4, where the same stylistic representation is used to give the results of each process. The value of 150m was chosen for the continuation because it was close to the figure selected as optimum for the project data. For the data shown, the differencing process is seen to give less noise, and reduced distortion of the low-frequency end of the spectrum, compared to the upward continuation. These advantages may not apply to all data spectra, and the second part of this thesis begins to address this by applying the process to a different dataset.

It is interesting to compare both differencing and downward continuation with low-pass filtering (fig. 6.4) and note that the latter loses virtually all frequencies beyond the cutoff and has no attenuating effect on noise below the cutoff. The one good point is the absence of distortion in the passband.

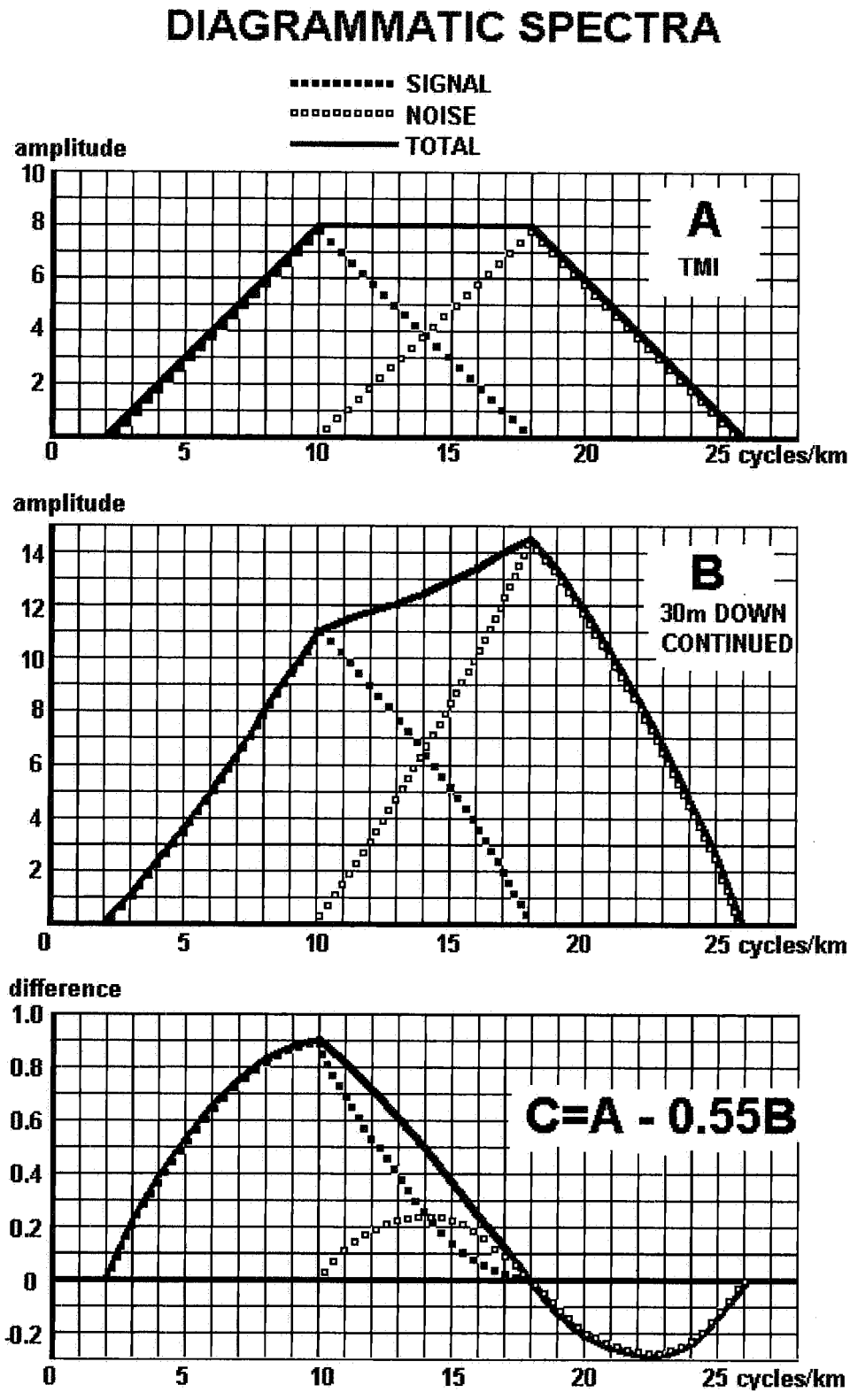

fig. 6.3 Diagrammatic example of the Differencing Process. A low-pass filter would be used to remove that part of the third diagram lying beyond 18 cycles/km.

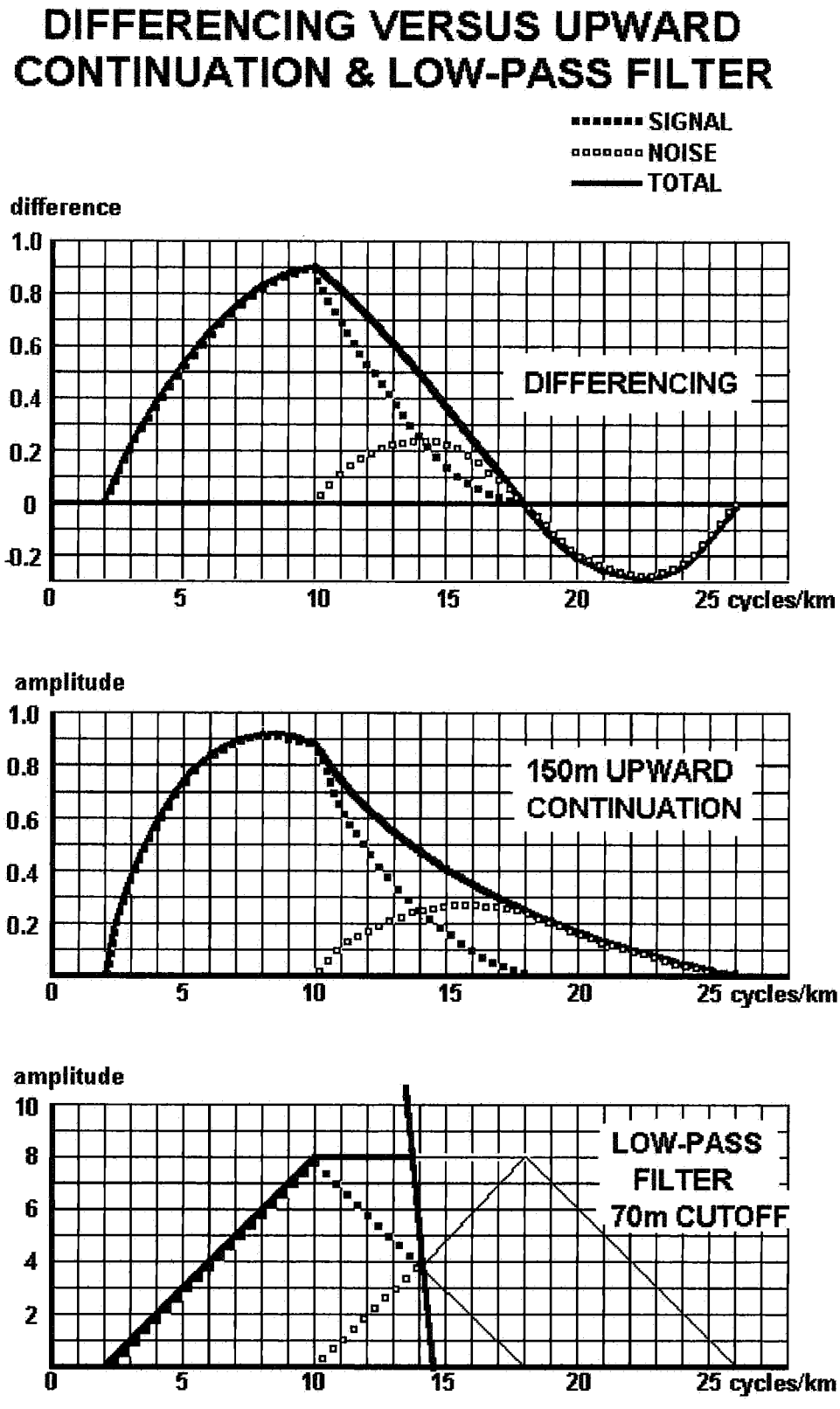

fig. 6.4 Comparing in diagrammatic form the effects of differencing, upward continuation, and low-pass filtering, on the simplified frequency spectrum.

The relationship between differencing and the first vertical derivative requires some examination. Experimentation with different continuation factors and subtraction coefficients gave the following results:

50m down cont; subtraction coeff. of 0.5 gave subjectively best image.

40m	0.6
30m	0.7
20m	0.8
10m	0.9
7m	0.95
5m	0.97

A graph is not plotted, for good reason: the figures are subject to some uncertainty, as the choice between coefficients requires perception of *very* minor differences in images, and a plotted curve tends to lend undeserved authority to its data.

Even without plotting the results, a regression line would appear to indicate that in the limit as the downward continuation approaches infinitesimally close to zero, the subtraction coefficient approaches unity, and the process gives the first vertical derivative (or its negative). Yet the differencing images do not resemble that of the first vertical derivative, appearing more like the TMI image. This is the clue to the effectiveness of differencing; the optimum parameters are such that there is a small excess of TMI data over continued data.

Suppose we take the amplitude of the TMI data to be a function A_0;
The amplitude of the continued data to be A_x;
The subtraction coefficient to be K;
Then the differencing amplitude function will be given by:

$$A_D = A_0 - K.A_x \qquad (1)$$

If $C = 1 - K$, we can re-write the above:

$$A_D = (C + K)A_0 - K.A_x \qquad (2)$$

or

$$= C.A_0 + K(A_0 - A_x) \qquad (3)$$

Since the first vertical derivative (FVD) $= (A_x - A_0)/x$ as x tends to 0, the above expression can be written:

$$A_D = C.A_0 - D.(FVD) \qquad (4)$$

where $D = -Kx$

In equation (4) the relationship between C and D will be optimised for each dataset, in a manner analogous to my selection of degree of downward continuation and subtraction coefficient. Equation (4) agrees with the results I obtained if C is > 0; The proportion of TMI amplitude, albeit small, gives the differenced image its resemblance to the TMI image.

This assertion was tested by subtracting from the TMI grid 75 times the first vertical derivative values. The value of 75 was selected because the relativity of ranges of TMI and 75xFVD was similar to the relativity of ranges for TMI and the downward continuation values. (The process in effect was one of selecting a suitable relationship for the C and D coefficients of equation (4) above). The end result is fig. 6.5. The similarity to fig. 4.2, the original differencing image, is obvious and confirms the relationship indicated by equation (4).

In summary, it can be seen that appropriate choice of coefficients enable the combination of TMI and first vertical derivative in a manner which provides more information than either in isolation.

6.3 The Vertical Derivatives

The first and second vertical derivatives in this case offer little in terms of structure delineation or resolution of features, due mainly to the basalt signal clouding the derivative image. The delineation of structures was more successful when applied to a filtered image. However one use which only became apparent with hindsight was the fact that both the first and second derivatives of the unfiltered data were able to pick out all the 'features of interest' (basalt plugs) found by the differencing method, registering them as highs (ref appendix E). Whilst they are not the only highs in the derivative images, and it is not possible to interpret them from these images, it does reinforce the belief that these features are real and not artifacts of processing.

6.4 Automatic Gain Control

AGC was similar to the vertical derivatives in that the basalt signal compromised its operation on unfiltered data. As mentioned in chapter 5, it appeared useful on filtered data, but this emphasizes the priority of finding an effective means of filtering first.

fig. 6.5 TMI data minus (75 times the first vertical derivative). The figure of 75 was selected to optimise the appearance of the image. It may be regarded as a scaling factor, producing a range for the FVD values that is comparable to the range of the TMI values.

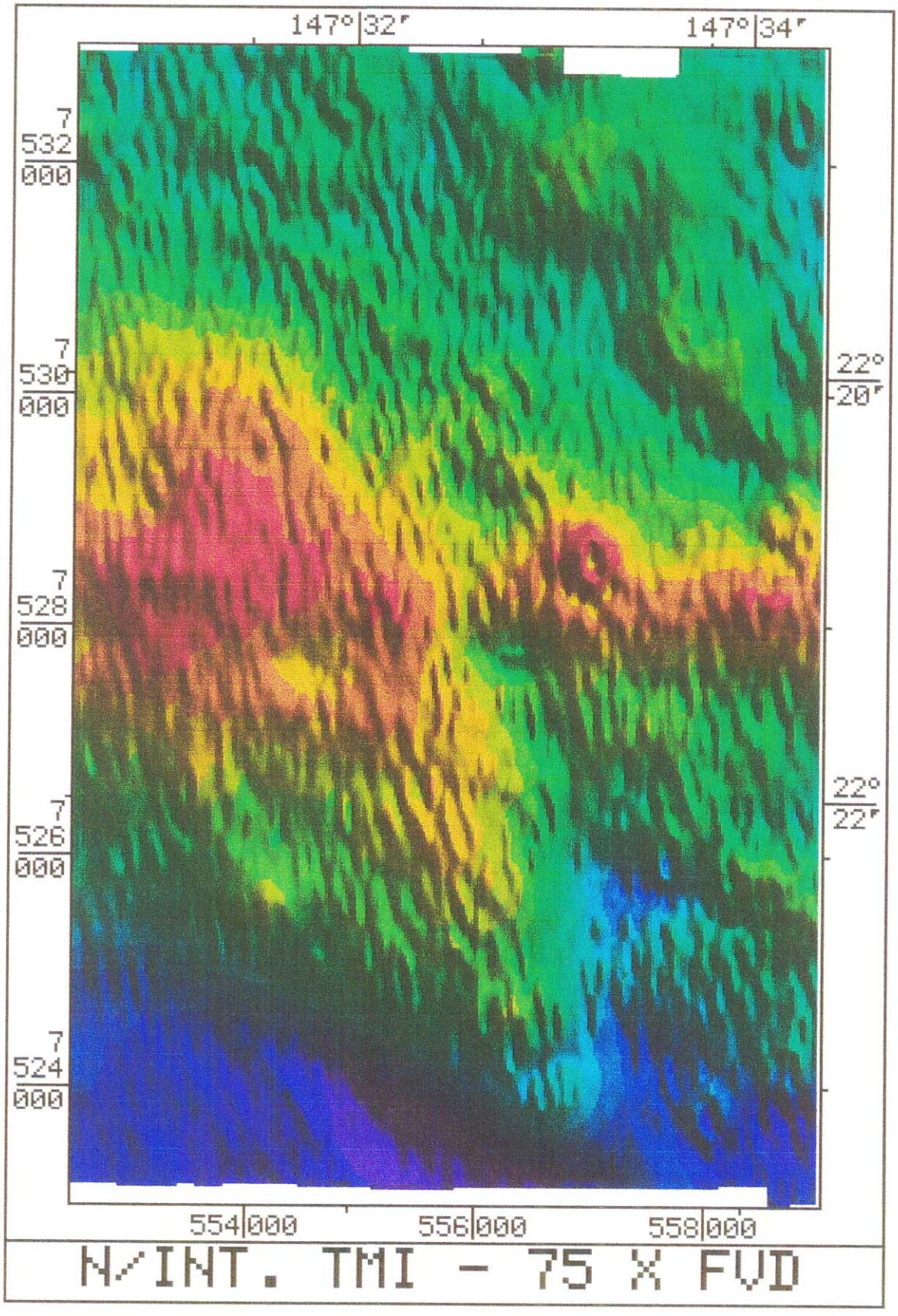

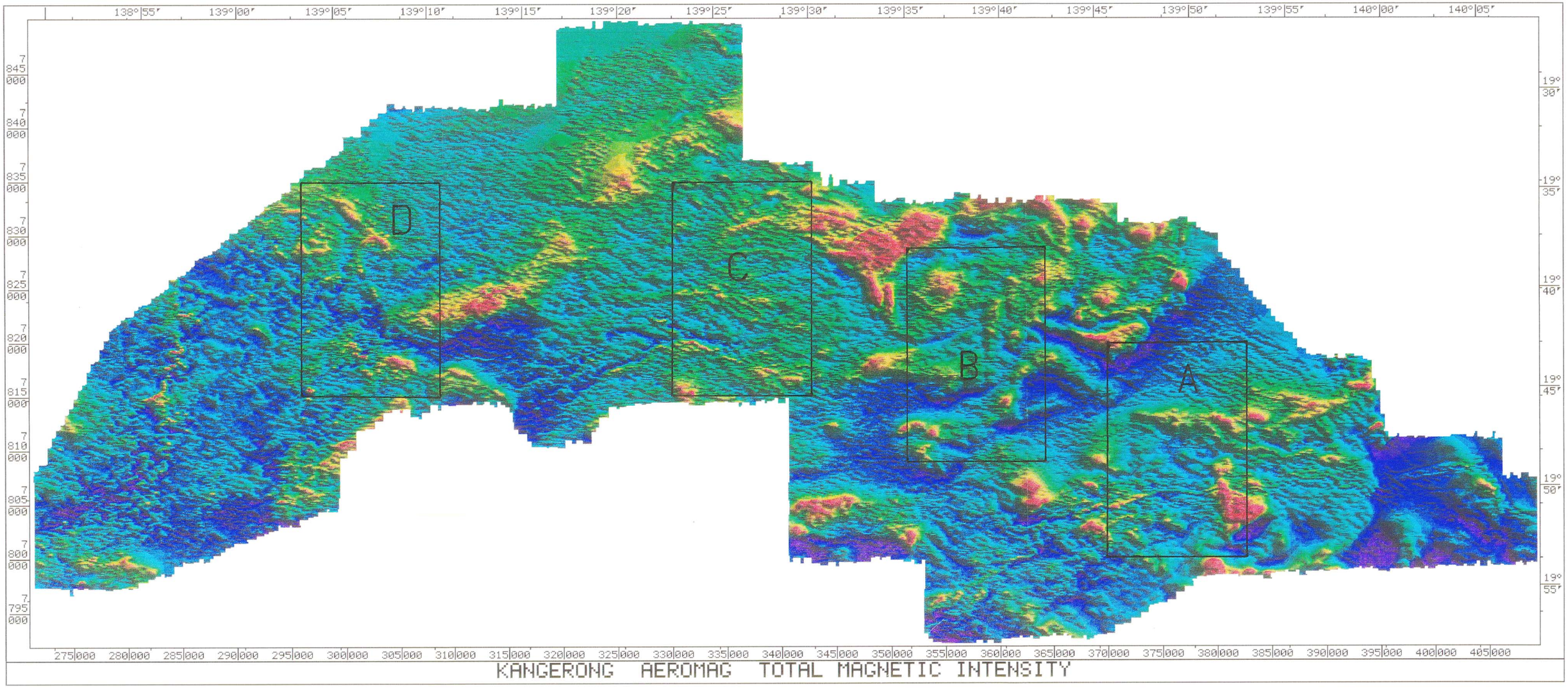
138°55′
139°00′
139°05′
139°10′
139°15′
139°20′
139°25′
139°30′
139°35′
139°40′
139°45′
139°50′
139°55′
140°00′
140°05′
7 845 000
7 840 000
7 835 000
7 830 000
7 825 000
7 820 000
7 815 000
7 810 000
7 805 000
7 800 000
7 795 000
19° 30′
19° 35′
19° 40′
19° 45′
19° 50′
19° 55′
D
C
B
A
275000 280000 285000 290000 295000 300000 305000 310000 315000 320000 325000 330000 335000 340000 345000 350000 355000 360000 365000 370000 375000 380000 385000 390000 395000 400000 405000
KANGERONG AEROMAG TOTAL MAGNETIC INTENSITY

Chapter 7

The Kangerong Dataset

7.1 Selection of Subsets

The entire Kangerong TMI image is shown on fig. 7.1 (foldout). Again it was convenient to use smaller subsets, and four were chosen arbitrarily as shown. Each subset is the same as the Miclere subset in terms of data quantity, but covers four times the area due to doubling of the flightline separation and of the gridding interval.
Compared to Miclere only a limited number of processes were applied to these subsets. Low-pass filters (Butterworth) with 600m cutoff; upward continuation of 100m, and the differencing method were applied to all, and the results compared. It turns out that the results and remarks applicable to areas 'A' and 'B' are the same, as are areas 'C' and 'D', so only the images, and remarks, for 'A' and 'C' are included.
TMI images for areas 'A' and 'C' are figs. 7.2 and 7.8 respectively.

7.2 Area 'A' Low-Pass Filtering

Butterworth low-pass filters were applied with cutoff wavelengths of 600 and 1000 metres (refer figs. 7.3 and 7.4). In the 600m filtered image, as in the TMI image, there is a clear arcuate feature tending roughly east-west at the 7805000 grid line. This feature is quite possibly a fault, and its resolution therefore important in the interpretation of the image. In fig. 7.4, however, this feature has all but disappeared. It must be concluded that a cutoff of 1000m gives unacceptable loss of resolution; yet this image still appears to contain significant basalt signal. Reduced separation of basalt and basement compared to Miclere would account for this.
Based on those results a cutoff of 600m was considered optimum, rather than the 1000m for Miclere.

7.3 Area 'A' Upward Continuation

Upward continuation was similar to low-pass filtering, in that an upward movement of 100m was deemed more appropriate than the 180m selected as optimum for Miclere. The resulting image (fig. 7.5) closely resembles fig. 7.2, and both retain the basalt signal to a distracting degree.

fig. 7.2 Area 'A' Total Magnetic Intensity. Range 49350 to 50947 nT.

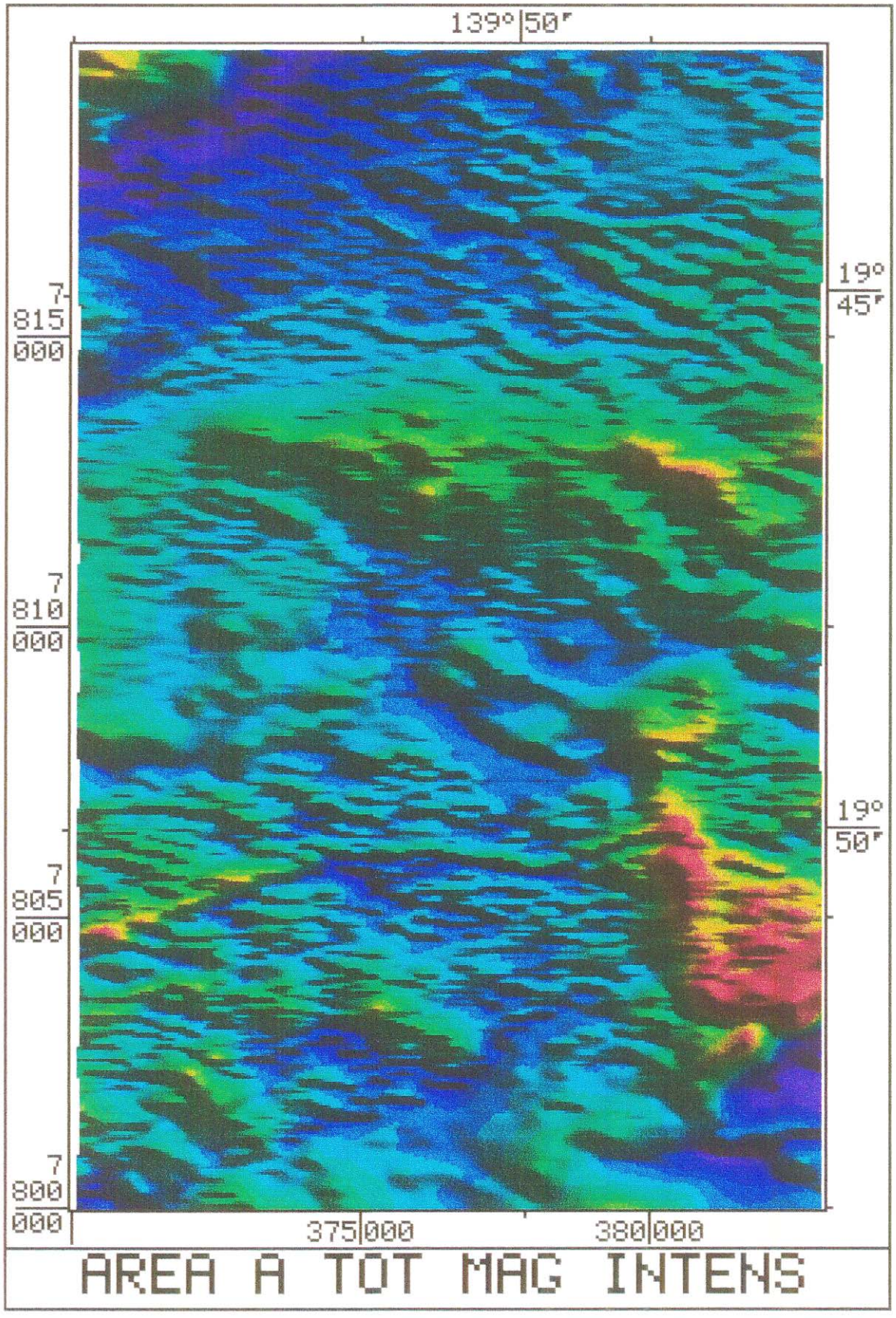

fig. 7.3 Area 'A' low-pass filtered: 2D Butterworth filter, 600m cutoff. Range 49369 to 50934 nT.

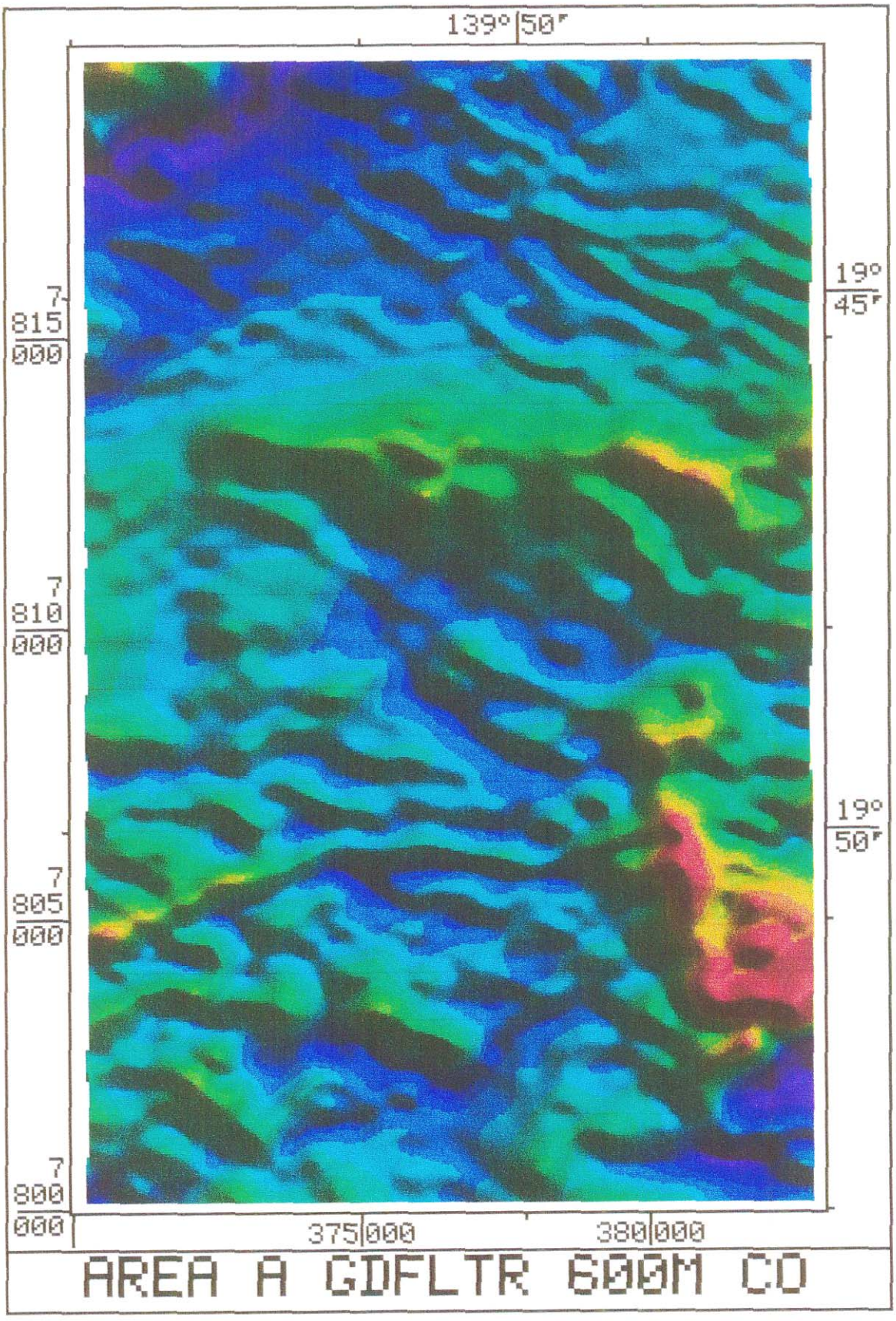

fig. 7.4 Area 'A' low-pass filtered: 2D Butterworth filter, 1000m cutoff. Range 49336 to 50929 nT.

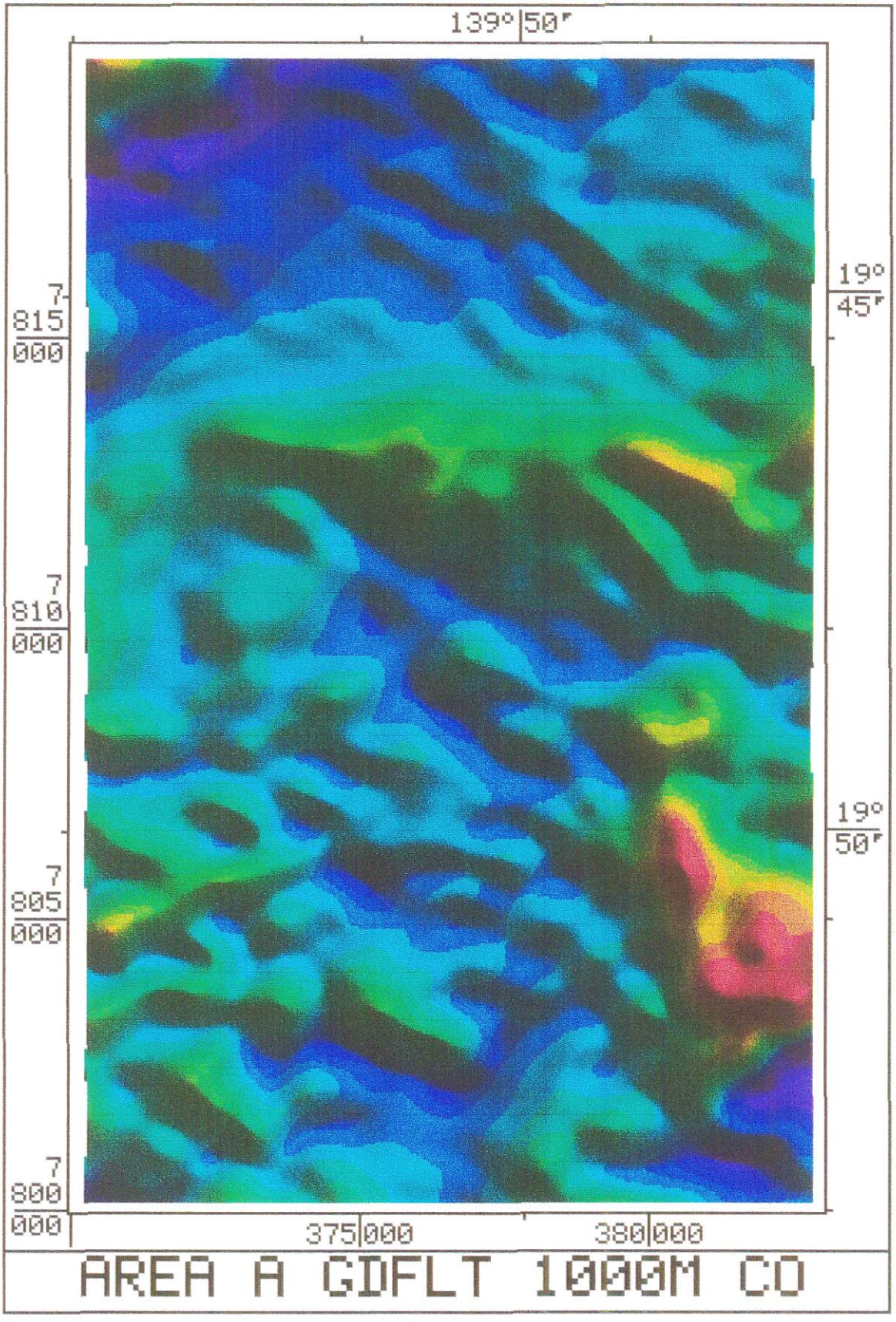

fig. 7.5 Area 'A' upward continuation by 100m. Range 49468 to 50764 nT.

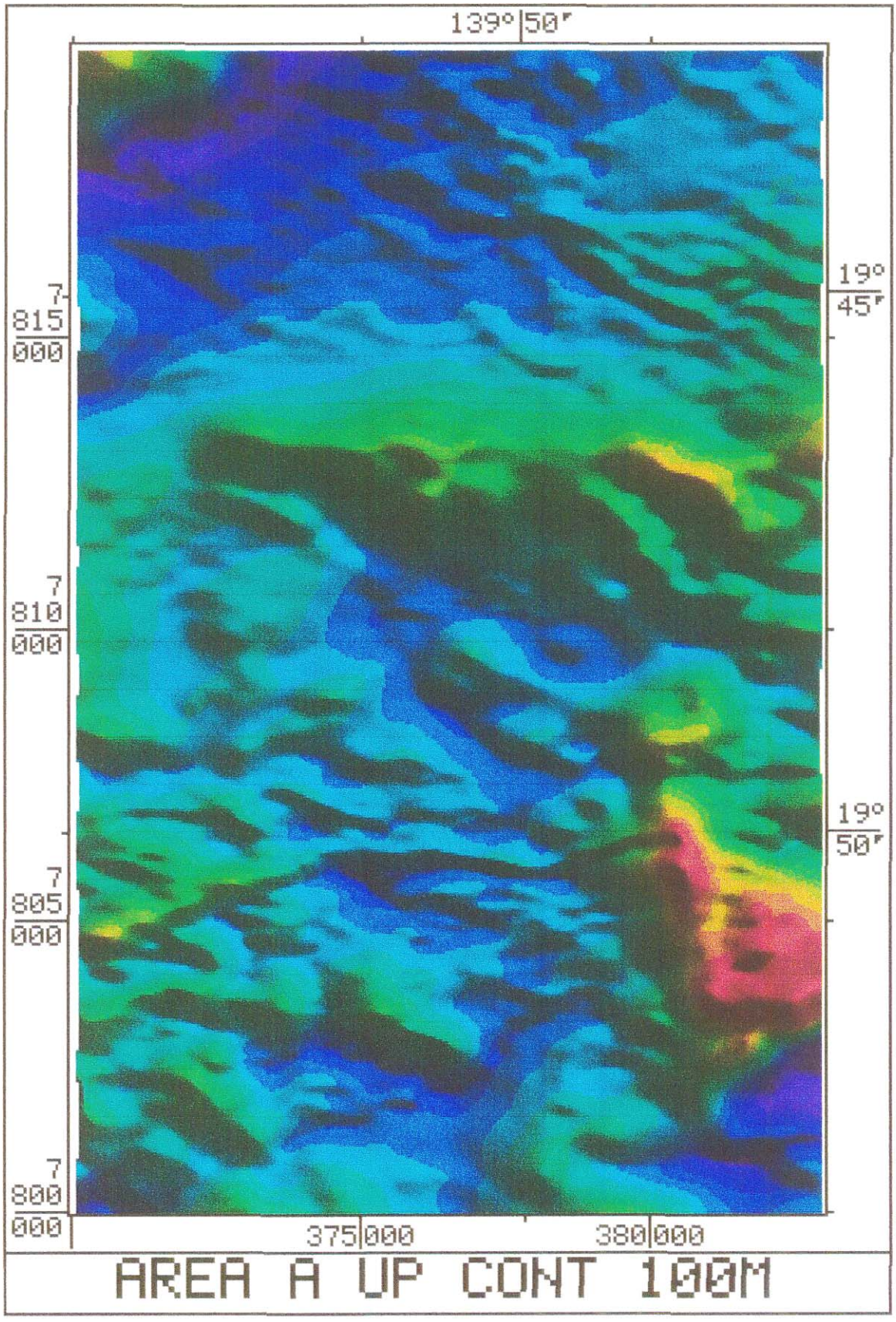

fig. 7.6 Area 'A': differencing process. Downward continuation by 10m, multiplied by 0.83, then subtracted from the TMI data. Range 8399 to 8648 nT.

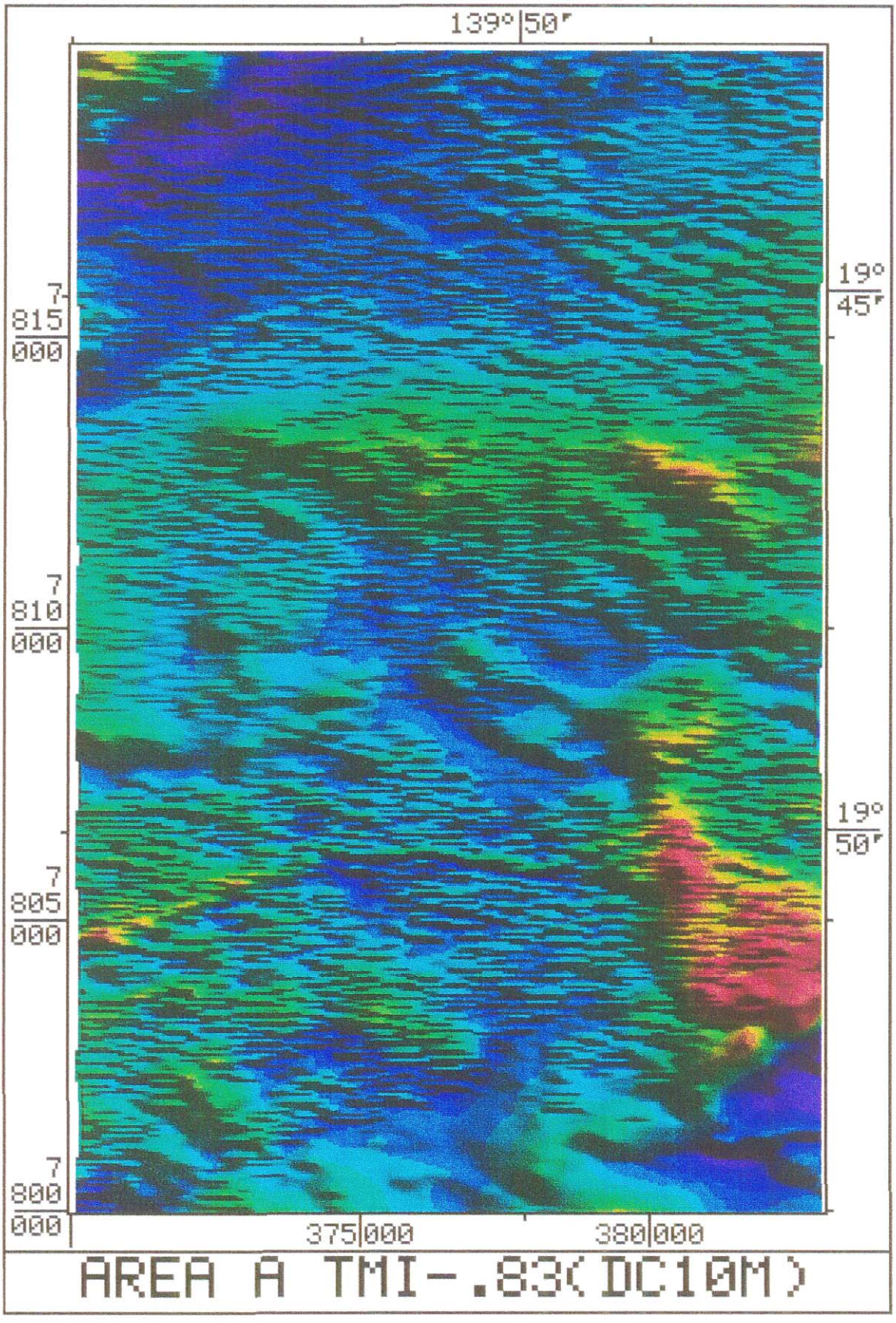

fig. 7.7 Previous image (fig. 7.6) with a Butterworth low-pass filter of 500m cutoff applied as a 'cleanup filter' to remove high frequency noise.

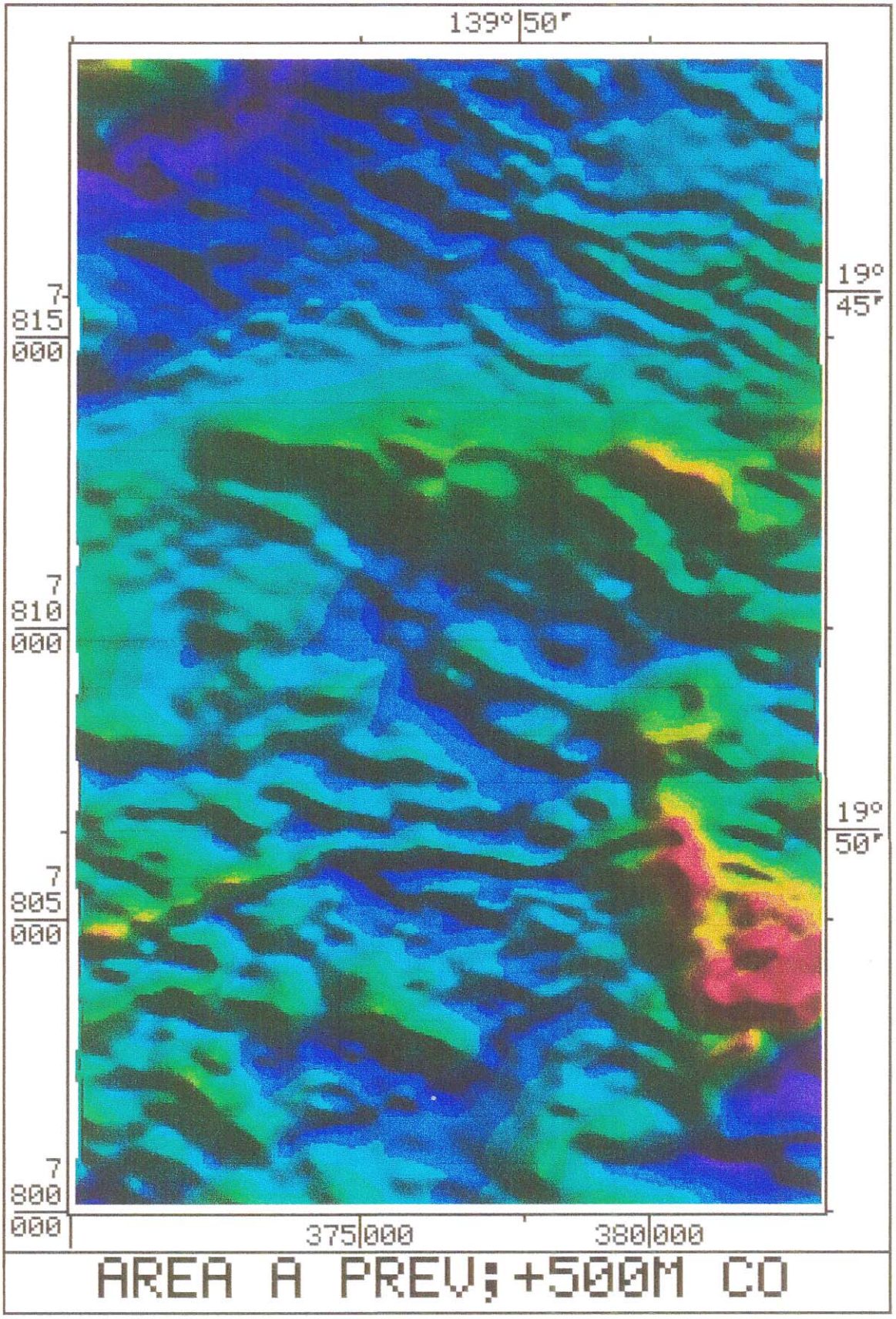

7.4 Application of Differencing

Differencing was tried using both 10m and 20m downward continuation, and a variety of subtraction coefficients. The best results were obtained with a 10m continuation and a subtraction coefficient of 0.83. This gave just marginally superior results to the coefficient of 0.9 used for Miclere. The result of this process is fig. 7.6. There is pronounced east-west lineation, or high-frequency signal, produced as a result of the downward continuation emphasizing the small high-frequency variations along the North-South flightlines. (In the Miclere dataset the flightlines were East-West, and this signal was evidenced by a North-South lineation). These high-frequency variations originate with the collection of the data, in which sampling is done every 7 metres along the flight path but each 400 metres, i.e., flightline spacing, lateral to the path. This high frequency signal necessitates a clean-up filter, and one with a cutoff equal to or greater than the flightline spacing is needed. In this case 500m was required for a presentable result. The final outcome, fig. 7.7, is virtually indistinguishable from figs. 7.3 and 7.5, the 600m low-pass and the 100m upward continued images, respectively.

7.5 Area 'C' Low-Pass Filtering

A Butterworth filter with 600m cutoff was applied with fig. 7.9 showing the result. As with area 'A' , this value of cutoff leaves much of the basalt signal, giving an image difficult to interpret, although free of the highest frequencies so evident in the original (fig. 7.8). Again, to use a longer cutoff would eliminate the subtle structural features.

7.6 Area 'C' Upward Continuation

An upward continuation of 100m was applied to 'C' with fig.7.10 the result. As with 'A' there is almost no discernable difference between the images from 600m low-pass filtering, and 100m upward continuation.

7.7 Area 'C' Differencing

Differencing was applied using the Miclere formula of 10m downward continuation and a subtraction coefficient of 0.9 . The unfiltered result is shown in fig. 7.11, and is interesting because there are several small 'highs' visible through the high frequency noise, which do not appear on the low-pass filtered image, or appear with reduced intensity. A cleanup

fig. 7.8 Area 'C' Total Magnetic Intensity. Range 49431 to 50518 nT

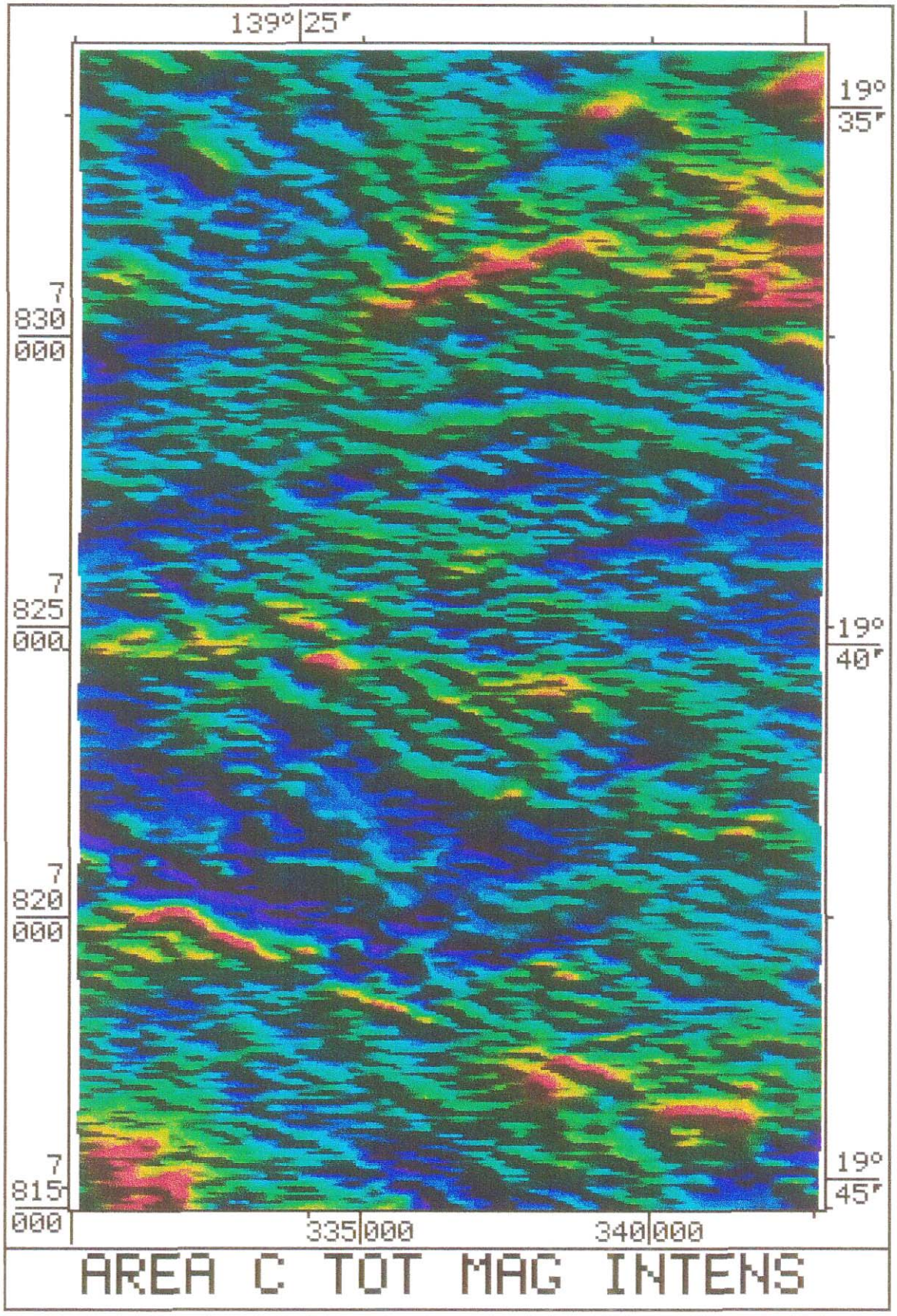

fig. 7.9 Area 'C' low-pass filtered: 2D Butterworth filter, 600m cutoff. Range 49588 to 50499 nT.

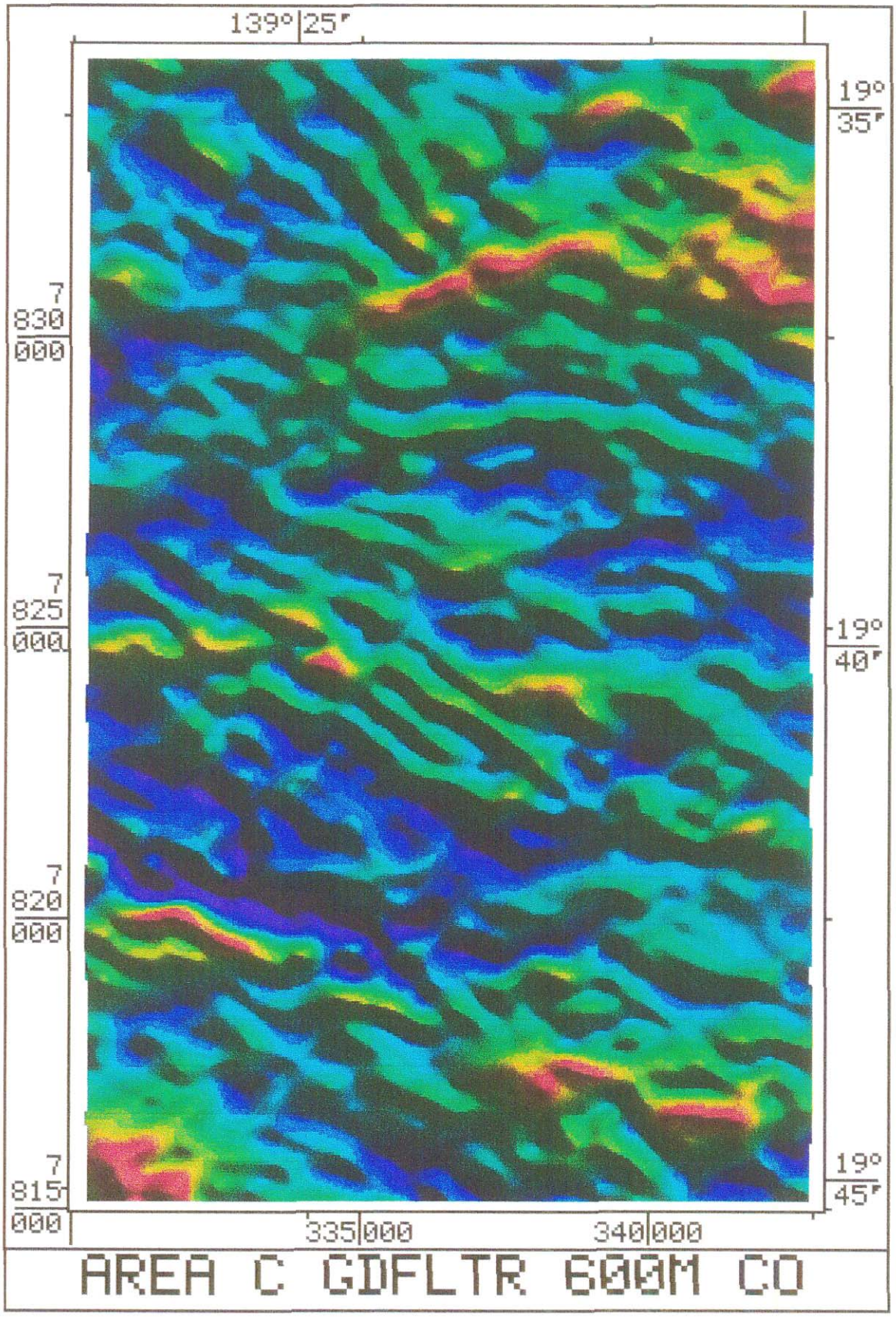

fig.7.10 Area 'C' upward continuation by 100m. Range 49752 to 50373 nT.

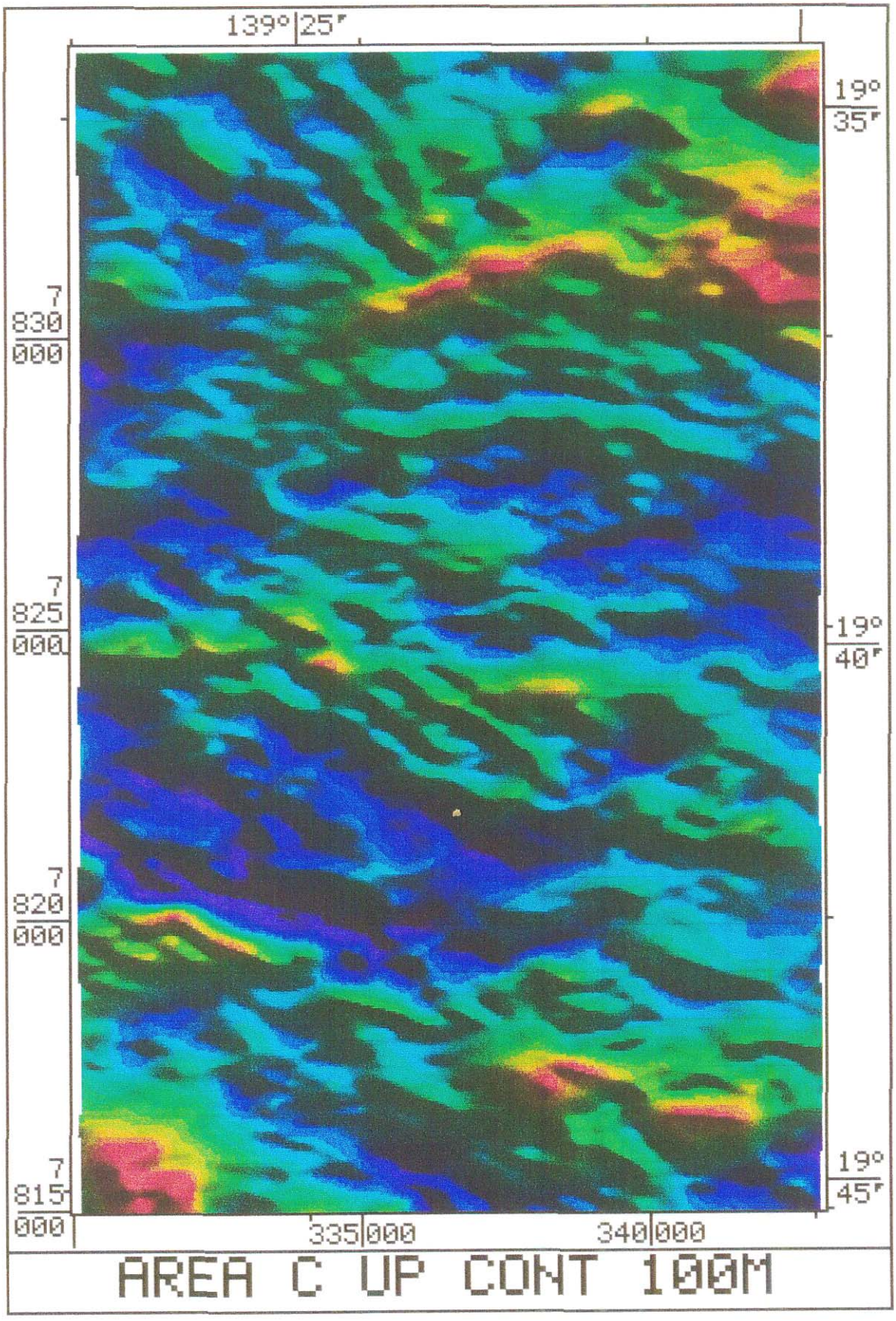

fig. 7.11 Area 'C': differencing process. Downward continuation by 10m, multiplied by 0.9, then subtracted from the TMI data. Range 4814 to 5077 nT.

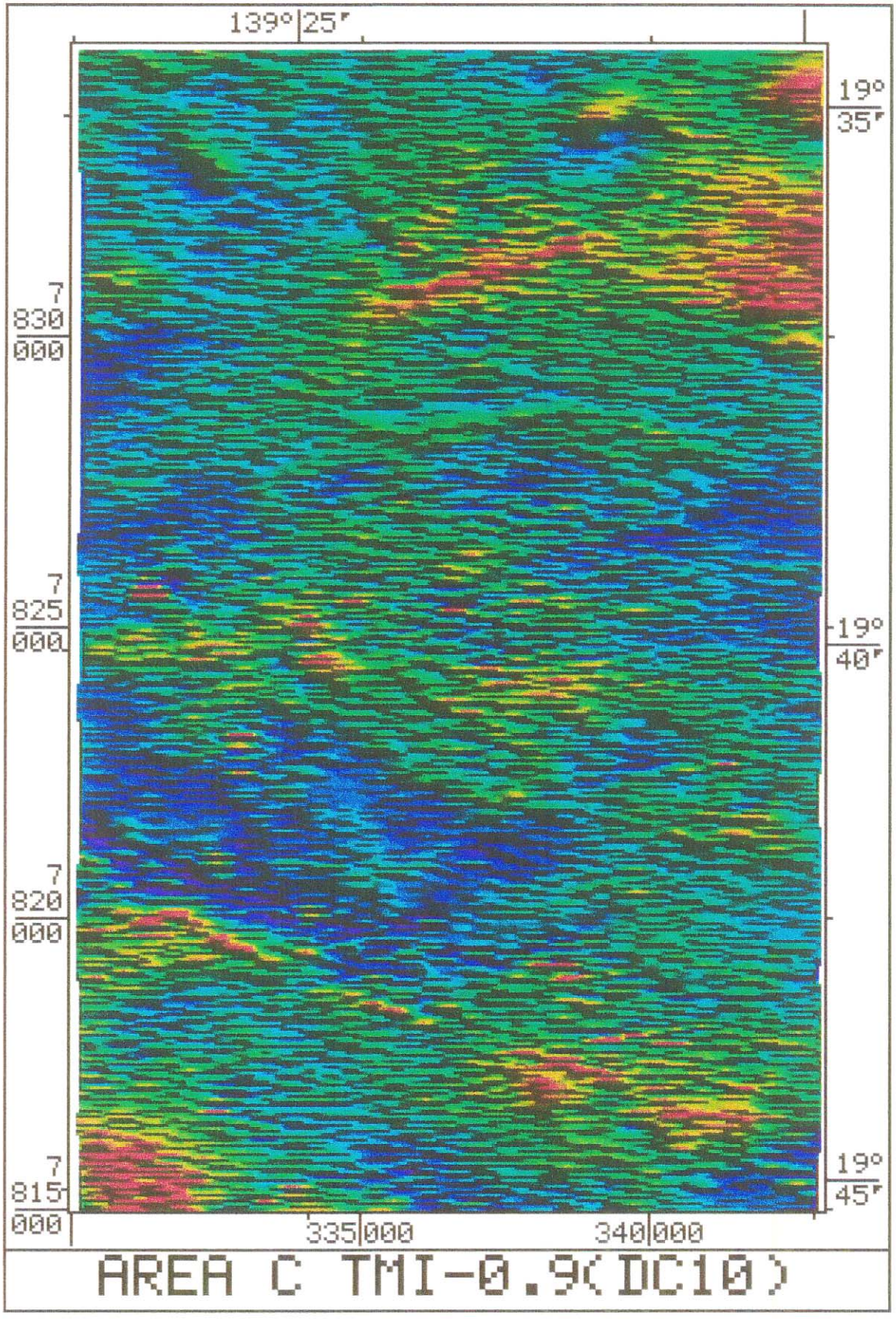

fig. 7.12 Previous image (fig. 7.11) with a Butterworth low-pass filter of 250m cutoff applied to reduce high frequency noise.

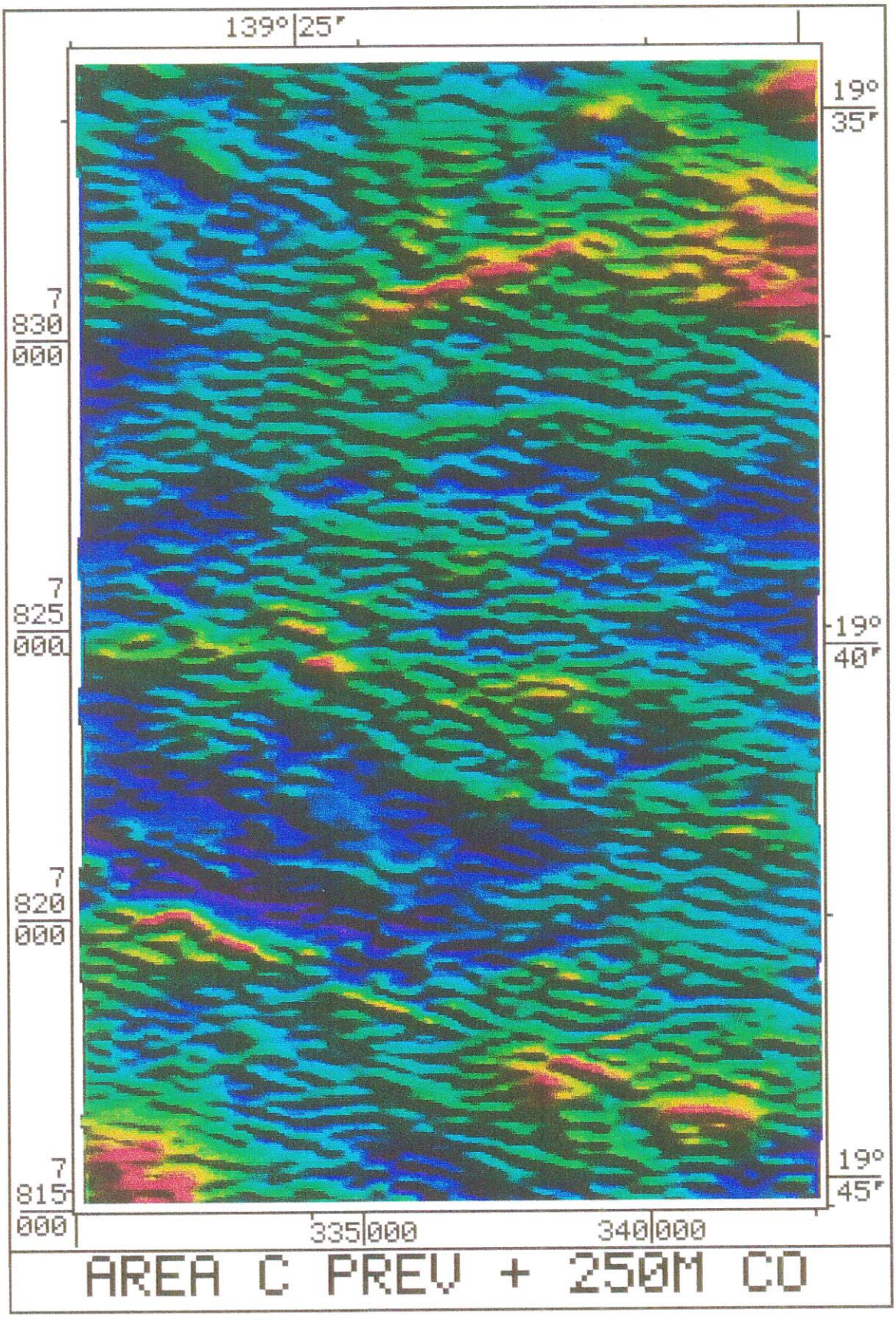

filter of any reasonable cutoff smooths off these highs, however, as is shown in fig. 7.12. Here a cutoff of 250m was used as a cleanup, and it was clearly inadequate in that task, yet it has rendered inconspicuous these small highs.

This raised the question as to whether these highs represented geological information or just noise. This will be discussed in detail in the next chapter, but it is worth noting that these ephemeral highs are visible (in most instances) in the original TMI image (fig. 7.8) and in the first vertical derivative image (not included). This suggests that they are real and not artifacts.

Chapter 8

Discussion

It was hoped that the process of differencing would prove as useful on the Kangerong data as it had on Miclere, but clearly this has not been so. It would appear to be no worse than other filters and processes, but more was expected. The performance of this process requires scrutiny.

If we leave for later the validity of the process itself, we may first compare the two datasets used in this project. They differ in that Kangerong has 400m flightline spacing, double that of Miclere. This is appropriate in that the model of a potential gold deposit is based on the nearby Mount Leyshon, a diatreme 1500 metres in diameter (ref. Paull *et al*, 1990). In contrast, according to in-company documents there were a number of possible models considered for possible gold deposition in the Miclere area, including the Mount Leyshon type but also hydrothermal alteration zones/structurally controlled deposits of smaller extent, necessitating the closer flightlines.

The flightline separation limits the resolution available, both in extent and also in depth. The latter is the source of a problem, for anecdotal evidence suggests much reduced separation of the basalt and the underlying source rocks in the Kangerong area. This view is supported by the effects of filtering done in this project, where structural information was lost if the basalt signal was largely removed. This indicates a low degree of separation. Fig. 6.4 can indicate the nature of the problem. If the basalt (noise source) and signal source rocks are closer, the 'signal' and 'noise' curves overlap to a greater extent, and the effectiveness of all three illustrated processes is reduced. Differencing should still offer an advantage, but it may be difficult to discern.

A possible factor is that there may not be any targets of suitable size and properties to show the differencing process to advantage. Differencing was applied to two different subsets of the Miclere area before the process found - and resolved - the basalt plugs. When re-examining the earlier subsets, the reason seems clear: there was nothing there to resolve! If this is the case for the subsets in Kangerong, the verdict on the process is still open.

So is the process of differencing still valid, and more importantly, of use? There are two positives to come from the Kangerong dataset. The first is based on the observation that the differencing images with 500 metre cutoff cleanup filter were indistinguishable from

the low-pass filtered images with a 600 metre cutoff. The 100 metre difference is slight, but does indicate that the differencing process has done something. (By comparison, with Miclere a 300 metre cleanup was used, for an image comparable to,or better than, a low-pass filter with 800 metre cutoff).

The second positive is the small 'highs' in the unfiltered differencing image (fig. 7.11). Their correspondence to similar features on both the TMI and first vertical derivative images rules against processing artifacts. Without resolving them more clearly it cannot be positively said that they are not some form of acquisition noise, but circumstantial evidence is in favour of them being real features, in that they occur in the general vicinity of other, more substantial highs, and are not randomly distributed.

Chapter 9

Conclusions

Although differencing is not an unqualified success, the fact that it can be useful in some situations is enough to merit attention and it deserves further investigation on that score. Perhaps equally important is the way it has been shown to be equivalent to a combination of TMI and first vertical derivatives, for this raises the question of combining TMI with other derivatives, or combining the results of other processes. The increasing speed of computing makes such experimentation very easy. The possibilities are interesting.

References

Blair, D. P. and Spathis, A. T. (1980). 'Some aspects of digital filtering'. Technical Report No. 118, C.S.I.R.O. Division of Applied Geomechanics, 30pp.

Kuo, F. F. (1962). 'Network analysis and synthesis'. John Wiley, New York. p339

Mudge, S. T. (1991).'New developments in resolving detail in aeromagnetic data'. *Exploration Geophysics,* 22, pp 277 - 284.

Paull, P. L., Hodkinson, I. P., Morrison, G. W., and Teale, G. S. (1990). 'Mount Leyshon Gold Deposit' in *Geology of the Mineral Deposits of Australia and Papua New Guinea* (Ed. F. E. Hughes). The Australasian Institute of Mining and Metallurgy: Melbourne. pp1471 - 1481.

Rajagopalan, S. (1987). The use of 'Automatic Gain Control' to display vertical magnetic gradient data. *Exploration Geophysics,* 18, pp 166 - 169.

Rajagopalan, S., and Milligan, P. (1995). 'Image enhancement of aeromagnetic data using Automatic Gain Control'. *Exploration Geophysics*, 25, pp 173 - 178.

Stanley, J. M., Sertsrivanit, S., and Clark, P. J. (1992). 'Magnetic exploration beneath a near-surface magnetic noise source'. *Exploration Geophysics*, 23, pp 323 - 326.

Appendix A

Low-Pass (Butterworth) Filtered Images

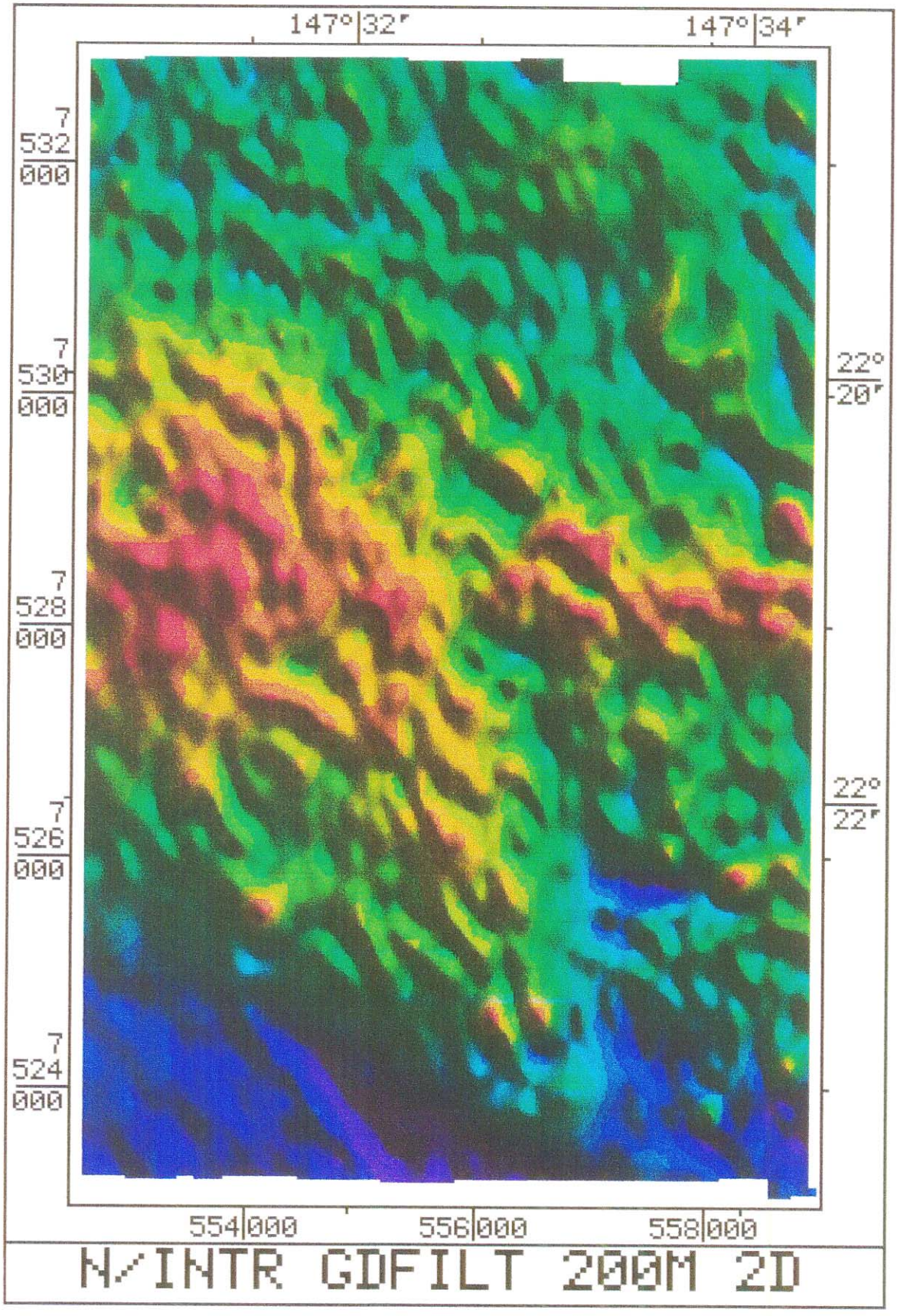
147° 32'
147° 34'
7 532 000
7 530 000
7 528 000
7 526 000
7 524 000
22° 20'
22° 22'
554 000
556 000
558 000
N/INTR GDFILT 200M 2D

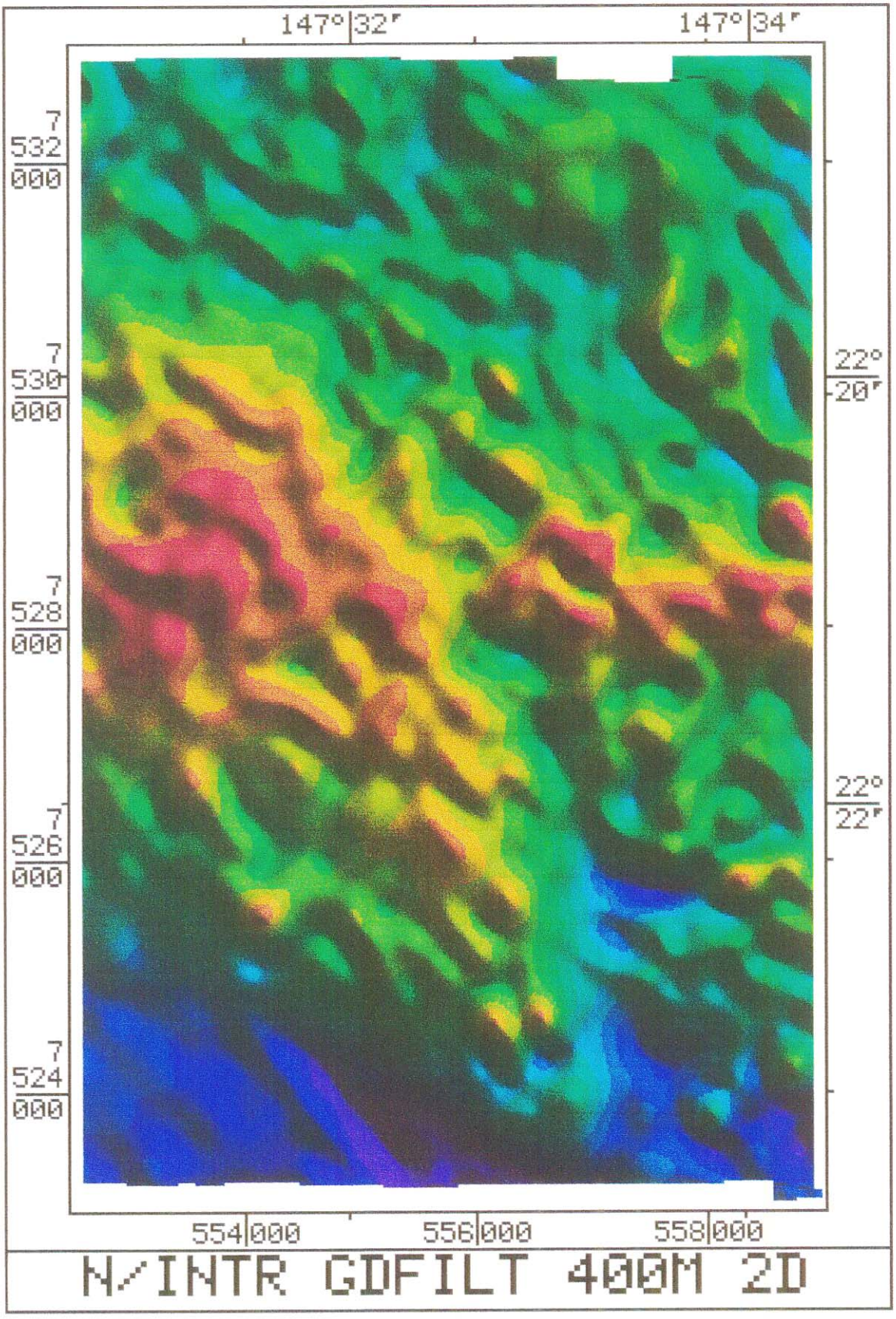
147° 32'
147° 34'
7 532 000
7 530 000
7 528 000
7 526 000
7 524 000
22° 20'
22° 22'
554 000
556 000
558 000
N/INTR GDFILT 400M 2D

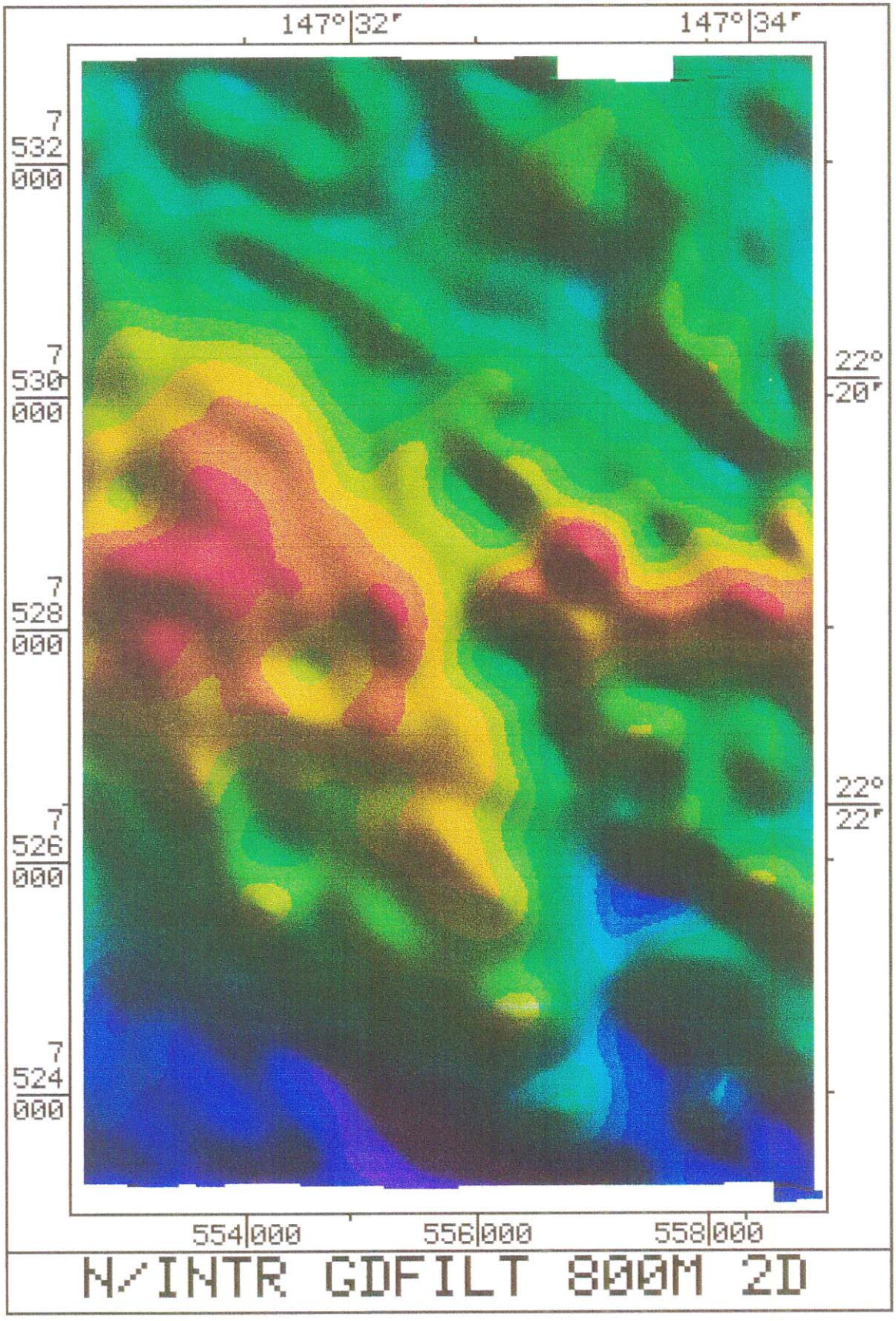
147° 32'
147° 34'
7532000
7530000
7528000
7526000
7524000
22° 20'
22° 22'
554000
556000
558000
N/INTR GDFILT 800M 2D

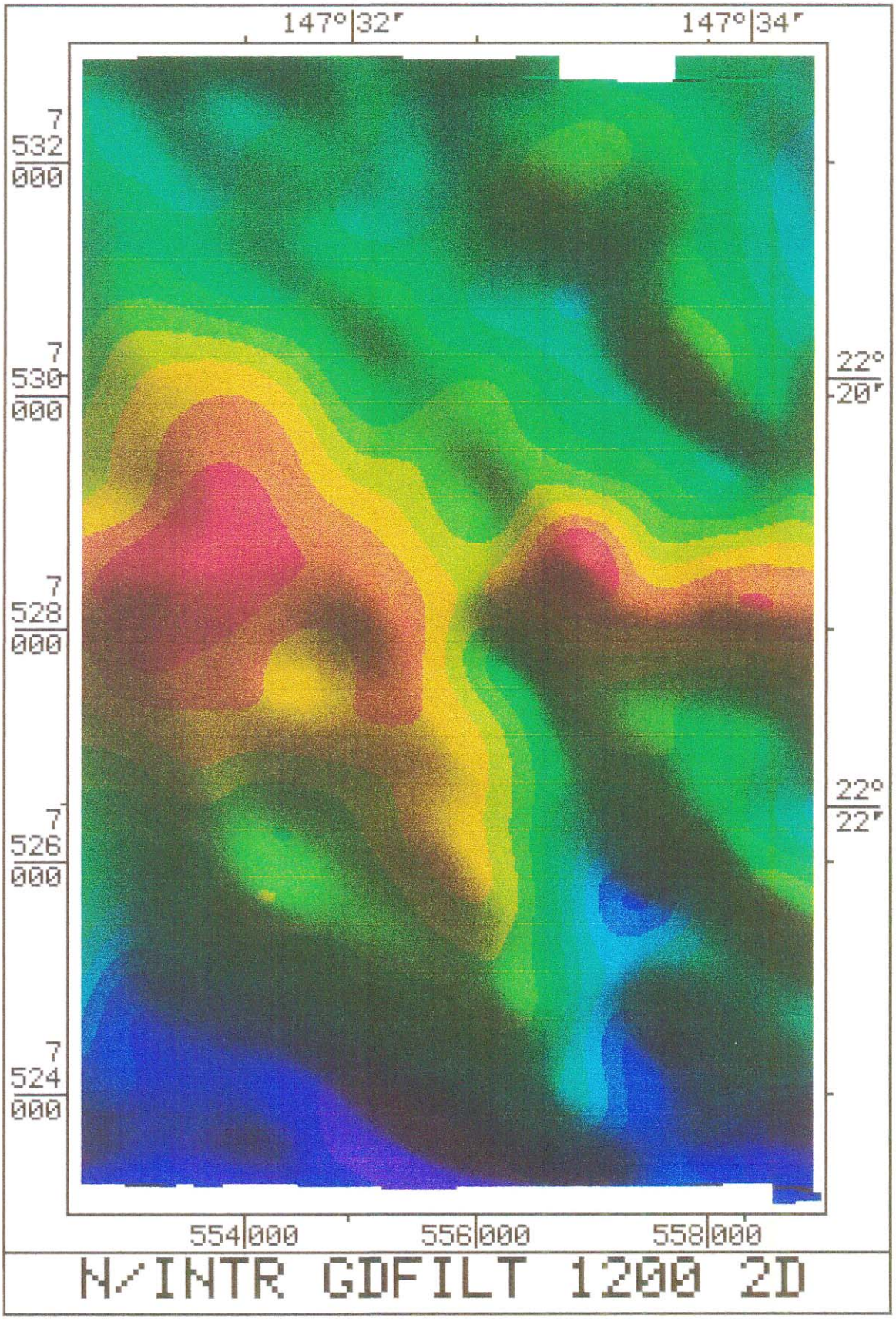
147° 32'
147° 34'
7 532 000
7 530 000
7 528 000
7 526 000
7 524 000
22° 20'
22° 22'
554 000
556 000
558 000
N/INTR GDFILT 1200 2D

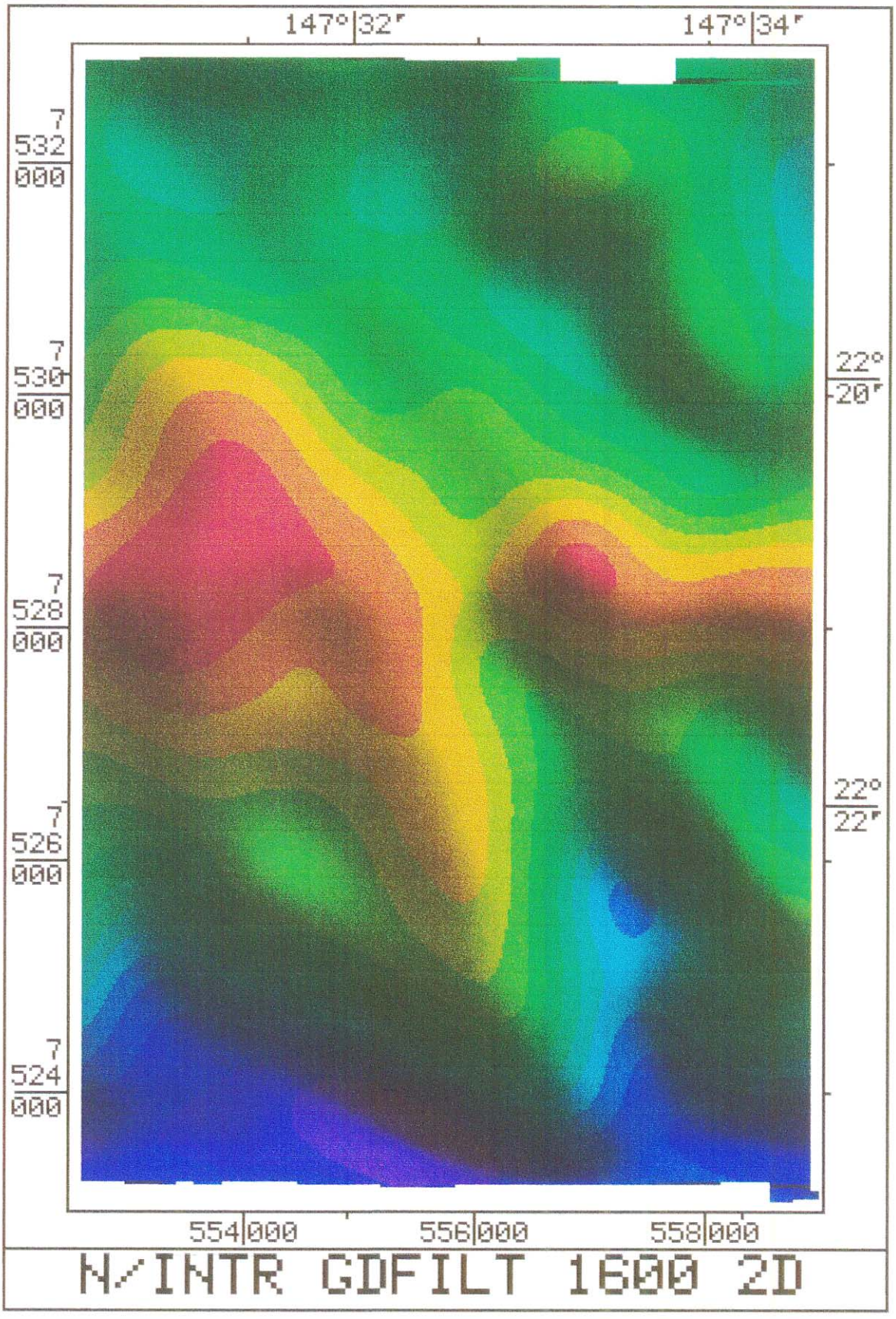
147°32'
147°34'
7532000
7530000
7528000
7526000
7524000
22°20'
22°22'
554000
556000
558000
N/INTR GDFILT 1600 2D

Appendix B

Averaging Window Filtered Images

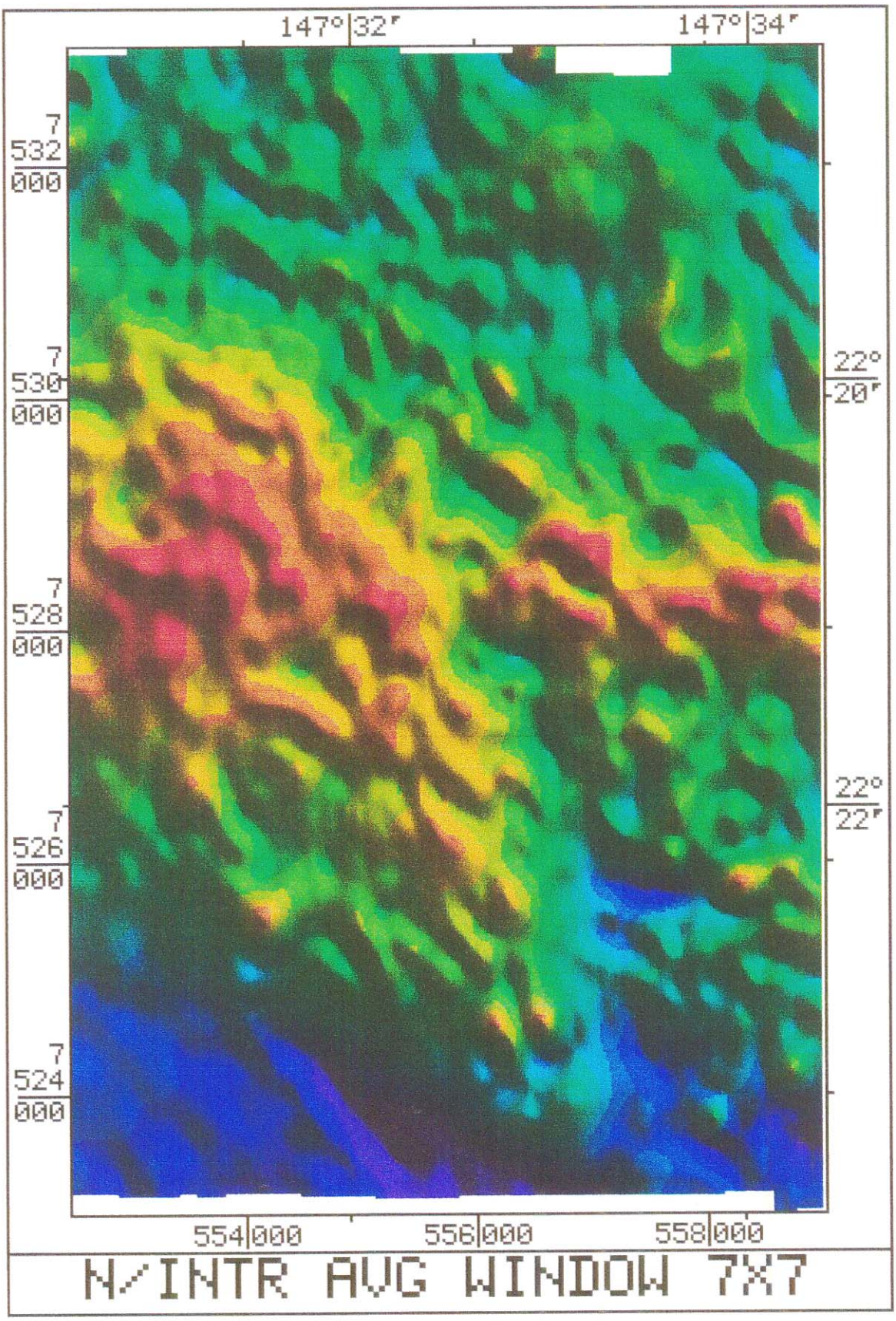
147° 32′
147° 34′
7 532 000
7 530 000
7 528 000
7 526 000
7 524 000
22° 20′
22° 22′
554 000
556 000
558 000
N/INTR AVG WINDOW 7X7

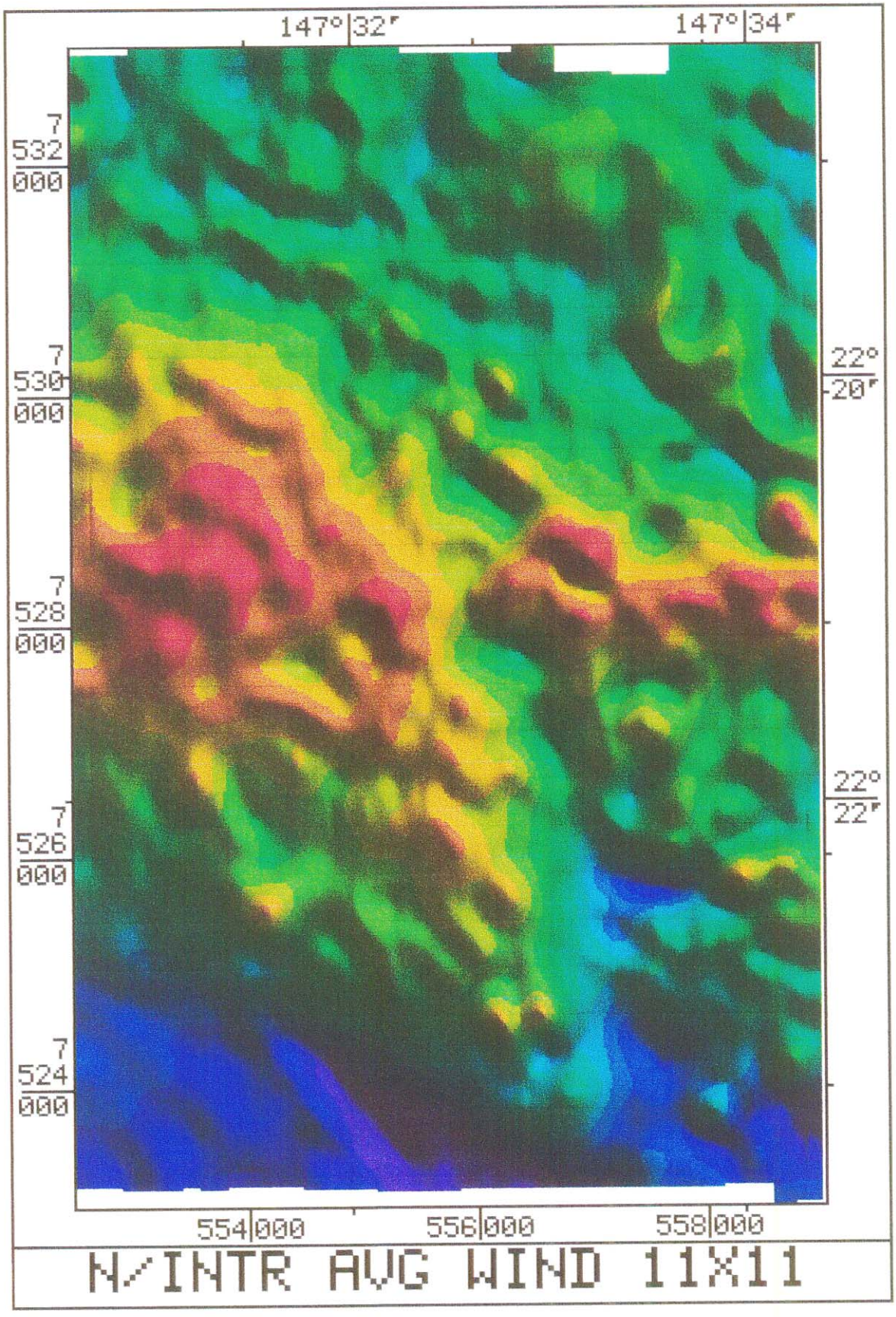
147° 32'
147° 34'
7 532 000
7 530 000
7 528 000
7 526 000
7 524 000
22° 20'
22° 22'
554 000
556 000
558 000
N/INTR AVG WIND 11X11

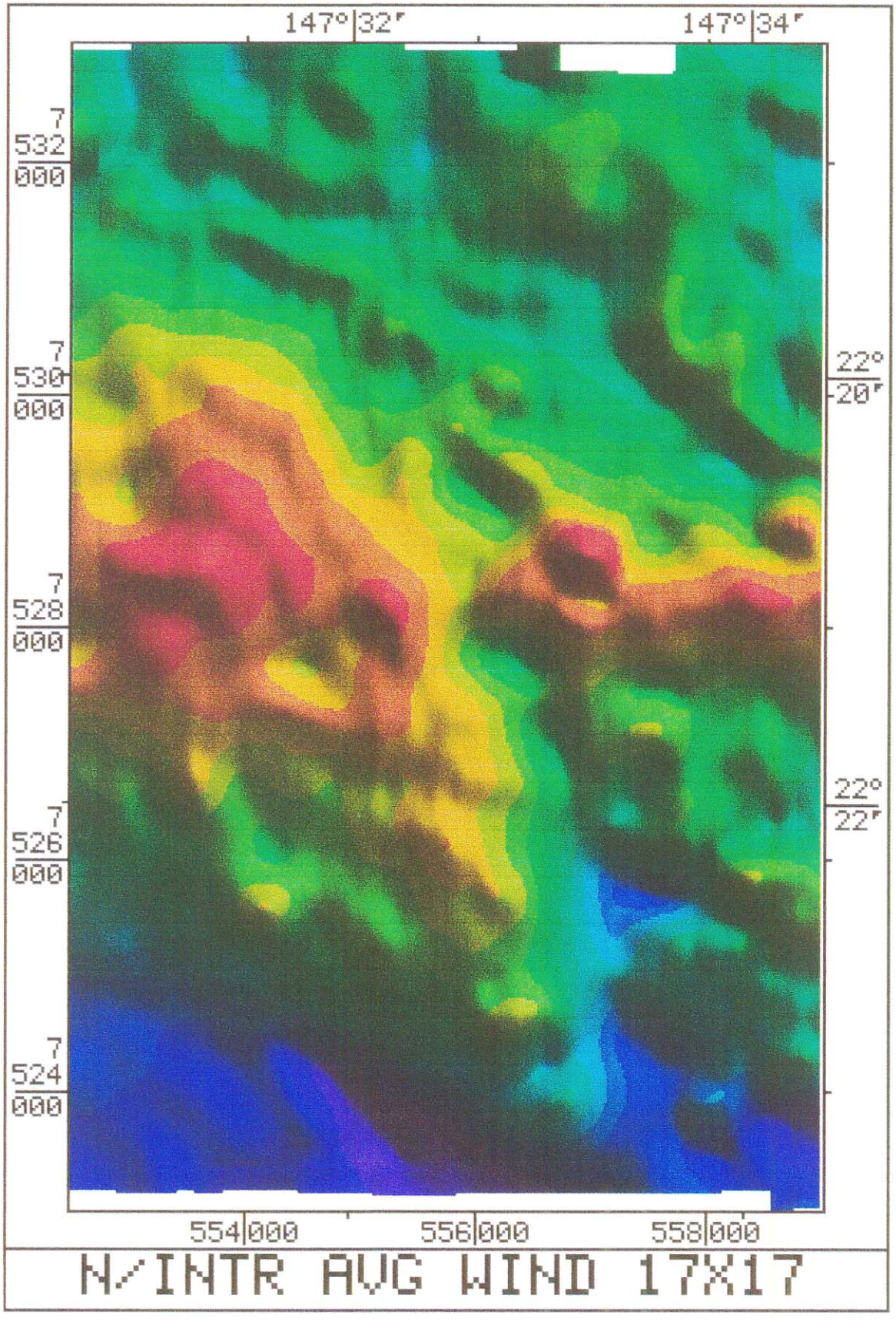
147° 32'
147° 34'
7 532 000
7 530 000
7 528 000
7 526 000
7 524 000
22° 20'
22° 22'
554 000
556 000
558 000
N/INTR AVG WIND 17X17

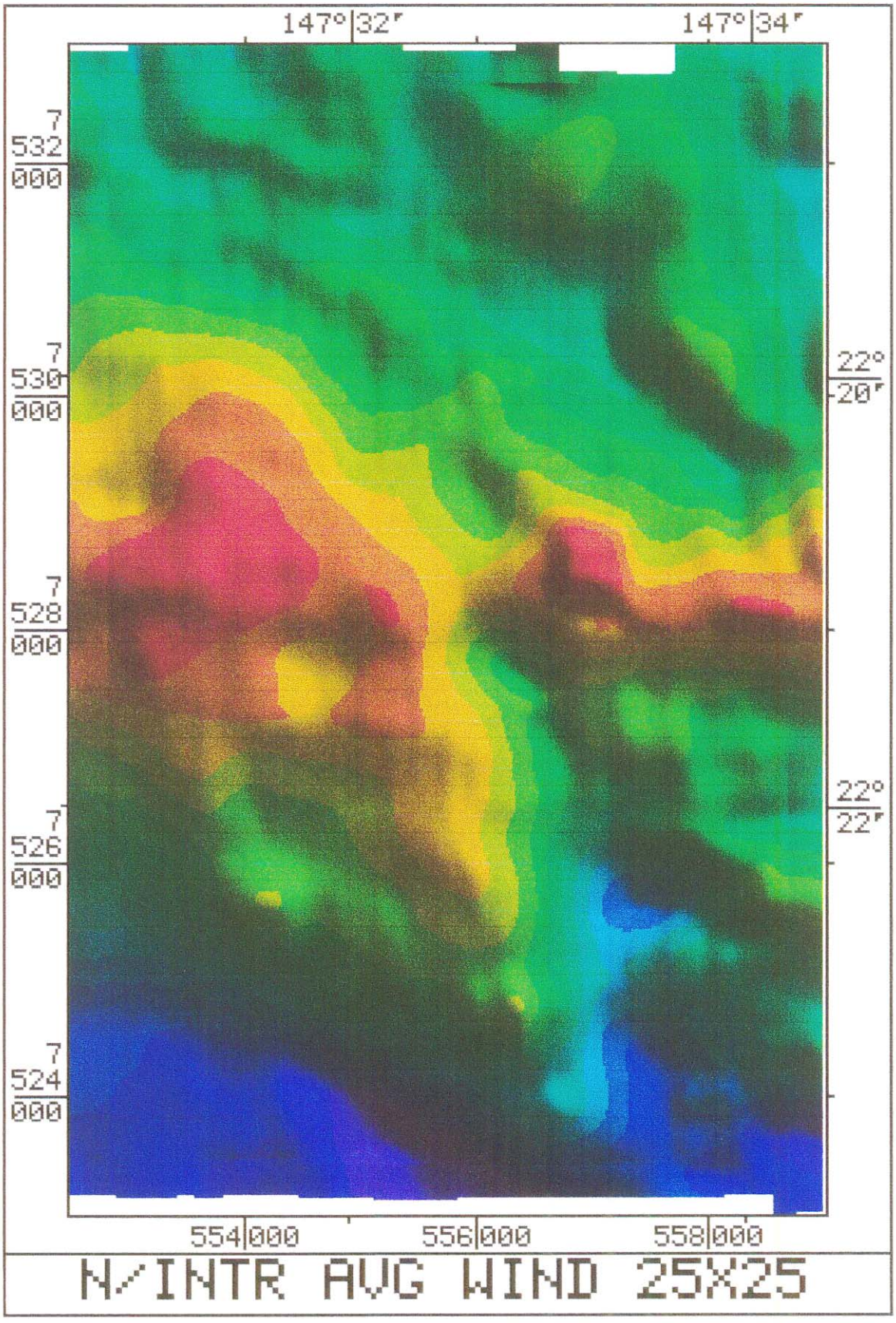
147° 32'
147° 34'
7 532 000
7 530 000
7 528 000
7 526 000
7 524 000
22° 20'
22° 22'
554 000
556 000
558 000
N/INTR AVG WIND 25X25

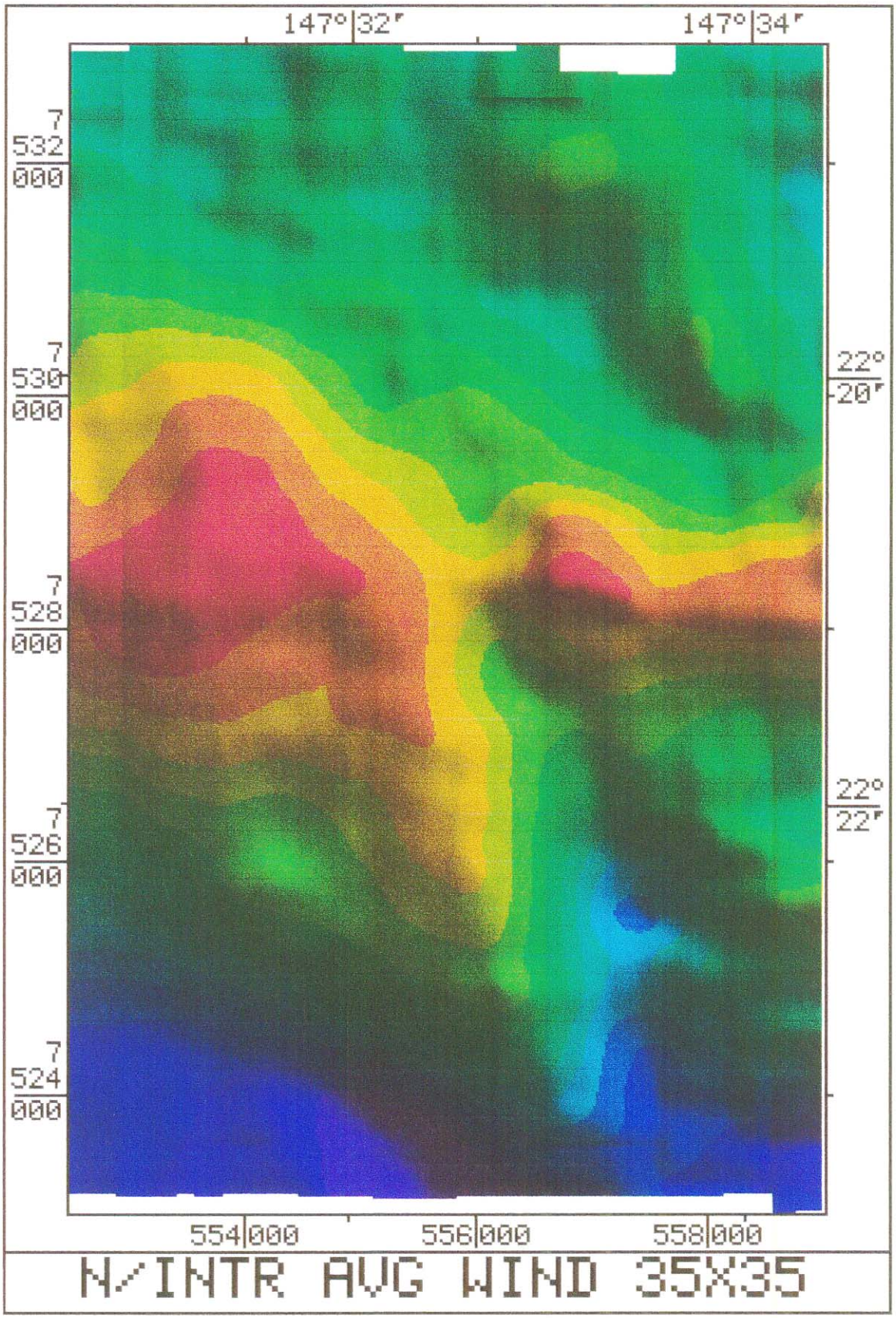
147°32′
147°34′
7532000
7530000
7528000
7526000
7524000
22°20′
22°22′
554000
556000
558000
N/INTR AVG WIND 35X35

Appendix C

Median Window Filtered Images

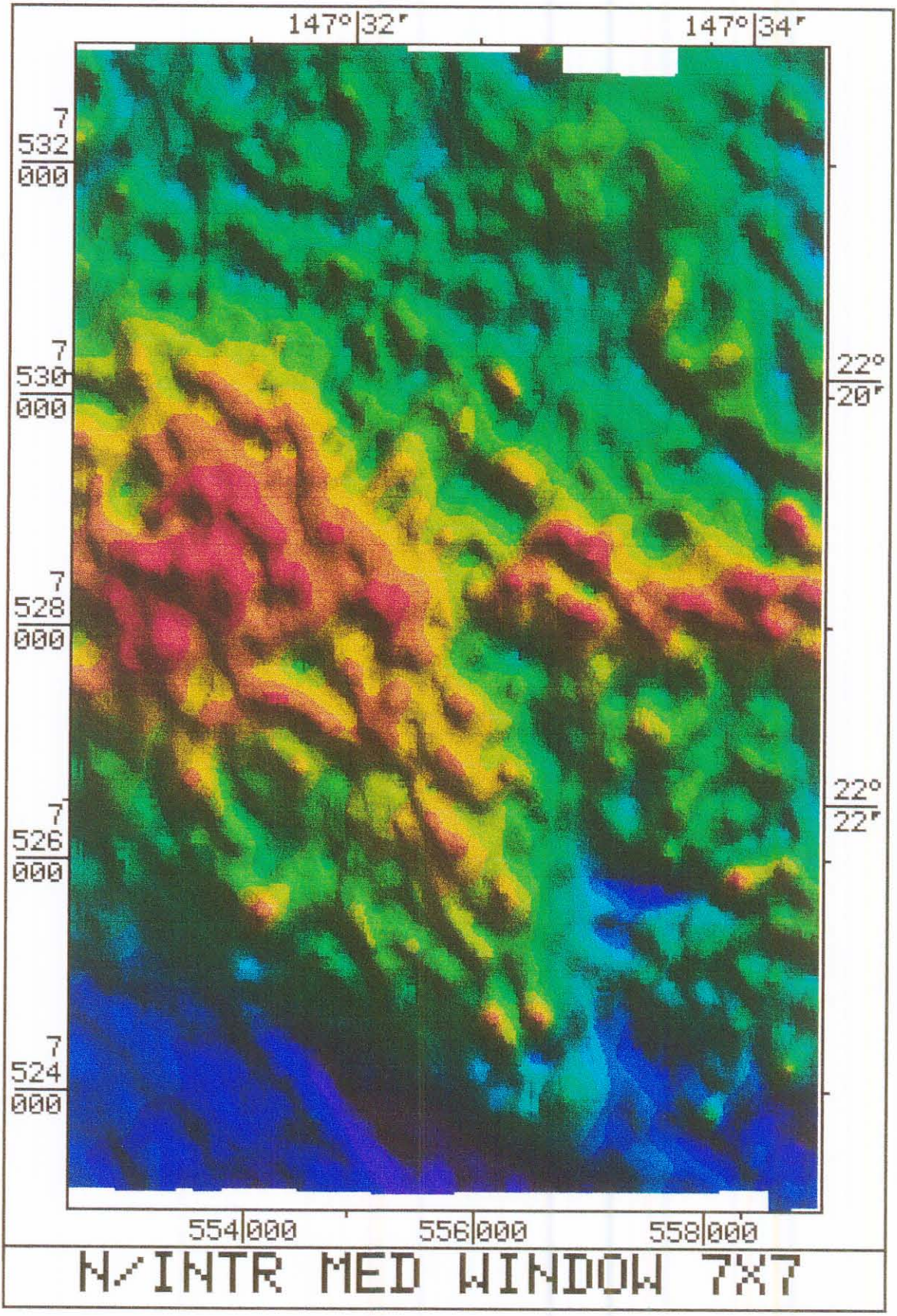
147° 32′
147° 34′
7 532 000
7 530 000
7 528 000
7 526 000
7 524 000
22° 20′
22° 22′
554 000
556 000
558 000
N/INTR MED WINDOW 7X7

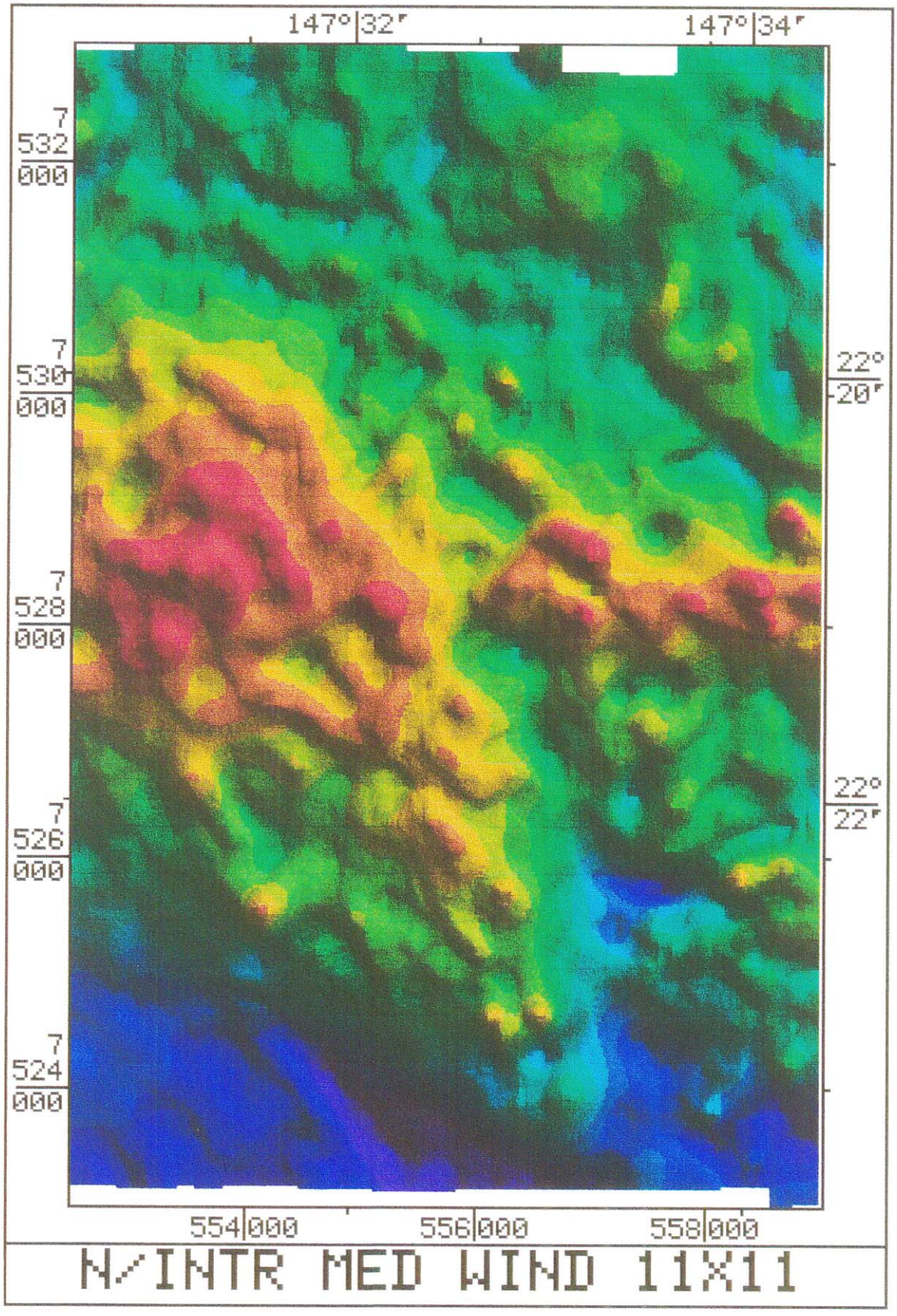
147°32'
147°34'
7532000
7530000
7528000
7526000
7524000
22°20'
22°22'
554000
556000
558000
N/INTR MED WIND 11X11

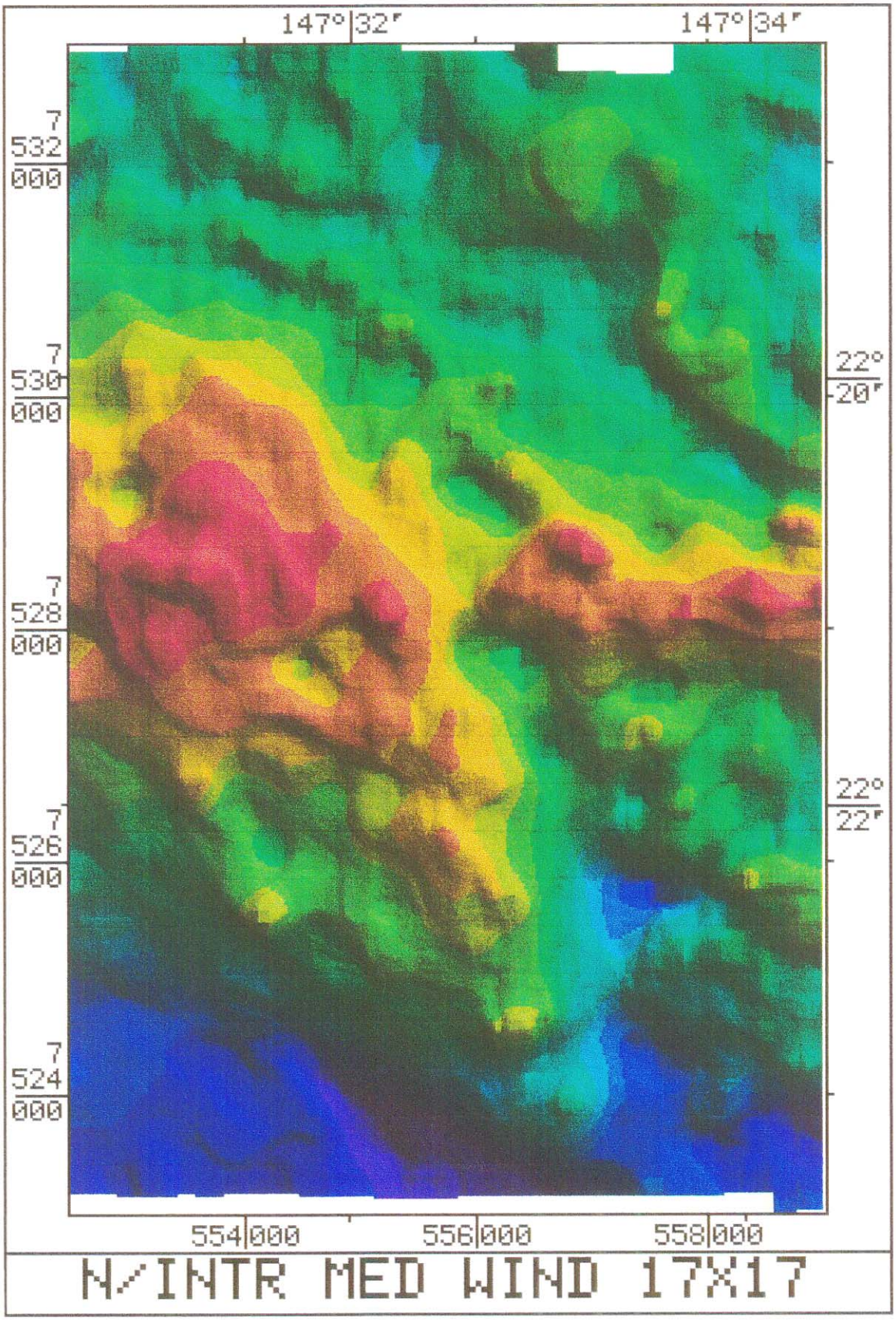
147° 32′
147° 34′
7 532 000
7 530 000
7 528 000
7 526 000
7 524 000
22° 20′
22° 22′
554 000
556 000
558 000
N/INTR MED WIND 17X17

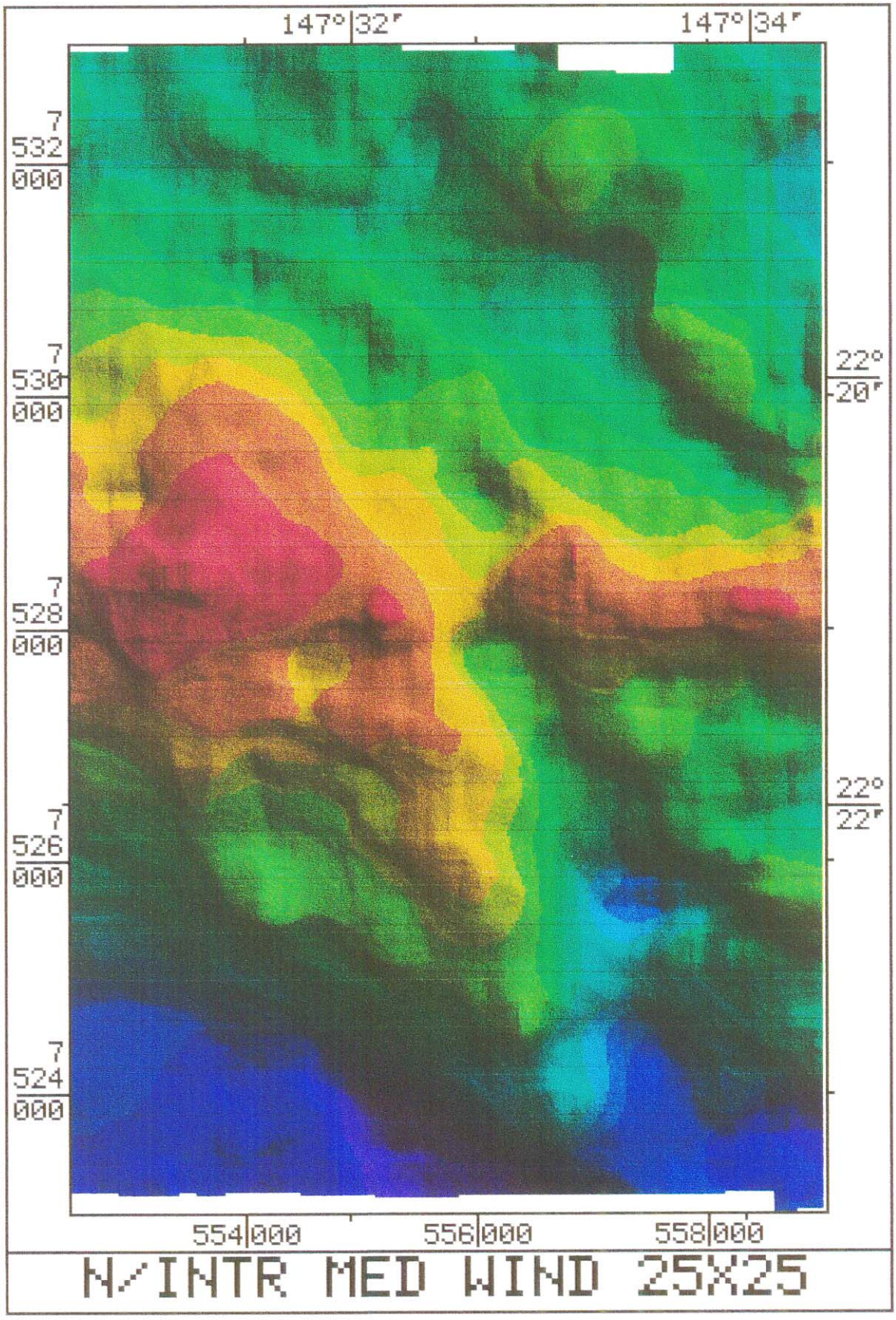
147° 32'
147° 34'
7532000
7530000
7528000
7526000
7524000
22° 20'
22° 22'
554000
556000
558000
N/INTR MED WIND 25X25

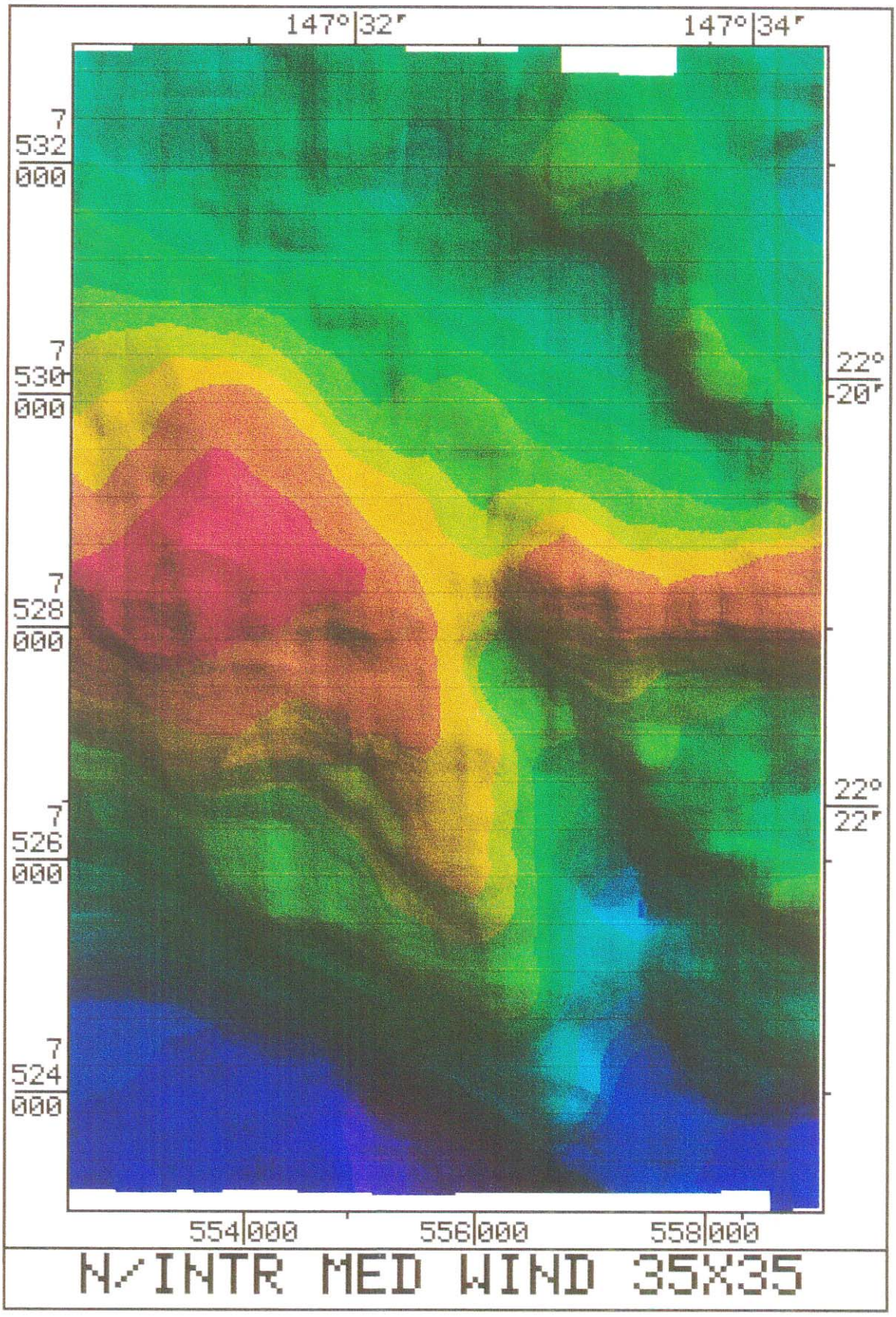
147° 32'
147° 34'
7 532 000
7 530 000
7 528 000
7 526 000
7 524 000
22° 20'
22° 22'
554 000
556 000
558 000
N/INTR MED WIND 35X35

Appendix D

Upward Continued Images

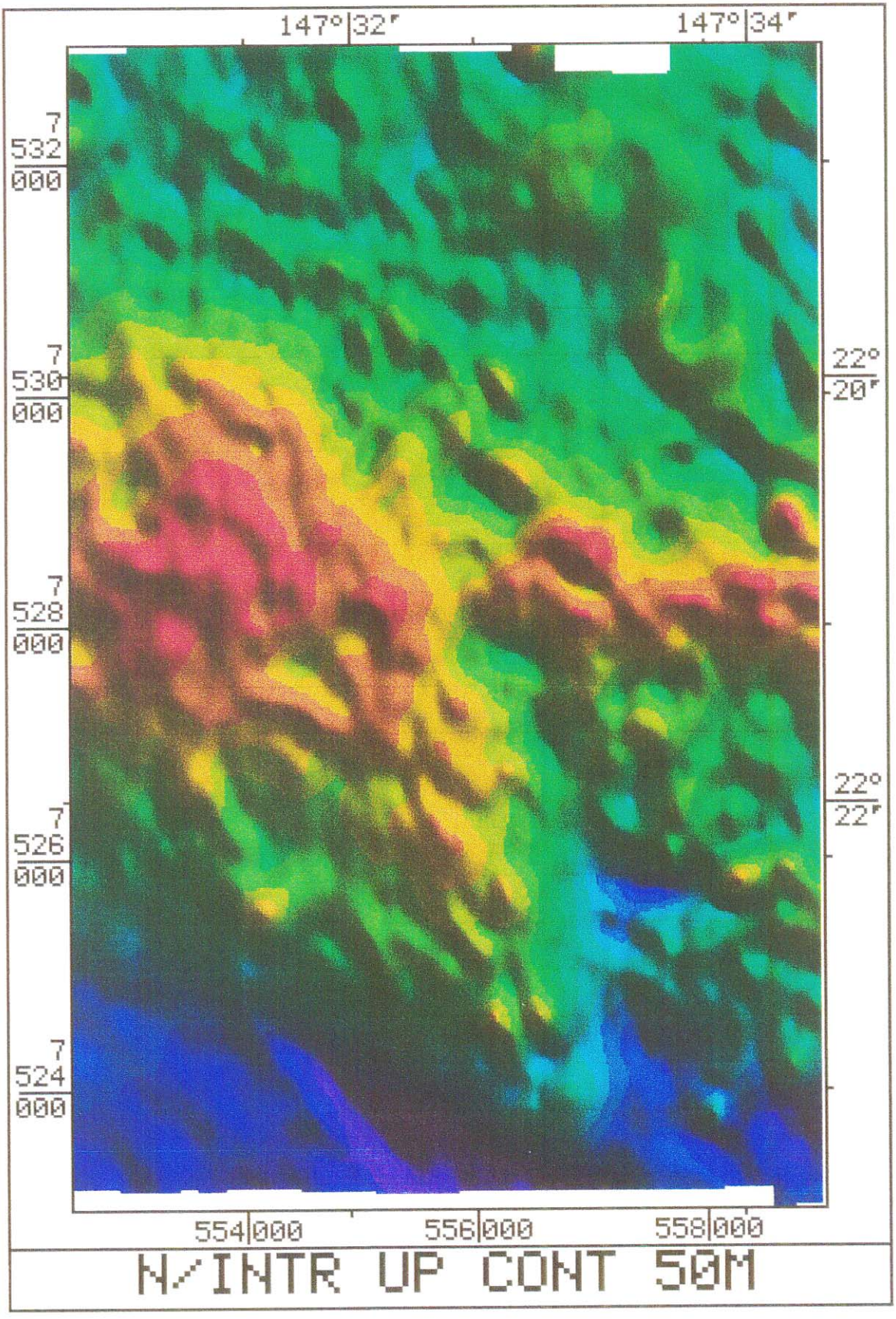
147° 32′
147° 34′
7 532 000
7 530 000
7 528 000
7 526 000
7 524 000
22° 20′
22° 22′
554 000
556 000
558 000
N/INTR UP CONT 50M

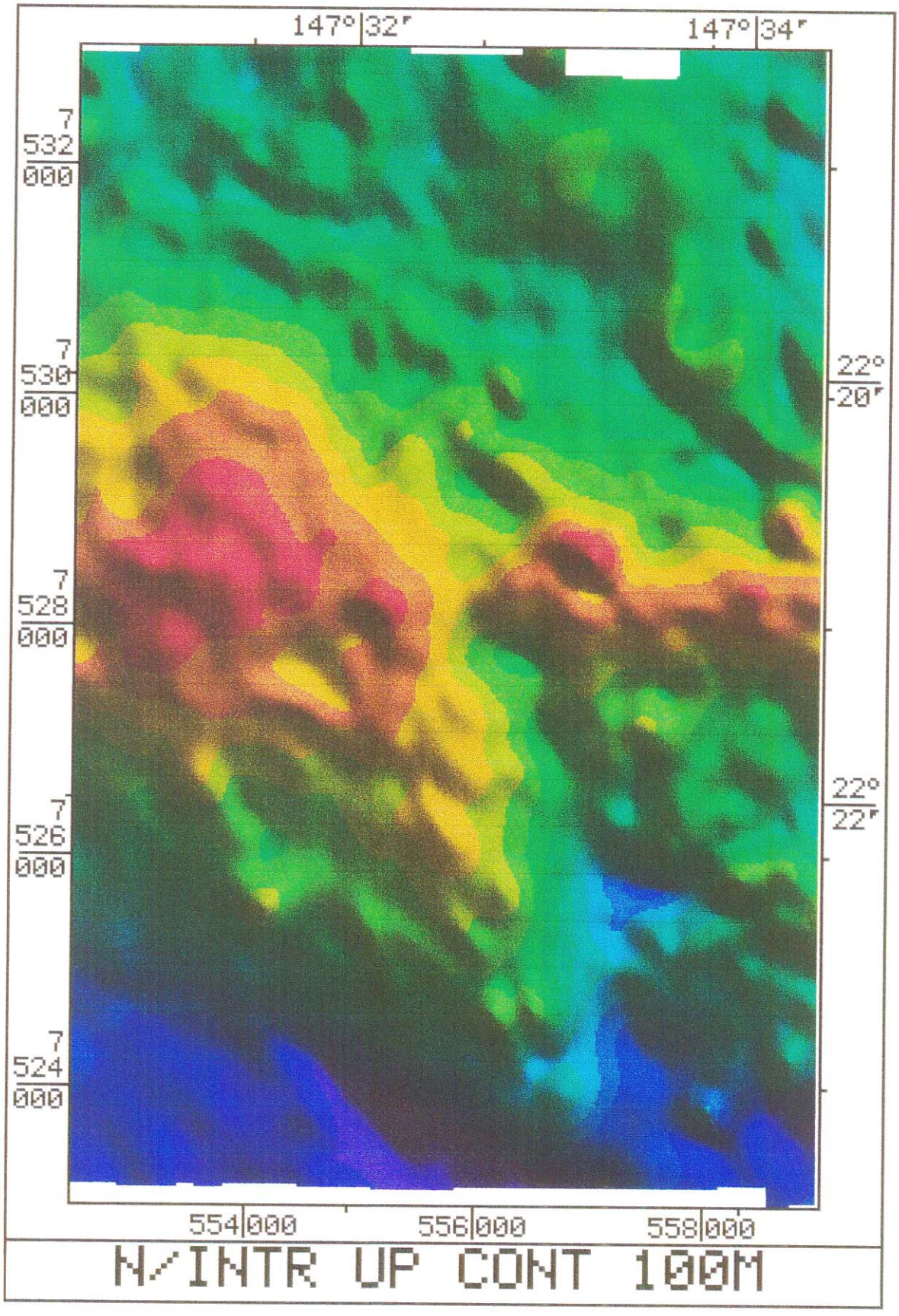
147° 32′
147° 34′
7 532 000
7 530 000
7 528 000
7 526 000
7 524 000
22° 20′
22° 22′
554 000
556 000
558 000
N/INTR UP CONT 100M

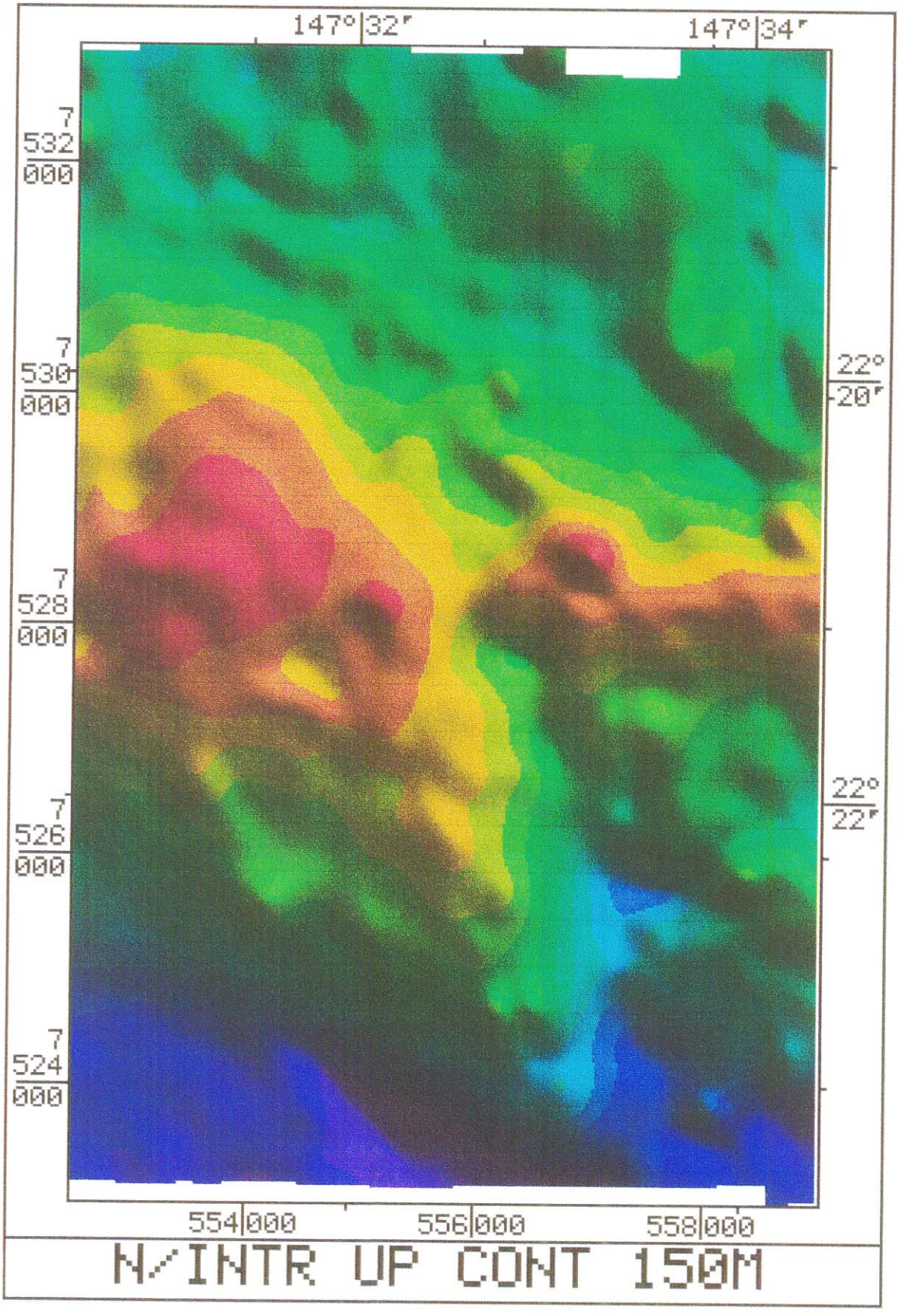
147° 32'
147° 34'
7 532 000
7 530 000
7 528 000
7 526 000
7 524 000
22° 20'
22° 22'
554 000
556 000
558 000
N/INTR UP CONT 150M

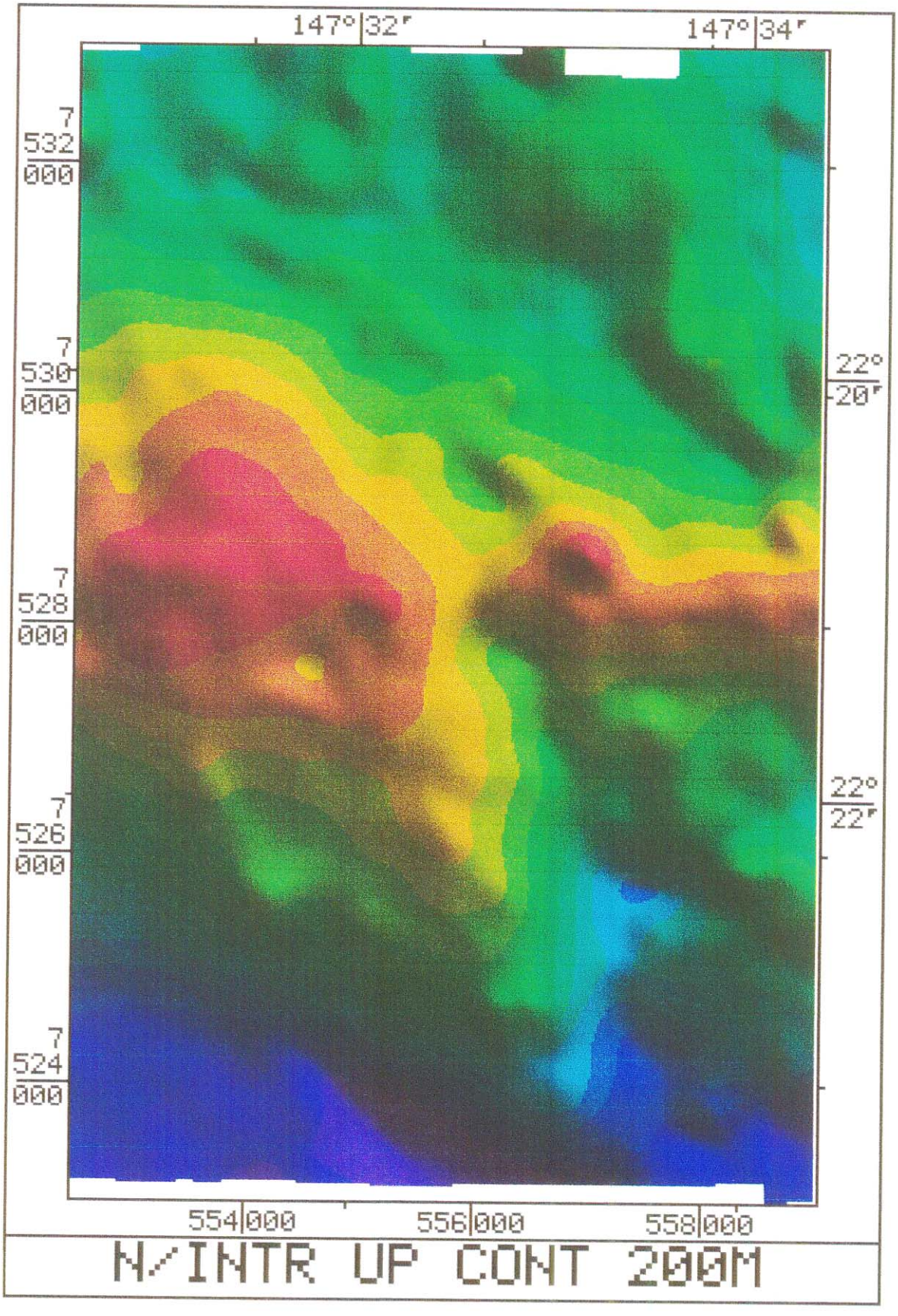
147° 32′
147° 34′
7 532 000
7 530 000
7 528 000
7 526 000
7 524 000
22° 20′
22° 22′
554 000
556 000
558 000
N/INTR UP CONT 200M

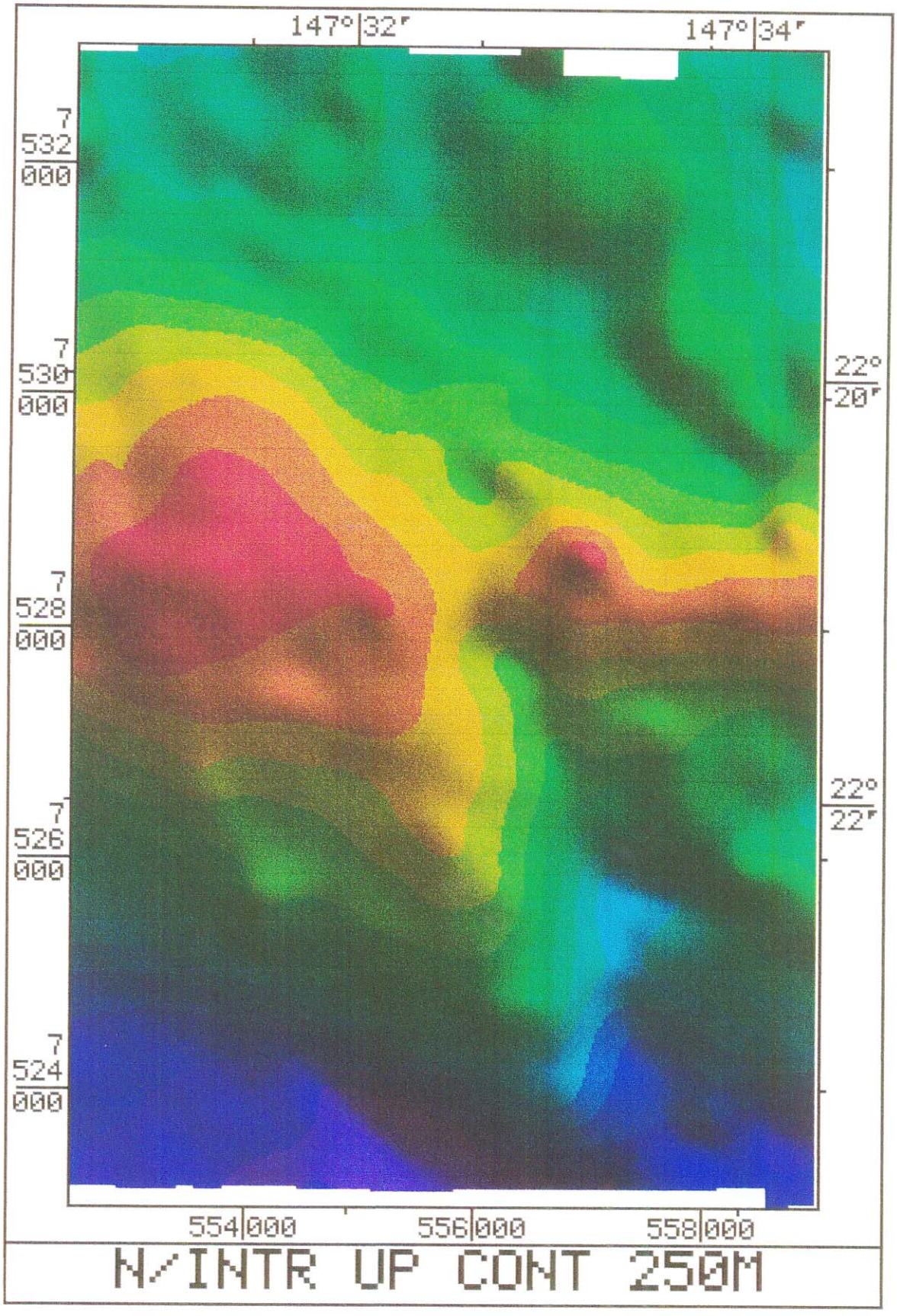
147° 32'
147° 34'
7 532 000
7 530 000
7 528 000
7 526 000
7 524 000
22° 20'
22° 22'
554 000
556 000
558 000
N/INTR UP CONT 250M

Appendix E

Vertical Derivatives Downward Continuation

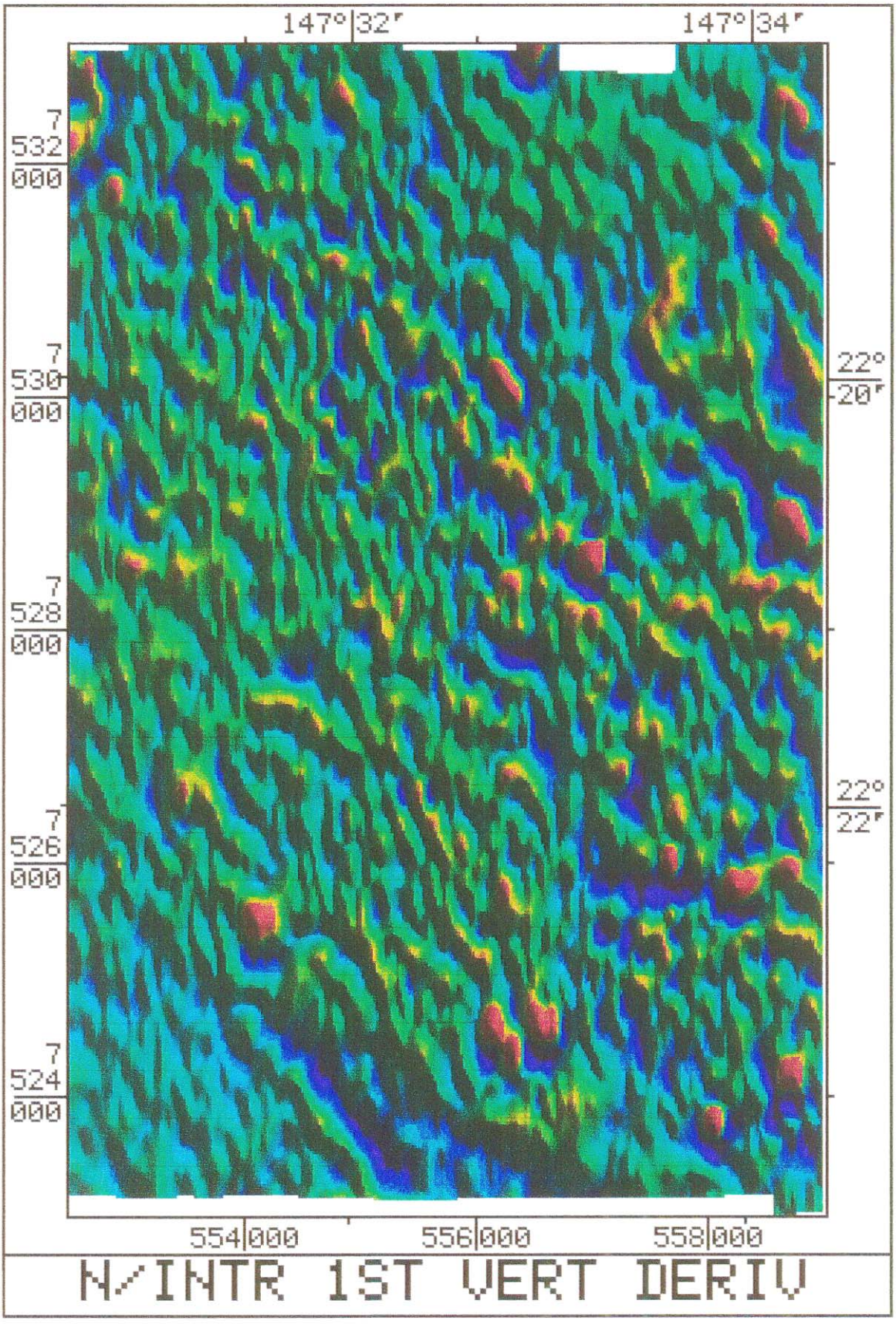
147°32'
147°34'
7532000
7530000
7528000
7526000
7524000
22°20'
22°22'
554000
556000
558000
N/INTR 1ST VERT DERIV

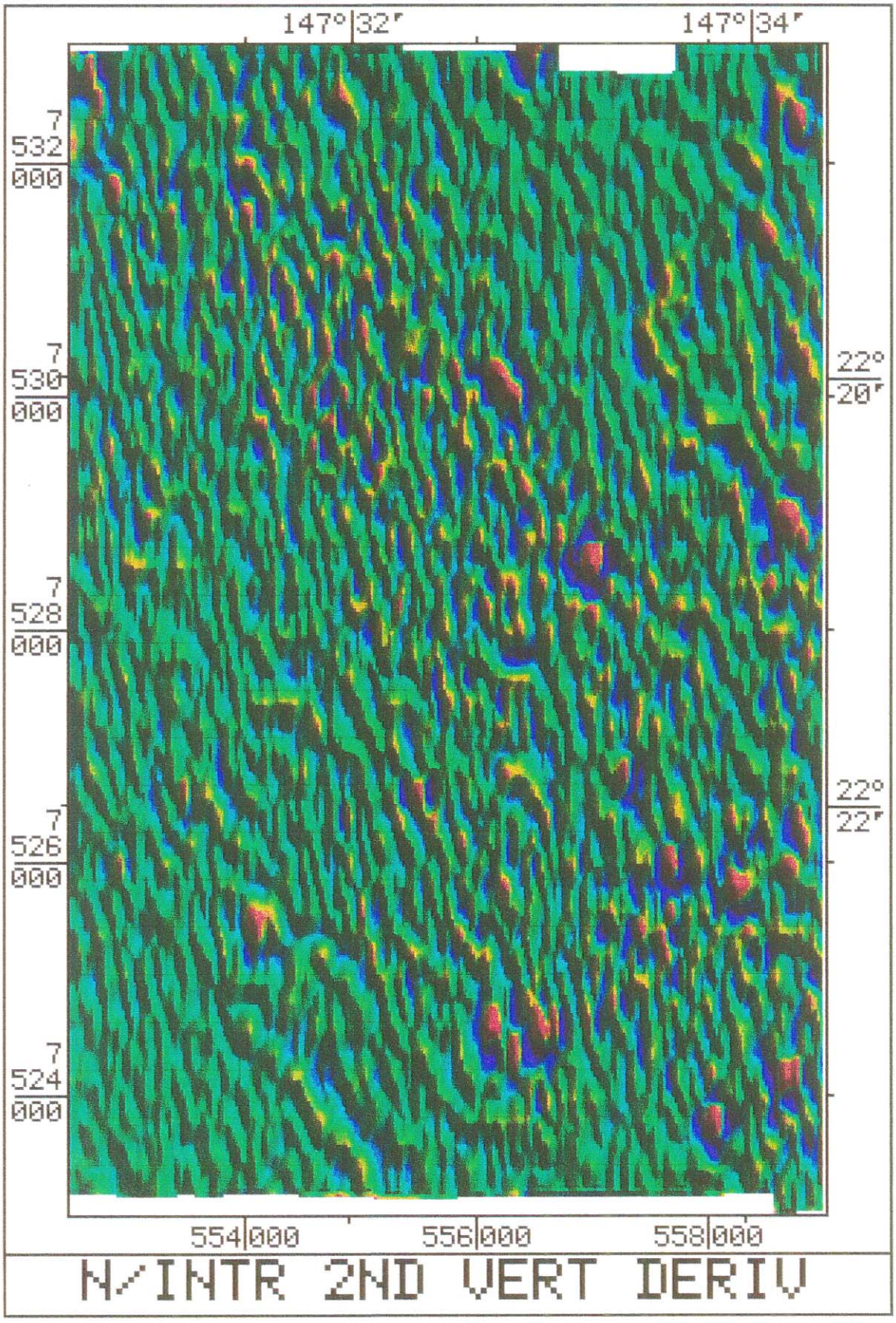
147°32'
147°34'
7532000
7530000
7528000
7526000
7524000
22°20'
22°22'
554000
556000
558000
N/INTR 2ND VERT DERIV

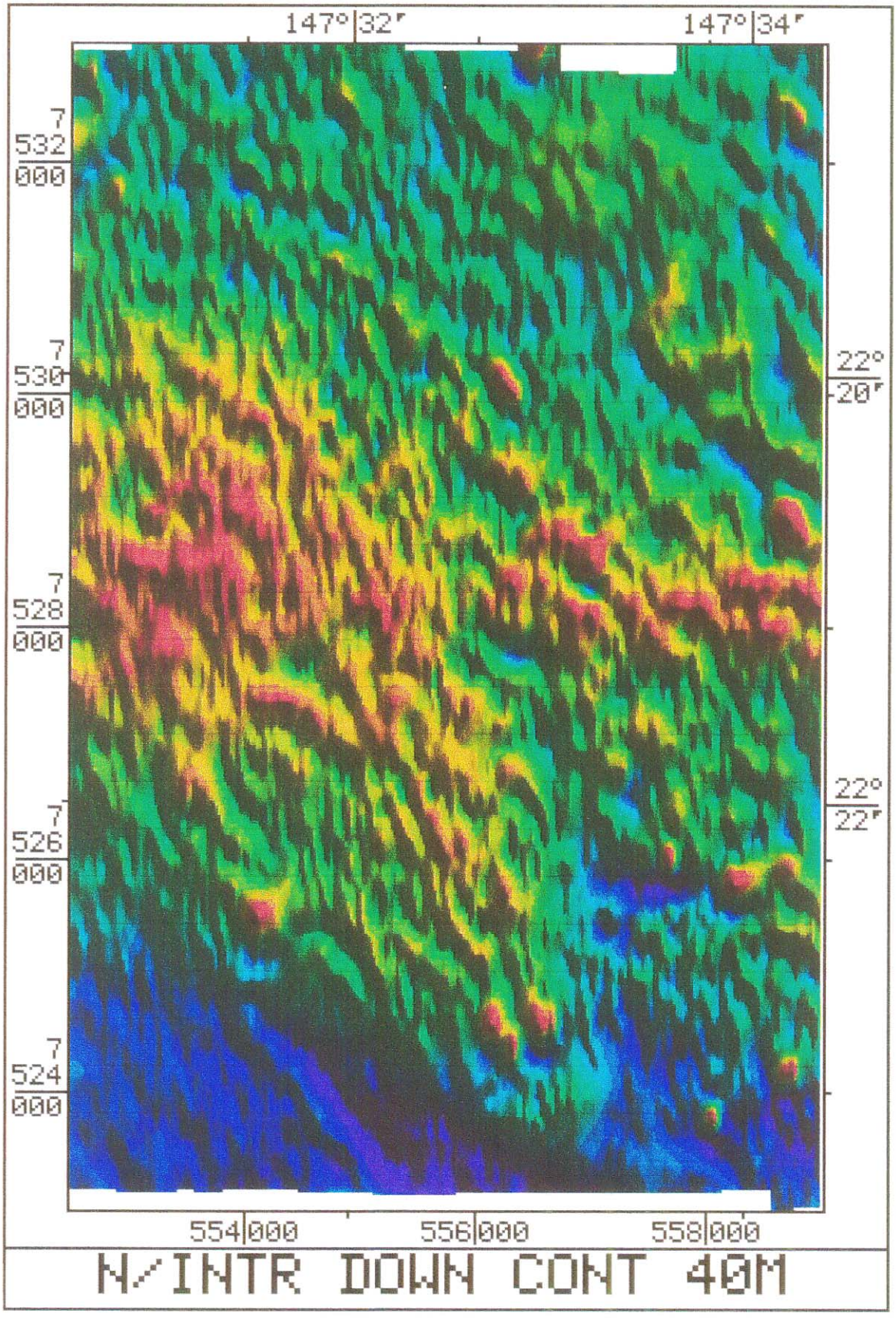
147° 32′
147° 34′
7 532 000
7 530 000
7 528 000
7 526 000
7 524 000
22° 20′
22° 22′
554 000
556 000
558 000
N/INTR DOWN CONT 40M

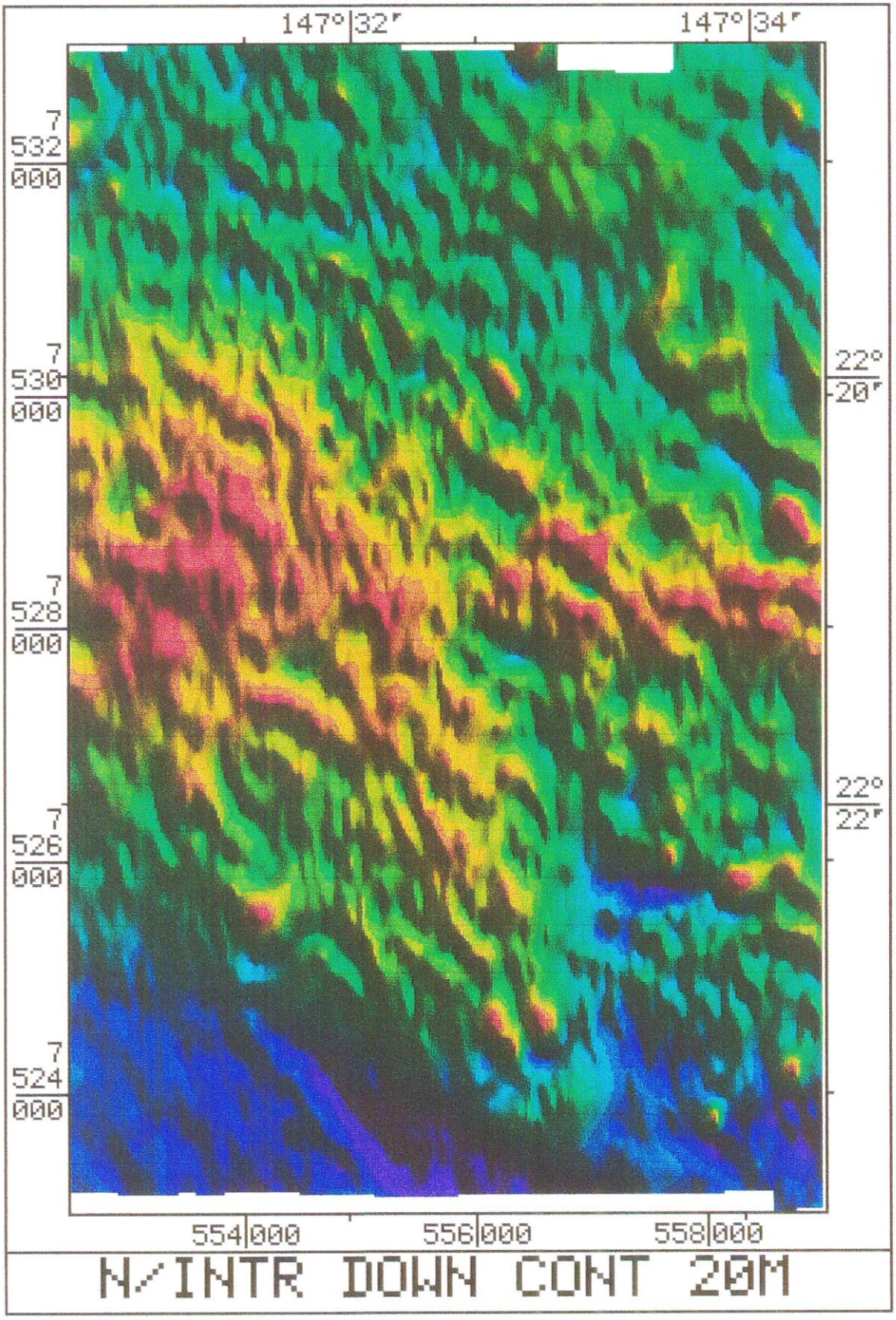
147°32'
147°34'
7532000
7530000
7528000
7526000
7524000
22°20'
22°22'
554000
556000
558000
N/INTR DOWN CONT 20M

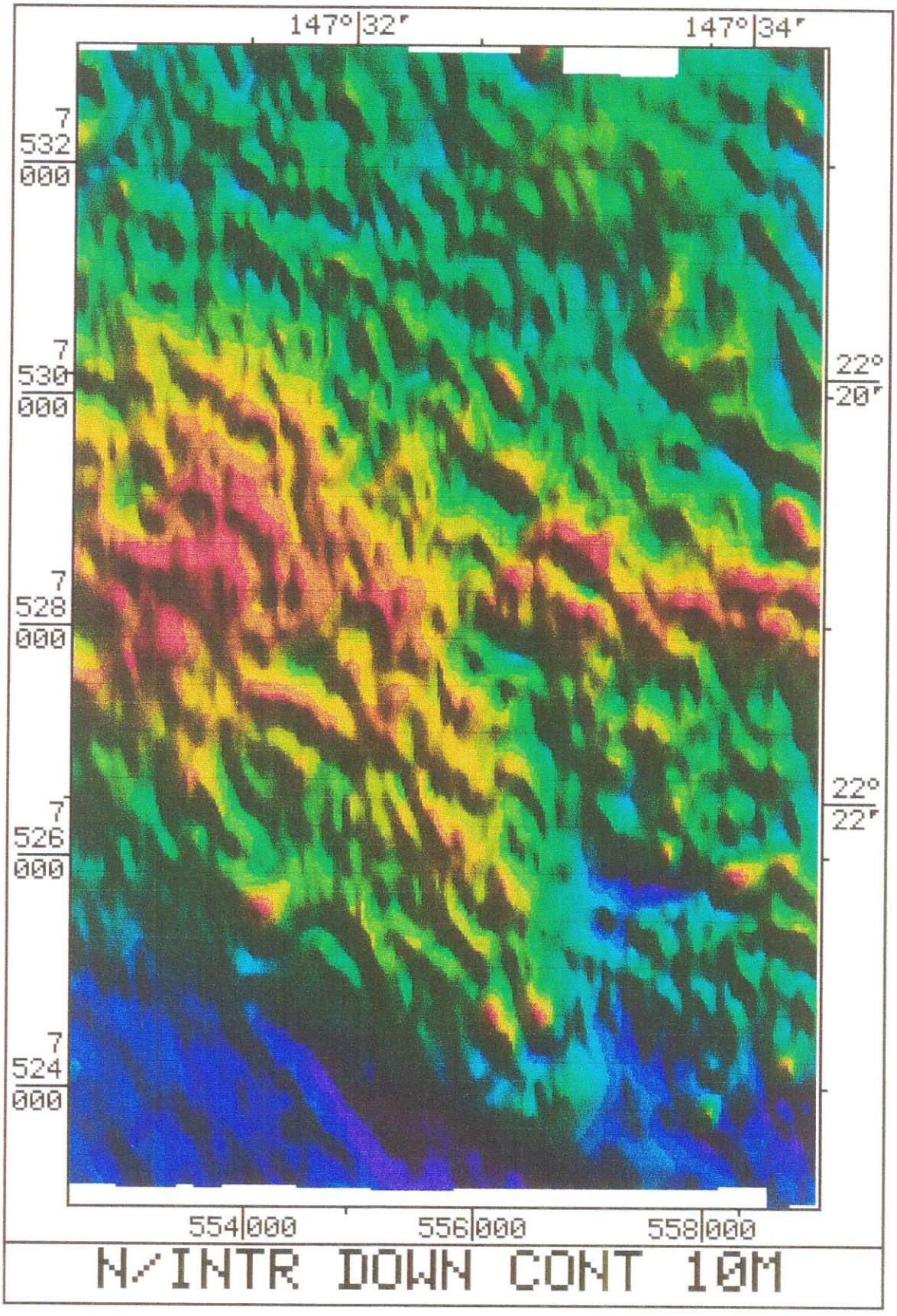
147° 32'
147° 34'
7 532 000
7 530 000
7 528 000
7 526 000
7 524 000
22° 20'
22° 22'
554 000
556 000
558 000
N/INTR DOWN CONT 10M

Appendix F

Comparison of Gridding Algorithms

fig. F1

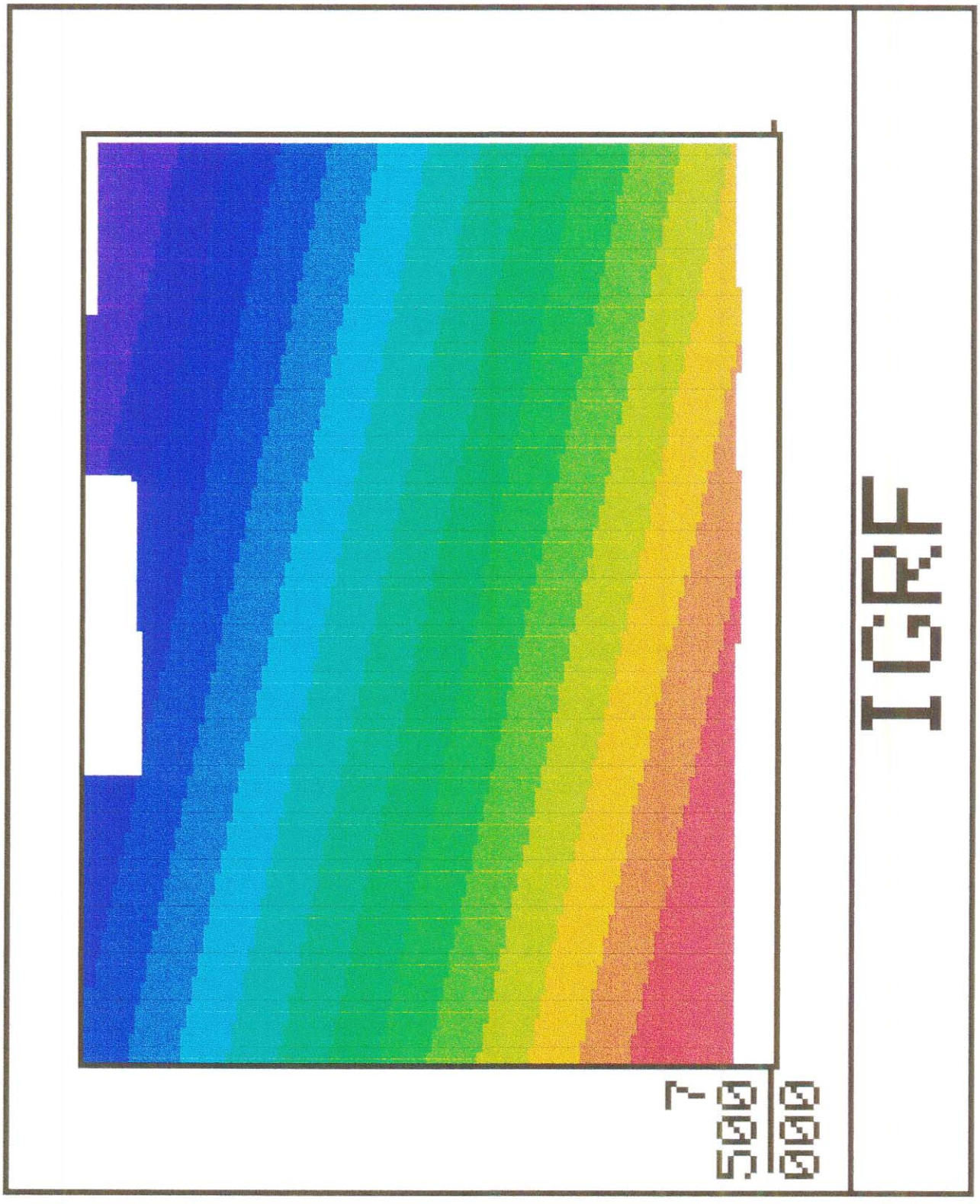

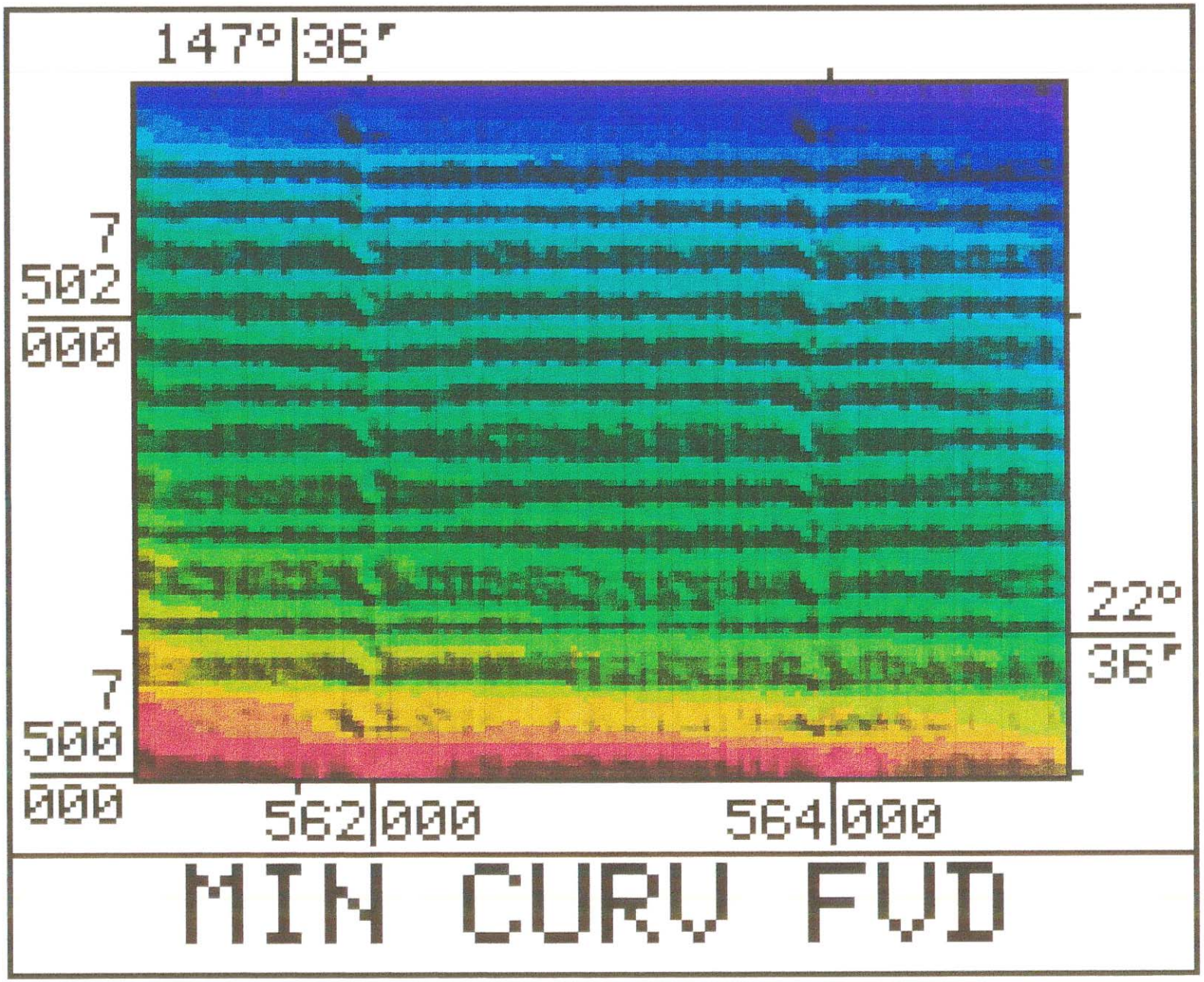

fig. F2

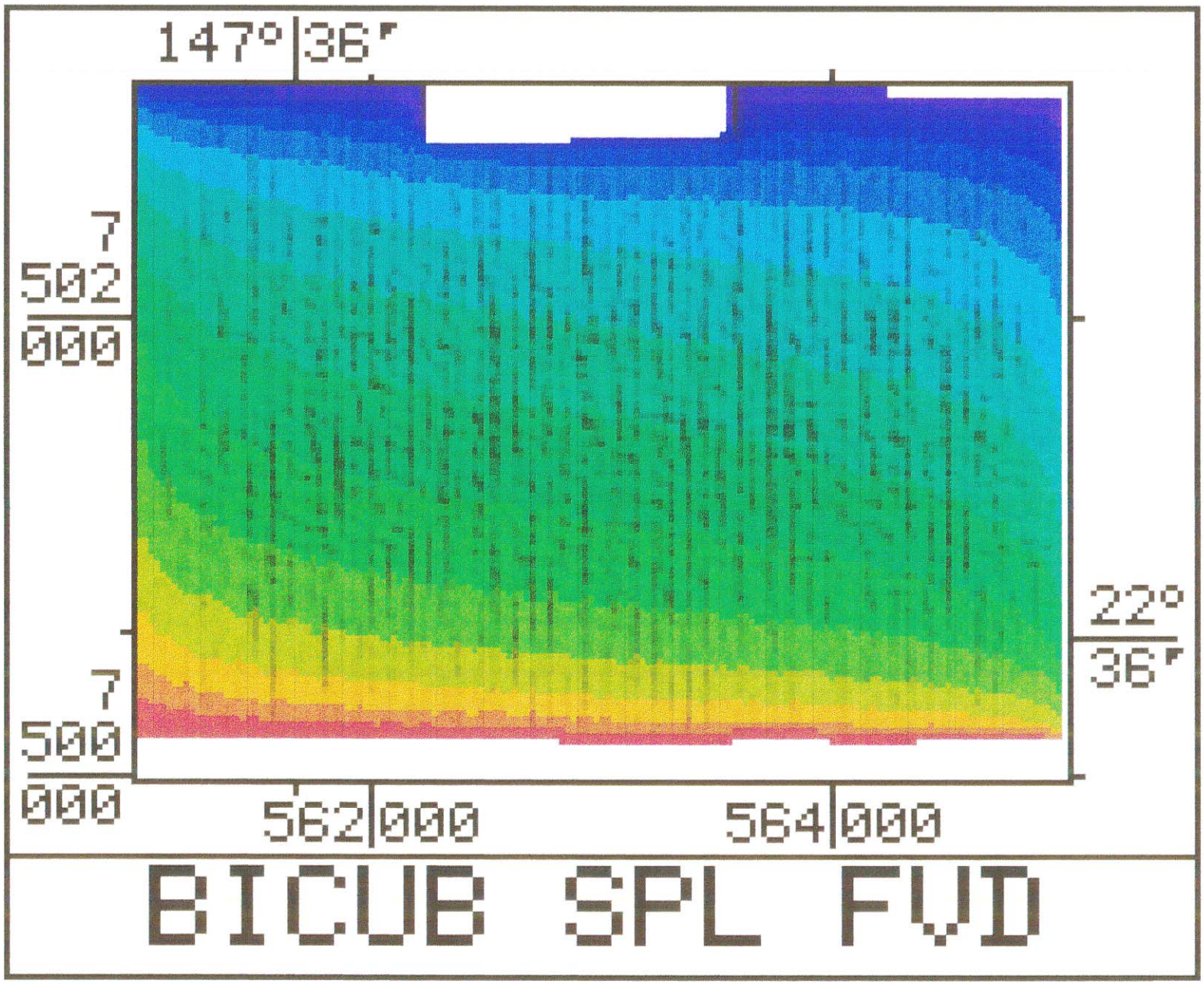

fig. F3

Appendix G

Drillhole Log Data

KEY TO ABBREVIATIONS

TOT	Total depth of drillhole
QSED	Thickness of Quaternary sediments
TBAS	Thickness of basalt
TSED	Depth to base of Tertiary sediments
PSED	Depth to base of Permian sediments
D TO B	Depth to basement
BCODE	Basement code, as follows:
B1	Anakie Metamorphics
B2	Granitoids
B3	Drummond Succession
***	D to B undetermined (>150m)

P2 PROSPECT	DATE	HOLE	TYPE	AMGEAST	AMGN0RTH	DEPTHS: TOT	QSED	TBAS	TSED	PSED	D TO B	BCODE
WATERBORE		57971	R	550830.05	7489813.32	73.50	3.00				3.00	B1
WATERBORE	1/81	62206	R	566095.54	7485572.00	54.00	1.00					
WATERBORE	6/82	62413	R	549128.91	7515154.56	57.91	1.00	11.43				
WATERBORE		62481	R	567334.75	7498193.81	116.50	1.00	109.00			109.00	B1
WATERBORE	1/64	62492	R	565962.14	7517141.04	42.67	1.00					
WATERBORE	8/82	62505	R	574548.39	7520060.15	20.00	1.00					
WATERBORE	8/82	62506	R	576556.26	7520770.80	20.00	1.00					
WATERBORE	8/82	62508	R	576276.51	7520040.29	20.00	1.00					
WATERBORE	9/83	67132	R	571388.52	7525083.23	18.00	1.00					
WATERBORE	1/86	67264	R	557645.55	7493688.99	51.50	1.00	12.00	27.00	49.00	49.00	B1
WATERBORE	7/85	67505	R	562820.23	7521647.47	33.50	1.00					
WATERBORE	1/88	84245	R	566683.32	7513919.18	36.50	1.00					
WATERBORE		84303	R	571147.56	7498164.30	36.60	1.00					
WATERBORE	9/88	84422	R	565895.34	7519347.60	44.00	1.00					
WATERBORE		84527	R	565485.98	7487999.92	99.40	1.00	68.00				
WATERBORE		84528	R	564575.95	7488551.81	94.00	1.00	65.00				
WATERBORE		84529	R	564303.04	7488839.71	94.80	1.00	64.00				
WATERBORE		84530	R	564457.73	7489447.74	93.50	1.00	62.00				
WATERBORE		84655	R	576023.87	7504926.55	108.00	1.00					
WATERBORE	1/90	84786	R	554717.70	7535989.20	66.00	1.00					
WATERBORE	8/90	89078	R	561497.26	7488830.50	27.43	1.00					
WATERBORE	1/91	89118	R	565307.81	7535816.62	48.70	1.00					
WATERBORE	1/91	89119	R	567008.03	7535442.98	35.00	11.50					
WATERBORE	1/92	89206	R	568962.39	7491407.62	72.00	1.00					
WATERBORE	1/92	89207	R	576126.35	7497203.10	39.00	1.00					
WATERBORE	1/92	89209	R	572889.54	7491677.38	31.50	1.00					
WATERBORE	2/92	89460	R	555950.00	7525404.59	87.00	1.00					
WATERBORE	3/91	89463	R	574586.60	7519950.72	22.86	1.00					
WATERBORE	6/71	90004	R	549801.00	7532162.82	54.86	1.00	45.42			45.42	B1
WATERBORE	6/71	90005	R	543866.98	7531583.58	18.29	1.00	18.29			18.29	B1
WATERBORE	2/73	90006	R	549192.62	7532689.52	51.82	1.00	45.11			45.11	B1
WATERBORE		90050	R	557625.20	7490248.35	33.00	1.00	7.00				
CLERMONT BASIN	9/80	CB001	R	568323.00	7478956.48	35.54	14.50	0.00		21.90	21.90	B1
CLERMONT BASIN	9/80	CB002	R	565770.72	7481918.11	36.54	3.00	0.00				
CLERMONT BASIN	4/81	CB003	R	570442.35	7471682.73	78.72	3.50	70.00			70.00	B1
CLERMONT BASIN	4/81	CB004	R	568399.61	7472096.08	71.56	20.00	0.00	60.00		60.00	B1
CLERMONT BASIN	6/81	CB005	R	573033.12	7471499.67	72.00	67.00	0.00			67.00	B1
CLERMONT BASIN	7/81	CB006	R	568600.00	7480000.00	61.30	1.00	26.80			26.80	B2
CLERMONT BASIN	8/81	CB007	PR	566000.15	7481001.30	201.00	1.00	13.00	15.00	198.00	198.00	B1
CLERMONT BASIN	7/81	CB008	R	565009.26	7481938.28	36.00	16.80	0.00			16.80	B1
CLERMONT BASIN	8/81	CB009	PR	566393.40	7489003.54	153.00	2.00	47.50	0.00	141.90	141.90	B1
CLERMONT BASIN	8/81	CB010	R	573600.70	7472100.87	85.49	84.74	0.00			84.74	B1
CLERMONT BASIN	8/81	CB011	PR	570904.03	7476865.43	54.90	26.00	39.20		46.40	46.40	B1
CLERMONT BASIN	8/81	CB013	R	573055.67	7475929.31	17.86	4.50				17.86	B2?
EPC443	7/88	CLN1R	R	548000.00	7554350.00	240.00	5.80	163.00	166.50		240.00	***
EPC443	8/88	CLN2R	R	563900.00	7523150.00	84.00	0.50	52.50	54.00		54.00	B1
EPC443	8/88	CLN3R	R	570650.00	7521800.00	115.00	0.50	72.00	80.50		80.50	B3?

P3	PROSPECT	DATE	HOLE	TYPE	AMGEAST	AMGN0RTH	DEPTHS: TOT	QSED	TBAS	TSED	PSED	D TO B	BCODE
EPC443		8/88	CLN4R	R	572000.00	7509850.00	144.00	1.00	122.00			122.00	B1
EPC443		8/88	CLN5R	R	550055.00	7520600.00	77.00	0.80	53.50			53.50	B1
EPC443		8/88	CLN6R	R	555250.00	7550850.00	282.00	16.00	131.50	167.00		282.00	***
EPC443		8/88	CLN7R	R	553250.00	7545000.00	264.00	7.00	170.00	186.00		264.00	***
EPC443		9/88	CLN8R	R	558450.00	7537900.00	250.00	1.50	148.50	185.00		250.00	***
EPC443		9/88	CLN9R	R	540400.00	7542500.00	162.00	28.00	99.00	129.00		129.00	B1
EPC443		9/88	CLN10R	R	540300.00	7552000.00	150.00	8.50	84.00	135.00		135.00	B1
EPC443		9/88	CLN11R	R	544700.00	7548550.00	121.00	25.00	75.00	103.00		103.00	B3
EPC443		9/88	CLN12R	R	553850.00	7530700.00	198.00	2.00	119.00	121.00		198.00	***
EPC443		9/88	CLN13C	D	548000.00	7554350.00	240.00	7.00	126.00	166.50		240.00	***
EPC443		10/88	CLN14R	R	563200.00	7509950.00	113.00	2.00	65.50	79.00		79.00	B2
EPC443		10/88	CLN16R	R	577600.00	7504340.00	191.00	4.00	178.00			178.00	B2
EPC443		10/88	CLN20R	R	577850.00	7480550.00	162.00	1.00	121.40	124.50		124.50	B1
EPC443		6/89	CLN24R	R	551500.00	7543050.00	400.00	6.00	170.00		388.00	388.00	B2
EPC443		6/89	CLN25R	R	548060.00	7516500.00	172.00	0.20	23.00		164.00	164.00	B1
EPC443		7/89	CLN26C	D	548050.00	7516500.00	171.00	0.20	23.50		165.30	165.30	B1
EPC443		7/89	CLN27R	R	550950.00	7515250.00	96.56	1.00	34.00	87.00		94.60	B1
EPC443		8/89	CLN28R	R	549500.00	7514350.00	75.05	2.00	17.00	50.00	64.00	64.00	B1
EPC443		8/89	CLN29R	R	548575.00	7516500.00	91.10	1.00	16.50		80.80	80.80	B1
EPC443		8/89	CLN30R	R	548125.00	7515475.00	49.75	16.00				16.00	B1
EPC443		8/89	CLN31R	R	548475.00	7517425.00	38.00	1.00	30.00			30.00	B1
EPC443		8/89	CLN32R	R	549100.00	7516600.00	29.00	2.00	12.00			12.00	B1
EPC443		8/89	CLN33R	R	547865.00	7516645.00	56.50	3.00	10.00	24.00			
EPC443		8/89	CLN34R	R	547850.00	7516650.00	304.81	1.00	18.00	25.00		304.81	***
EPC443		8/89	CLN35R	R	556500.00	7523100.00	93.37	1.00	70.00	71.60		71.60	B1
EPC443		8/89	CLN36C	D	547865.00	7516645.00	91.00	0.50	11.00	23.60			
EPC443		8/89	CLN37R	R	548125.00	7515475.00	96.00	5.00	10.50	49.00	83.80	83.80	B1
EPC443		8/89	CLN38R	R	547650.00	7518400.00	16.00	1.00				1.00	B1
EPC443		8/89	CLN39R	R	548150.00	7518400.00	262.00	2.50	12.10	22.80		262.00	***
EPC443		8/89	CLN40R	R	558240.00	7526350.00	131.00	0.50	114.50	115.50		115.50	B2
EPC443		8/89	CLN41R	R	548350.00	7519600.00	68.00	2.00	23.60			23.60	B1
EPC443		9/89	CLN42R	R	551800.00	7528000.00	84.66	1.00	61.50	69.50		69.50	B1
EPC443		9/89	CLN43R	R	548475.00	7517425.00	126.00	0.50	34.00	37.00	112.80	112.80	B1
EPC443		9/89	CLN44R	R	552200.00	7531000.00	35.00	0.80					
EPC443		9/89	CLN45R	R	549000.00	7519550.00	195.85	2.00	8.00			167.00	B1
EPC443		9/89	CLN46R	R	552230.00	7531000.00	292.43	0.80	119.00	142.00		292.43	***
EPC443		9/89	CLN47R	R	549500.00	7519500.00	63.00	2.00	32.00	37.00		37.00	B1
EPC443		9/89	CLN48R	R	550600.00	7526000.00	83.67	1.00	46.00			46.00	B1
EPC443		9/89	CLN49R	R	547775.00	7514500.00	127.00	6.00			63.70	63.70	B1
EPC443		10/89	CLN50R	R	561050.00	7540300.00	335.00	1.00	169.00	206.00		335.00	***
EPC443		9/89	CLN51R	R	547650.00	7514700.00	167.00	27.00			93.80	93.80	B1
EPC443		10/89	CLN52R	R	569950.00	7526750.00	181.25	2.00	121.00	163.00		163.00	B2
EPC443		10/89	CLN53R	R	572725.00	7525100.00	141.00	0.50	64.50	91.50		91.50	B3?
EPC443		10/89	CLN54R	R	554150.00	7548075.00	361.80	20.00	170.00	171.00	350.00	350.00	B3
EPC443		10/89	CLN55R	R	566650.00	7513475.00	162.00	1.00	122.00			122.00	B1
EPC443		10/89	CLN63R	R	550000.00	7544650.00	96.00	3.50	70.20		77.20	77.20	B3
EPC443		10/89	CLN64R	R	549950.00	7549850.00	200.00	7.50	140.50	171.20		200.00	***

P4	PROSPECT	DATE	HOLE	TYPE	AMGEAST	AMGN0RTH	DEPTHS: TOT	QSED	TBAS	TSED	PSED	D TO B	BCODE
	EPC443	10/89	CLN65R	R	543900.00	7542600.00	107.00	2.00	83.50			83.50	B3
	EPC443	11/89	CLN66R	R	552450.00	7525350.00	184.00	2.50	94.50	99.00		184.00	***
	EPC443	11/89	CLN67R	R	552000.00	7519150.00	112.00	1.00	68.00	94.00		94.00	B1
	EPC443	11/89	CLN68C	D	548150.00	7516650.00	143.90	1.00	19.00		143.60	143.60	B1
	EPC443	7/90	CLN70R	R	535600.00	7548400.00	151.00	46.00	94.00	140.00		140.00	B1
	EPC443	7/90	CLN71R	R	551700.00	7538600.00	242.00	7.00	111.00	187.00		242.00	***
	EPC443	7/90	CLN72R	R	549275.00	7537800.00	86.00	3.00	77.00	83.00		83.00	B2
	EPC443	8/90	CLN73R	R	553050.00	7534975.00	201.00	1.00	122.00	155.10		201.00	***
	EPC443	8/90	CLN74R	R	562790.00	7508510.00	125.00	1.00	55.00				
	EPC443	8/90	CLN77R	R	562780.00	7508510.00	129.50	1.00	53.00	75.00	128.10	128.00	B2
	KURRAJONG	1994	KJRC001	RC	553600.00	7532430.00	128.00	3.00					
	KURRAJONG	1994	KJRC002	RC	546710.00	7529200.00	150.00	3.00	84.00	86.00		86.00	B3
	KURRAJONG	1994	KJRC003	RC	560230.00	7527790.00	114.00	3.00	96.00			96.00	B1
	KURRAJONG	1994	KJRC004	RC	559540.00	7526790.00	150.00	3.00	124.00			124.00	B1
	KURRAJONG	1994	KJRC005	RC	556240.00	7533990.00	174.00	3.00	138.00			174.00	***
	KURRAJONG	1994	KJRC006	RC	558380.00	7529200.00	96.00	3.00	82.00			82.00	B1
	KURRAJONG	1994	KJRC007	RC	547860.00	7534700.00	84.00	3.00	48.00			48.00	B3
	KURRAJONG	1995	KJRC008	RC	559600.00	7525350.00	134.00	3.00	130.00	134.00			
	KURRAJONG	1995	KJRC009	RC	549930.00	7526000.00	78.00	3.00	50.00	60.00		60.00	B1
	KURRAJONG	1995	KJRC010	RC	551140.00	7524220.00	120.00	3.00	100.00	106.00		106.00	B1
	KURRAJONG	1995	KJRC011	RC	575250.00	7530020.00	50.00	3.00	6.00	44.00		44.00	B3
	KURRAJONG	1995	KJRC012	RC	574890.00	7531350.00	62.00	3.00	30.00	58.00		58.00	B3
	KURRAJONG	1995	KJRC013	RC	558720.00	7523610.00	150.00	3.00	136.00	138.00		138.00	B1
	KENLOGAN BASIN	9/80	KL001	DD	565113.20	7501371.51	27.43	0.10	20.00		25.44	25.44	B1
	KENLOGAN BASIN	9/80	KL002	DD	566026.31	7501979.86	24.40	0.90	21.12		22.80	22.80	B1
	KENLOGAN BASIN	9/80	KL003	PR	564826.04	7500084.47	71.62	0.50	19.90			19.90	B1
	KENLOGAN BASIN	9/80	KL004	PR	564883.32	7501238.27	78.27	0.50	47.00	59.00		59.00	B1
	KENLOGAN BASIN	7/80	KL005	R	567117.88	7503263.94	66.76	1.20	60.00			60.00	B2
	KENLOGAN BASIN	3/81	KL006	PR	567549.90	7504242.63	113.62	1.50	110.00			110.00	B2
	MICLERE BASIN	8/80	MC001	R	556424.49	7502923.90	30.64	1.00			29.50	29.50	B1
	MICLERE BASIN	8/80	MC002	DD	557131.32	7502277.37	47.75	1.10	14.50	34.50	44.69	44.69	B1
	MICLERE BASIN	9/80	MC003	R	558303.73	7503169.34	8.69	6.20				6.20	B1
	MICLERE BASIN	9/80	MC004	PR	559254.94	7504278.62	30.70	29.70				29.70	B1
	MICLERE BASIN	9/80	MC005	R	560163.06	7504632.23	2.74	0.10				0.10	B1
	MICLERE BASIN	9/80	MC006	R	561134.49	7504605.48	6.19	3.00				3.00	B1
	MICLERE BASIN	9/80	MC007	PR	561731.16	7505203.46	30.82	0.60					
	MICLERE BASIN	4/81	MC010	R	554976.14	7500059.85	83.55	1.00	10.00	33.00		33.00	B1
	MICLERE BASIN	4/81	MC011	R	554980.39	7501201.41	56.59	27.00				27.00	B1
	MICLERE BASIN	6/81	MC012	R	555076.48	7503971.59	67.20	3.00					
	MICLERE BASIN	6/81	MC013	R	555000.26	7502997.61	67.10	1.00					
	MICLERE BASIN	6/81	MC014	R	556001.12	7499000.91	28.09	1.00			25.00	25.00	B1
	MICLERE BASIN	6/81	MC015	PR	556998.19	7497999.84	38.20	1.00	11.30	12.00	34.70	34.70	B1
	MICLERE BASIN	6/81	MC016	R	559699.61	7499000.00	73.66	2.00	23.80	42.00		42.00	B1
	MICLERE BASIN	6/81	MC017	DD	559617.33	7499003.11	52.60	2.00	22.45	34.73		34.73	B1
	MICLERE BASIN	6/81	MC018	PT	559782.31	7499483.40	83.70	10.00	38.00	60.00		60.00	B1
	MICLERE BASIN	6/81	MC019	PR	556401.56	7502000.03	110.20	2.00			102.60	102.60	B1

P5 PROSPECT	DATE	HOLE	TYPE	AMGEAST	AMGN0RTH	DEPTHS: TOT	QSED	TBAS	TSED	PSED	D TO B	BCODE
MICLERE BASIN	6/81	MC020	R	558400.00	7502000.04	17.96	2.00			10.00	10.00	B1
MICLERE BASIN	6/81	MC021	R	556400.70	7501000.14	72.76	2.00	55.00				
MICLERE BASIN	6/81	MC022	R	557399.74	7501000.46	49.10	13.00	21.00	23.00			
MICLERE BASIN	6/81	MC023	R	558400.63	7501000.00	18.50	7.00				7.00	B1
MICLERE BASIN	6/81	MC024	R	559600.73	7501000.63	42.36	1.00	9.00	34.00		34.00	B1
MICLERE BASIN	6/81	MC025	R	555000.90	7498999.23	23.86	2.00	10.00		19.00	19.00	B1
MICLERE BASIN	6/81	MC027	R	555000.74	7497000.78	8.76	3.00				3.00	B1
MICLERE BASIN	7/81	MC028	DD	559599.83	7501007.87	27.30	0.80	11.00				
MICLERE BASIN	7/81	MC029	R	555601.83	7501300.41	102.00	1.00			95.40	95.40	B1
MICLERE BASIN	7/81	MC030	R	555681.85	7502997.94	20.70	2.00			7.00	7.00	B1
MICLERE BASIN	7/81	MC031	R	555398.91	7497001.32	54.30	17.00			35.00	35.00	B1
MICLERE BASIN	8/81	MC032	PR	556399.52	7503900.20	55.10	1.00	13.30	15.00	45.30	45.30	B1
MICLERE BASIN	8/81	MC034	R	557299.85	7499000.16	72.00	3.00			66.20	66.20	B1
SPRINGS BASIN	8/80	SB001	PR	565008.34	7497984.04	22.97	0.30	17.60	21.54		21.54	B1
SPRINGS BASIN	8/80	SB002	PR	565875.12	7498240.28	83.61	0.10	77.00	80.00		80.00	B1
SPRINGS BASIN	5/81	SB003	PR	566845.18	7498053.76	68.59	0.10	65.50			65.50	B1
SPRINGS BASIN	5/81	SB004	R	567881.04	7498160.03	116.50	1.00	109.00			109.00	B1
SPRINGS BASIN	8/80	SB005	PR	563980.26	7498021.66	76.00	3.20	65.30		71.50	71.50	B1
SPRINGS BASIN	8/80	SB006	R	563000.00	7498000.00	46.40	0.20	35.10	45.10		45.10	B1
SPRINGS BASIN	9/80	SB007	PR	561957.39	7498039.63	23.10	12.20	22.80			22.80	B1
SPRINGS BASIN	9/80	SB008	R	560848.67	7498000.89	64.62	2.50	51.90		64.10	64.10	B1
SPRINGS BASIN	9/80	SB009	R	560457.31	7500083.77	46.72	1.10	46.10			46.10	B1
SPRINGS BASIN	3/81	SB010	PR	558391.94	7495292.65	51.72	1.50	14.72	19.00	39.00	39.00	B1
SPRINGS BASIN	3/81	SB011	PR	558871.70	7494275.29	126.99	1.00	98.00		123.00	123.00	B2
SPRINGS BASIN	4/81	SB012	PR	561999.37	7492015.29	42.84	1.50	17.00		32.00	32.00	B1
SPRINGS BASIN	6/81	SB013	PR	561878.84	7490947.22	108.60	0.50	70.00		107.00	107.00	B1
SPRINGS BASIN	4/81	SB015	R	559637.61	7491512.66	62.54	1.00	17.00	38.00	50.00	50.00	B1
SPRINGS BASIN	4/81	SB016	PR	558469.14	7491775.70	62.48	1.00	41.00	43.00	55.00	55.00	B1
SPRINGS BASIN	5/81	SB018	PR	562083.88	7492656.84	57.52	0.50	39.00	52.00		52.00	B1
SPRINGS BASIN	5/81	SB019	R	562038.04	7494209.58	17.47	11.00				11.00	B1
SPRINGS BASIN	5/81	SB020	R	559000.53	7496000.24	8.43	0.50					
SPRINGS BASIN	5/81	SB021	PR	560000.33	7496999.91	41.54	1.00	27.17		38.00	38.00	B1
SPRINGS BASIN	5/81	SB022	R	563000.21	7499000.29	41.69	36.00				36.00	B1
SPRINGS BASIN	5/81	SB023	R	564000.07	7499000.00	20.50	16.00				16.00	B1
SPRINGS BASIN	5/81	SB024	PR	564000.74	7499972.43	23.00	0.50	8.00	19.00		19.00	B1
SPRINGS BASIN	5/81	SB028	R	566000.00	7503999.98	137.50	1.00	118.00			118.00	B1
SPRINGS BASIN	6/81	SB029	PR	566042.12	7505070.94	110.80	1.00	88.00	100.60		100.60	B2
SPRINGS BASIN	8/81	SB030	R	566943.35	7505636.67	223.00	0.30	215.00			215.00	B2
SPRINGS BASIN	5/81	SB031	PR	567709.45	7507345.42	110.80	1.00	95.00	102.00		102.00	B1
SPRINGS BASIN	5/81	SB032	PR	563339.77	7491000.04	107.60	1.00	61.00		98.30	98.30	B1
SPRINGS BASIN	5/81	SB033	PR	566000.40	7490999.83	114.56	5.66	60.00	80.00	101.36	101.36	B1
SPRINGS BASIN	5/81	SB034	R	559092.74	7497001.38	8.55	0.25	1.00			1.00	B1
SPRINGS BASIN	6/81	SB035	R	558992.13	7491004.00	86.79	57.10				57.10	B1
SPRINGS BASIN	6/81	SB036	R	563000.28	7489000.00	85.04	1.00	61.50		82.00	82.00	B1
SPRINGS BASIN	6/81	SB037	PR	564914.63	7495132.23	126.00	0.50	94.00		120.00	120.00	B1
SPRINGS BASIN	6/81	SB038	R	561940.57	7491400.55	121.90	1.00	78.73	85.00	106.00	106.00	B1

P6 PROSPECT	DATE	HOLE	TYPE	AMGEAST	AMGN0RTH	DEPTHS: TOT	QSED	TBAS	TSED	PSED	D TO B	BCODE
SPRINGS BASIN	7/81	SB039	R	565999.78	7495999.85	66.46	1.50	58.00			58.00	B1
SPRINGS BASIN	7/81	SB042	R	564903.60	7494001.05	54.26	1.00	47.00			47.00	B1
SPRINGS BASIN	7/81	SB046	R	565105.82	7492158.46	36.26	0.25	12.00		23.10	23.10	B1
SPRINGS BASIN	7/81	SB047	PR	563693.68	7497000.97	69.43	1.00	64.00	66.00		66.00	B1
SPRINGS BASIN	8/81	SB048	R	566639.20	7496960.47	133.76	0.30	114.80			114.80	B1
SPRINGS BASIN	8/81	SB049	R	567301.12	7498900.24	103.36	0.50	96.00			96.00	B1
SPRINGS BASIN	8/81	SB050	PR	567698.65	7500401.46	147.40	0.50	104.00			104.00	B1
SPRINGS BASIN	8/81	SB051	PR	566800.39	7503201.56	165.67	0.70	162.00			162.00	B1
SPRINGS BASIN	8/81	SB052	PR	563398.12	7503197.80	91.70	1.00	72.30		80.90	80.90	B1
SPRINGS BASIN	8/81	SB053	PR	564777.55	7505781.07	138.00	1.00	126.00			126.00	B1
SPRINGS BASIN	8/81	SB054	PR	561650.60	7497002.15	96.87	0.25	80.00	85.00	88.30	88.30	B1
SPRINGS BASIN	8/81	SB055	PR	558249.54	7494358.02	115.00	1.00	66.60		105.80	105.80	B1
STRATHFIELD	1994	STRC001	RC	562730.00	7505185.00	66.00	1.00	44.00	54.00		54.00	B1
STRATHFIELD	1994	STRC002	RC	562741.00	7506270.00	36.00	1.00	17.00			17.00	B1
STRATHFIELD	1994	STRC003	RC	562900.00	7507220.00	54.00	1.00	40.00			40.00	B1
STRATHFIELD	1994	STRC004	RC	561920.00	7507190.00	30.00	2.00				2.00	B1
STRATHFIELD	1994	STRC005	RC	562280.00	7508230.00	24.00	1.00					
STRATHFIELD	1994	STRC006	RC	563150.00	7508310.00	90.00	1.00	68.00		76.00	76.00	B2
STRATHFIELD	1994	STRC007	RC	562280.00	7508220.00	72.50	1.00	38.00		54.00	54.00	B2
STRATHFIELD	1994	STRC008	RC	564300.00	7509310.00	102.00	1.00	88.00		98.00	98.00	B1
STRATHFIELD	1994	STRC009	RC	561404.00	7510855.00	96.00	1.00	66.00		78.00	78.00	B2
MICLERE	1994	STRC010	RC	561270.00	7509490.00	72.00	1.00	38.00		59.00	59.00	B1
MICLERE	1994	STRC011	RC	561300.00	7508300.00	60.00	1.00	42.00	48.00		48.00	B1
MICLERE	1994	STRC012	RC	560540.00	7507170.00	48.00	2.00				2.00	B1
STRATHFIELD	1994	STRC013	RC	560280.00	7510270.00	102.00	8.00	34.00		52.00	52.00	B1
MICLERE	1994	STRC014	RC	560220.00	7509200.00	48.00	1.00	4.00	18.00		18.00	B1
MICLERE	1994	STRC015	RC	560180.00	7507810.00	48.00	2.00				2.00	B1
STRATHFIELD	1994	STRC016	RC	567240.00	7505280.00	123.00	1.00	118.00				
STRATHFIELD	1994	STRC017	RC	566530.00	7506430.00	104.00	1.00					
STRATHFIELD	1994	STRC018	RC	565890.00	7505530.00	96.00	1.00	89.00				
STRATHFIELD	1994	STRC019	RC	564280.00	7505790.00	120.00	1.00	90.00			108.00	B1
STRATHFIELD	1994	STRC020	RC	564890.00	7505640.00	77.00	1.00	70.00				
STRATHFIELD	1994	STRC021	RC	563530.00	7506600.00	84.00	1.00	54.00		64.00	64.00	B1
STRATHFIELD	1994	STRC022	RC	565350.00	7508230.00	132.00	1.00	84.00				
STRATHFIELD	1994	STRC023	RC	564650.00	7510290.00	150.00	1.00	94.00		118.00	118.00	B2
STRATHFIELD	1994	STRC024	RC	563070.00	7511550.00	120.00	1.00	78.00		108.00	108.00	B2
STRATHFIELD	1994	STRC025	RC	563800.00	7510870.00	114.00	1.00	76.00		96.00	96.00	B2
STRATHFIELD	1994	STRC026	RC	564990.00	7511900.00	114.00	1.00	82.00			82.00	B2
STRATHFIELD	1994	STRC027	RC	559940.00	7511430.00	90.00	1.00	58.00			58.00	B1
STRATHFIELD	1994	STRC028	RC	559510.00	7512250.00	36.00	1.00	12.00			12.00	B1
STRATHFIELD	1994	STRC029	RC	557640.00	7514870.00	78.00	1.00	44.00	64.00		64.00	B1
STRATHFIELD	1994	STRC030	RC	557240.00	7525190.00	132.00	1.00	118.00			118.00	B1
STRATHFIELD	1994	STRC031	RC	558280.00	7514180.00	60.00	1.00	16.00			16.00	B1
STRATHFIELD	1994	STRC032	RC	560320.00	7517570.00	66.00	1.00	44.00			44.00	B1
STRATHFIELD	1994	STRC033	RC	556160.00	7523000.00	144.00	1.00	104.00			104.00	B1
STRATHFIELD	1994	STRC034	RC	557030.00	7525520.00	160.00	3.00	118.00			160.00	***
STRATHFIELD	1994	STRC035	RC	557530.00	7524870.00	134.00	3.00	117.00	126.00		126.00	B2

P7	PROSPECT	DATE	HOLE	TYPE	AMGEAST	AMGN0RTH	DEPTHS: TOT	QSED	TBAS	TSED	PSED	D TO B	BCODE
	STRATHFIELD	1994	STRC036	RC	554860.00	7527950.00	150.00	3.00	134.00	138.00		138.00	B1
	STRATHFIELD	1994	STRC037	RC	555900.00	7529140.00	144.00	3.00	132.00			132.00	B1
	STRATHFIELD	1994	STRC038	RC	555070.00	7529330.00	168.00	3.00	154.00			154.00	B1
	STRATHFIELD	1994	STRC039	RC	553930.00	7531300.00	125.00	3.00					
	STRATHFIELD	1994	STRC040	RC	557580.00	7525430.00	162.00	3.00	102.00	152.00		152.00	B1
	STRATHFIELD	1994	STRC041	RC	556940.00	7524920.00	144.00	3.00	130.00	132.00		132.00	B1
	STRATHFIELD	1994	STRC042	RC	558020.00	7527200.00	174.00	3.00	152.00			152.00	B2
	STRATHFIELD	1994	STRC043	RC	556340.00	7530500.00	162.00	3.00	129.00	148.00		148.00	B1
	STRATHFIELD	1994	STRC044	RC	553070.00	7523150.00	120.00	3.00	92.00			92.00	B1
	STRATHFIELD	1994	STRC045	RC	551380.00	7528040.00	114.00	3.00	82.00	88.00		88.00	B1
	STRATHFIELD	1994	STRC046	RC	556140.00	7527550.00	174.00	3.00	136.00				
	STRATHFIELD	1994	STRC047	RC	555260.00	7523370.00	156.00	3.00	132.00	138.00		138.00	B1
	MICLERE	1995	STRC048	RC	560410.00	7509470.00	42.00	3.00				6.00	B1
	MICLERE	1995	STRC049	RC	560600.00	7509050.00	42.00	3.00	18.00			18.00	B1
	STRATHFIELD	1995	STRC050	RC	557770.00	7523960.00	138.00	3.00	114.00	124.00		124.00	B1
	STRATHFIELD	1995	STRC051	RC	556800.00	7525980.00	150.00	3.00	124.00			150.00	***
	STRATHFIELD	1995	STRC052	RC	557070.00	7523000.00	150.00	3.00	122.00	136.00		136.00	B1
	STRATHFIELD	1995	STRC053	RC	555550.00	7524720.00	150.00	3.00	140.00			150.00	***
	STRATHFIELD	1995	STRC054	RC	554340.00	7524540.00	150.00	3.00	126.00	138.00		138.00	B2
	STRATHFIELD	1995	STRC055	RC	554630.00	7526300.00	144.00	3.00	128.00	134.00		134.00	B1
	STRATHFIELD	1995	STRC056	RC	553020.00	7525790.00	132.00	3.00	107.00	118.00		118.00	B1
	STRATHFIELD	1995	STRC057	RC	552340.00	7526840.00	118.00	3.00	78.00	88.00		88.00	B1
	STRATHFIELD	1995	STRC058	RC	557460.00	7528540.00	138.00	3.00	104.00	124.00		124.00	B1
	STRATHFIELD	1995	STRC059	RC	553400.00	7527980.00	138.00	3.00	126.00			126.00	B1
	WOLFANG BASIN	7/81	WB946	PR	566769.72	7487661.54	139.00	8.00	61.00		135.80	135.80	B1
	WOLFANG BASIN	7/81	WB947	PR	566385.21	7489621.38	141.00	1.00	36.40		109.60	109.60	B1

HOLE No.	FROM (DEPTH)	TO	COLOUR	CODE	OXID	DESCRIPTION	COMMENTS	DEPTHCODE	WATER	M/ALOGY	Qz	S2	MAG SUS	D TO B
KJRC002	0.00	4.00	GYBL	SL	WO	BLACK SOIL PRECOLLAR	NO SAMPLE	O5	D	-	-	-	29	88.00
KJRC002	4.00	12.00	LBN	BS	WO	CLAY-RICH, REMNANT FINE BS CLASTS (OXIDISED)		O3	D	-	-	-	31	88.00
KJRC002	12.00	28.00	YWBN	CY	WO	CLAY-RICH, AFTER BS PYROCLASTICS		O3	D	-	-	-	25	88.00
KJRC002	28.00	34.00	LBN	BS	WO	CLAY-RICH, REMNANT BS CLASTS		O3	D	-	-	-	27	88.00
KJRC002	34.00	84.00	GY	BS	SR	FINE GRAINED BS	ZEOL AMYGDALES	O3	M	-	-	-	103	88.00
KJRC002	84.00	86.00	GYBN	SH	WO	GREY SH WITH COAL BANDS	PROBABLE PERMAIN SEDIMENTS	O2	M	-	2%	tr?	5	88.00
KJRC002	86.00	88.00	GYGN	SH	WO	SHALE	PROBABLE PERMIAN SEDIMENTS	O2	M	-	5%	-	5	88.00
KJRC002	88.00	150.00	GY	VFBX	FR	DA TO AD COMPOSITION VOLCANICLASTIC	PROBABLE DRUMMOND	B3	M	-	<1%	-	86	88.00
KJRC003	0.00	6.00	DBN	SL	WO	BLACK SOIL PRECOLLAR	NO SAMPLE	O5	D	-	-	-	180	
KJRC003	6.00	18.00	BLBU	BS	WO	FELDSPAR PORPHYRITIC BS	OXIDATION ON FRACTURES	O3	D	-	-	-	2500	
KJRC003	18.00	22.00	BLBU	BS	FR	FINE GRAINED BS	CARBONATE ON FRACTURES	O3	D	-	-	-	230	
KJRC003	22.00	32.00	GY	CY	FR	CLAY ALT BS PYROCLASTICS?	DISSEM & VEIN MARCASITE	O3?	D	MARC/PY	-	5	50	
KJRC003	32.00	34.00	BN	CY	WO	CLAY ALT BS PYROCLASTICS?		O3?	D	-	-	-	120	
KJRC003	34.00	38.00	DGN	CY	WO	CLAY ALT BS?	DISSEM MARCASITE	03?	D	MARC/PY	-	5	70	
KJRC003	38.00	48.00	DGY	BS	WO	FELD & AMPH PORPHYRITIC BS	WEATHERING ON FRACTURES	O3	D/W	-	-	-	280	
KJRC003	48.00	68.00	BLBU	BS	WO	FINE GRAINED BS	CARB & SMECTITE ON FRACTURES	03	D/W	-	-	-	350	
KJRC003	68.00	96.00	REBN	BS	WO	CLAY AFTER BS PYROCLASTICS?	PALEOSOL?	03	D/W	-	-	-	110	
KJRC003	96.00	108.00	GYGN	MSH	SP	MICACEOUS CLAY WITH VEIN QTZ & SCHIST FRAGMENTS	WEATHERED ANAKIE MM	B1	D/W	-	30	-	<30	
KJRC003	108.00	114.00	GYGN	MSH	SR	MICA SCHIST & VEIN QTZ	ANAKIE MM	B1	D	-	20	-	<30	
KJRC005	0.00	6.00	DBN	SL	WO	BLACK SOIL - PRECOLLAR	NO SAMPLE	O5	D	-	-	-	250	
KJRC005	6.00	14.00	BN	BS	WO	PERVASIVELY OXIDISED BS	CARB AMYGDALES	03	D	-	-	-	550	
KJRC005	14.00	30.00	BN	BS	WO	FINE GRAINED BS	OXID.FRACTS & CARBONATE AMYGDALES	03	D	-	-	-	750	
KJRC005	30.00	38.00	BNPU	BS	WO	VARIABLY WEATHERED BS	PALEOSOL UPPER , CARB ON WEATH. FRACT.	03	D	-	-	-	560	
KJRC005	38.00	52.00	GYBN	BS	WO	FINE GRAINED BS	WEATH,C/ATE & SMECTITES ON FRACTURES	03	D	-	-	-	270	
KJRC005	52.00	66.00	GYBL	BS	FR	FINE GRAINED BS		03	D	-	-	-	450	
KJRC005	66.00	84.00	GYBL	BS	FR	FINE GRAINED BS	SMECTITE AMYGDALES UPPER ZONE	03	D	-	-	-	430	
KJRC005	84.00	102.00	REBN	CY	WO	ALT/WEATHERED BS PYROCLASTICS?		03?	D	-	-	-	250	
KJRC005	102.00	110.00	PU	CY	WO	ALT/WEATHERED BS PYROCLASTICS?		03?	D	-	-	-	1800	
KJRC005	110.00	138.00	GYBL	BS	FR	FINE GRAINED BS - PORPHYRITIC FLOW CENTRE	C/ATE & SMECTITE AMYGDALES AT FLOW TOP	03	D	-	-	-	350	
KJRC005	138.00	174.00	WHGY	SGL	-	VEIN QTZ-RICH GRAVELS TO CONGLOMERATES	LOCAL SANDY CLAY BEDS	O4	W	-	40-90	-	<20	
KJRC007	0.00	6.00	DBN	SL	WO	BLACK SOIL - PRECOLLAR	NO SAMPLE	O5	D	-	-	-	150	
KJRC007	6.00	34.00	BLBN	BS	WO	PERVASIVELY OXIDISED FG BS	CARBONATE & SMECTITE ON FRACTURES	03	D	-	-	-	200	
KJRC007	34.00	38.00	BLGY	BS/SC	WO	MIXED BS & CARBONACOUES SEDIMENTS		03	M	-	-	-	<50	
KJRC007	38.00	48.00	BLGN	BS	FR	FINE GRAINED BS	SMECTITE & CARBONATE ON FRACTURES	03	D	-	-	-	200	
KJRC007	48.00	84.00	LBNGN	VF	SP	PERVASIVELY OXIDISED DACITIC VOLCANICLASTICS	MIXED PROVENANCE VOLCANICLASTIC ?	B3	W	-	5	-	150	
KJRC009	0.00	6.00	DBN	SL	WO	BLACK SOIL - PRECOLLAR	NO SAMPLE	O5	D	-	-	-	120	
KJRC009	6.00	16.00	BNGN	BS	WO	PERVASIVELY OXIDISED FG BS		O3	D	-	-	-	300	
KJRC009	16.00	20.00	REBN	BS	WO	CLAYS AFTER BS PYROCLASTICS		O3	D	-	-	-	120	
KJRC009	20.00	50.00	GYBL	BS	FR	FINE GRAINED BS	CARBONATE ON FRACTURES	O3	D/M	-	-	-	280	
KJRC009	50.00	52.00	BN	BS/SE	FR	MIXED BS AND SILCRETE		O3/O4	M/W	-	-	-	250	
KJRC009	52.00	60.00	CRYL	SC	WO	MICACEOUS SEDIMENT	ANAKIE MM PROVENANCE	O4	M/W	-	35	-	<30	
KJRC009	60.00	62.00	REBN	SC	WO	MICACEOUS CLAY WITH VEIN QTZ CLASTS	RESIDUAL SURFACE	01	M/W	-	45	-	<30	
KJRC009	62.00	68.00	LGN	SC	SP	MICACEOUS CLAY, VEIN QTZ & MSH FRAGMENTS	IN SITU WEATHERED ANAKIE MM	B1	M/W	-	25	-	<30	
KJRC009	68.00	78.00	DGN	MSH	SR	MICA SCHIST	ANAKIE METAMORPHICS	B1	M/W	-	20	-	<30	
STRC002	0.00	4.00	LDBN	SL	WO	BLACK SOIL - PRECOLLAR	NO SAMPLE	O5	D	-	-	-	433	17.00
STRC002	4.00	17.00	LBN	BS	WO	CLAY-RICH REM. PORPHYRITIC BS (OXIDISED) FRAGMENTS	REMNANT ZEOL IN MATRIX	O3	D	-	-	-	445	17.00
STRC002	17.00	36.00	CRYW	MSH	SP	CLAY-RICH, MSH & ANGULAR VEIN QTZ FRAGMENTS	WEATHERED BASEMENT	B1	M	-	15%		41	17.00

HOLE No.	FROM (DEPTH)	TO	COLOUR	CODE	OXID	DESCRIPTION	COMMENTS	DEPTHCODE	WATER	M/ALOGY	Qz	S2	MAG SUS	D TO B
STRC009	0.00	6.00	GYBN	SL	WO	BLACK SOIL - PRECOLLAR	NO SAMPLE	O5	D	-	-	-	213	78.00
STRC009	6.00	15.00	DBN	BS	WO	CLAY-RICH, REMNANT PORPHYRITIC BS (OXIDISED) FRAGMENTS		03	D	-	-	-	1112	78.00
STRC009	15.00	20.00	BN	BS	WO	CLAY-RICH, REMNANT PORPHYRITIC BS (OXIDISED) FRAGMENTS		03	D	-	-	-	1925	78.00
STRC009	20.00	30.00	YWBN	BS	WO	CLAY-RICH, REMNANT FINE BS (OXIDISED) FRAGMENTS		03	D	-	-	-	1886	78.00
STRC009	30.00	40.00	GY	BS	WO	FINE BASALT, OXIDISED ON FRACTURES		03	M	-	-	-	202	78.00
STRC009	40.00	66.00	GY	BS	WO	PORPHYRITIC BASALT, OXIDISED ON FRACTURES		03	M	-	-	-	521	78.00
STRC009	66.00	69.00	PK	SH	WO	PINK SILTY SHALE	PERMIAN SEDIMENTS?	O2	W	-	-	-	8	78.00
STRC009	69.00	78.00	YWCR	SGL	WO	CLAY-RICH, ROUNDED QTZ CLASTS	PERMIAN SEDIMENTS?	O2	W	-	10%	-	61	78.00
STRC009	78.00	90.00	DGN	DI	SP	CLAY-RICH WITH ABUNDANT SUBHEDRAL QTZ CRYSTALS	WEATHERED GRANITOID	B2	W	-	15%	-	40	78.00
STRC009	90.00	96.00	GYGN	DI	SR	MEDIUM HB-BIOT DIORITE	GRANITOID BASEMENT	B2	W	-	15%	-	1399	78.00
STRC019	0.00	6.00	GYBL	SL	WO	BLACK SOIL PRECOLLAR	NO SAMPLE	O5	D	-	-	-	270	108.00
STRC019	6.00	14.00	BN	BS	WO	CLAY-RICH, REMNANT BS FRAGMENTS		03	D	-	-	-	601	108.00
STRC019	14.00	20.00	BL	CY	WO	FINE BS, OXIDISED ON FRACTURES		03	D	-	-	-	44	108.00
STRC019	20.00	26.00	GN	BS	WO	CLAY AFTER BS?		03	D	-	-	-	234	108.00
STRC019	26.00	34.00	DBN	BS	WO	FINE BS, CLAYS ON FRACTURES	EOL AMYGDALES	03	D	-	-	-	214	108.00
STRC019	34.00	56.00	GY	BS	WO	FINE BS, CLAYS ON FRACTURES	ZEOL AMYGDALES & VEINS	03	M	-	-	-	214	108.00
STRC019	56.00	84.00	BL	SH	WO	CLAYS, COAL, INTERACTION WITH FINE BS		03	M	-	-	-	50	108.00
STRC019	84.00	90.00	GY	BS	WO	PERVASIVELY HYDRATED BS	ZEOL AMYGDALES	03	M	-	-	-	5	108.00
STRC019	90.00	96.00	GY	SC	WO	INTERBEDDED SHALES & QTZ SST	PERMIAN SEDIMENTS?	O2	M	-	20%	-	67	108.00
STRC019	96.00	104.00	YWBN	SS	WO	QTZ-RICH SST	PERMIAN SEDIMENTS?	O2	M	-	35%	-	5	108.00
STRC019	104.00	108.00	LGY	SH	WO	INTERBEDDED SHALE & QTZ SST	PERMIAN SEDIMENTS?	O2	W	-	15%	-	5	108.00
STRC019	108.00	120.0	GYGN	BSH	SP/R	WEATHERED CHLORITIC SCHIST	WEATHERED AMM BASEMENT	B1	W	-	15%	tr	5	108.00
STRC025	0.00	6.00	GYBL	SL	WO	BLACK SOIL PRECOLLAR	NO SAMPLE	O5	D	-	-	-	132	96.00
STRC025	6.00	20.00	YWBN	BS	WO	PERVASIVELY OXIDISED BS		O3	D	-	-	-	222	96.00
STRC025	20.00	24.00	GNGY	CY	WO	SHALE	INTERFLOW SEDIMENTS	O3	M	-	-	-	35	96.00
STRC025	24.00	76.00	BLGY	BS	WO	FINE BS, OXIDISED ON FRACTURES	ZEOL AMYGDALES	O3	M	-	-	-	260	96.00
STRC025	76.00	82.00	GNGY	CY	WO	SHALE	PERMIAN SEDIMENTS?	O2	W	-	-	-	5	96.00
STRC025	82.00	88.00	DBNBL	CY	WO	SHALE & COAL	PERMIAN SEDIMENTS?	O2	W	-	-	-	49	96.00
STRC025	88.00	96.00	WH	CY	WO	SHALE	PERMIAN SEDIMENTS?	O2	W	-	-	-	56	96.00
STRC025	96.00	106.00	GNGY	SC	SP	CLAY-RICH, ABUNDANT SUBHEDRAL QTZ CRYSTALS	WEATHERED GRANITOID BASEMENT	B2	W	-	20%	-	51	96.00
STRC025	106.00	114.00	GYGN	DI	SR	MEDIUM Hb-Biot DIORITE	GRANITOID BASEMENT	B2	W	-	20%	-	50	96.00
STRC031	0.00	6.00	GYBL	SL	WO	BLACK SOIL PRECOLLAR	NO SAMPLE	O5	D	-	-	-	102	16.00
STRC031	6.00	16.00	RELBN	CY	WO	CLAY-RICH, AFTER BS?	-	03	D	-	-	-	207	16.00
STRC031	16.00	20.00	LBNPK	SC	WO	CLAY-RICH, ABUNDANT SUB-ANGULAR VEIN QTZ	PALEO RESIDUALSURFACE?	01	D	-	15%	-	88	16.00
STRC031	20.00	36.00	PKLBN	SC	SP	CLAY-RICH, MICACEOUS, ABUNDANT ANGULAR VEIN QTZ	GOSSANOUS FRAGMENTS	B1	D	QTZ	5%	-	14	16.00
STRC031	36.00	60.00	GYGN	MSH	SR	GRAPHITIC MSH, SOME LEACHING	AMM BASEMENT	B1	D	QTZ	5%	I%	56	16.00
STRC032	0.00	6.00	BLGY	SL	WO	BLACK SOIL PRECOLLAR	NO SAMPLE	O5	D	-	-	-	87	45.00
STRC032	6.00	16.00	LGNBN	BS	WO	PERVASSIVELY OXIDISED BS		O3	D	-	-	-	76	45.00
STRC032	16.00	26.00	DRE	CY	WO	CLAY-RICH, AFTER BS PYROCLASTICS?		O3	D	-	-	-	109	45.00
STRC032	26.00	40.00	DPU	CY	WO	CLAY-RICH, AFTER BS PYROCLASTICS?		O3	D	-	-	-	1346	45.00
STRC032	40.00	44.00	DRE	CY	WO	CLAY-RICH, AFTER BS PYROCLASTICS?		O3	D	-	-	-	39	45.00
STRC032	44.00	52.00	LBNPK	SC	WO	CLAY-RICH, ABUNDANT SUB-ANGULAR VEIN QTZ	PALEO RESIDUAL SURFACE?	01	D		25%	-	41	45.00
STRC032	52.00	62.00	LBNYW	SC	PL	CLAY-RICH, MICACEOUS, SOME VEIN QTZ	WEATHERED AMM BASEMENT	B1	D	-	15%	-	29	45.00
STRC032	62.00	66.00	YWGN	BSH	SP	MICACEOUS SCHIST, OXIDISED	AMM BASEMENT	B1	M	-	15%	-	33	45.00

HOLE No.	FROM (DEPTH)	TO	COLOUR	CODE	OXID	DESCRIPTION	COMMENTS	DEPTHCODE	WATER	M/ALOGY	Qz	S2	MAG SUS	D TO B
STRC033	0.00	6.00	GYBL	SL	WO	BLACK SOIL PRECOLLAR	NO SAMPLE	O5	D	-	-	-	267	105.00
STRC033	6.00	18.00	LBN	BS	WO	CLAY-RICH, REMNANT FINE BS (OXIDISED)CLASTS		O3	D	-	-	-	218	105.00
STRC033	18.00	48.00	GY	BS	WO	FINE BS, OXIDISED ON FRACTURES	ZEOL AMYGDALES & FRACTURES	O3	M	-	-	-	511	105.00
STRC033	48.00	50.00	BN	BS	WO	CLAY-RICH, FEW REMNANT FINE BS (OXIDISED) CLASTS	FLOW BASE?	O3	M	-	-	-	1108	105.00
STRC033	50.00	64.00	GY	BS	WO	FINE BS, OXIDISED ON FRACTURES	ZEOL AMYGDALES & FRACTURES	O3	W	-	-	-	581	105.00
STRC033	64.00	88.00	REBN	CY	WO	CLAY-RICH, AFTER BS PYROCLASTICS?		O3	W	-	-	-	487	105.00
STRC033	88.00	94.00	GY	BS	WO	FINE BS,OXIDISED ON FRACTURES		O3	W	-	-	-	677	105.00
STRC033	94.00	104.00	REBN	CY	WO	CLAY-RICH, AFTER BS PYROCLASTICS?		O3	W	-	-	-	62	105.00
STRC033	104.00	132.00	PK	SC	PL	MICACEOUS CLAYS & VEIN QTZ	AMM BASEMENT?	B1	W	-	15%	-	37	105.00
STRC033	132.00	144.00	LGN	MSH	SP	CLAY-RICH, REMNANT MICACEOUS MSH CLASTS & VEIN QTZ	AMM BASEMENT	B1	W	-	15%	-	62	105.00
STRC042	0.00	6.00	DBN	SL	WO	BLACK SOIL - PRECOLLAR	NO SAMPLE	05	D	-	-	-	300	
STRC042	6.00	12.00	BLBU	BS	FR	WEAKLY PORPHYRITIC BS	ARBONATES ON FRACTURES	O3	D	-	-	-	1250	
STRC042	12.00	22.00	BLGY	BS	WO/FR	FINE GRAINED BS	CLAYS, C/ATES & SMECTITES ON FRACTURES	O3	D	-	-	-	550	
STRC042	22.00	56.00	REBN	CY	WO	CLAYS AFTER BS PYROCLASTICS?		O3	D	-	-	-	210	
STRC042	56.00	76.00	BLGN	BS	FR	FINE GRAINED BS	CLAYS ON FRACTURES	O3	D	-	-	-	220	
STRC042	76.00	78.00	DGN	SC	WO	FINE SANDSTONE	INTERFLOW SEDIMENTS	O3	D	-	-	-	30	
STRC042	78.00	102.00	REBN	CY	WO	CLAY AFTER BS PYROCLASTICS?		O3	D	-	-	-	80	
STRC042	102.00	128.00	BLBU	FR	FR	FINE GRAINED BS	CLAYS ON FRACTURES	O3	W	-	-	-	320	
STRC042	128.00	152.00	BNGY	SC	WO	MICACEOUS CLAY-RICH FINE SST	ANAKIE MM PROVENANCE	04	D	-	-	-	45	
STRC042	152.00	162.00	WH	SC	WO	CLAY WITH GRANITIC QTZ	WEATHERED GRANITOID?	01	D	-	30	-	<30	
STRC042	162.00	168.00	WHCR	GR	SP	CLAY WITH GRANITIC QTZ & FELDSPARS	WEATHERED GRANITOID	B2	D	PY	30	TR	<30	
STRC042	168.00	174.00	CRGN	GR	SR	GRANODIORITE/DIROITE	WEAKLY ALTERED, ESP. FeMg MINERALS	B2	W	PY	30	TR	<30	
STRC043	0.00	6.00	DBN	SL	WO	BLACK SOIL - PRECOLLAR	NO SAMPLE	O5	D	-	-	-	420	
STRC043	6.00	18.00	GYBN	BS	WO	VARIABLY OXIDISED FEINE GRAINED BS	SOME FRESH ZONES	O3	D	-	-	-	400	
STRC043	18.00	24.00	LBN	BS	WO	FINE GRAINED BASALT	UPPER SURFACE PALEOSOL	O3	D	-	-	-	650	
STRC043	24.00	36.00	GYBN	BS/CY	WO	FINE GRAINED BASALT	UPPER SURFACE PALEOSOL	O3	D	-	-	-	450	
STRC043	36.00	50.00	GNBL	BS/CY	WO	FINE GRAINED BASALT	WEATHERING & SMECTITES ON FRACTURES	O3	D	-	-	-	700	
STRC043	50.00	60.00	GYBN	BS	WO/FR	FINE GRAINED BASALT	SOME PERVASIVELY OXIDISED ZONES	O3	D	-	-	-	250	
STRC043	60.00	66.00	DBN	BS	WO/FR	PERVASIVELY OXID FINE GRAINED BS	CARB ON FRACTURES	O3	D/M	-	-	-	900	
STRC043	66.00	78.00	DBNBL	BS	FR	FINE GRAINED BS	CARB & WEATHERING ON FRACTURES	O3	D/M	-	-	-	350	
STRC043	78.00	84.00	REBN	CY	WO	CLAY - AFTER BS PYROCLASTICS		O3?	D/M	-	-	-	150	
STRC043	84.00	98.00	LBN	CY	WO	CLAY - AFTER BS PYROCLASTICS		O3?	D	-	-	-	30	
STRC043	98.00	106.00	GNBN	BS	FR	FINE GRAINED BS	OXIDES & CARB ON UPPER/LOWER SURFACES	O3	D	-	-	-	250	
STRC043	106.00	129.00	GNBN	BS	FR	FINE GRAINED BS	OXIDES, CARB, SMECTITES ON SURFACES	O3	D/M	-	-	-	70	
STRC043	129.00	148.00	CRYL	SC	SP	MICACEOUS SANDY CLAY - ANAKIE MM PROV	DEEPLY WEATHERED ANAKIE MM?	O1/B1	D/M	-	15	-	<30	
STRC043	148.00	162.00	DYL	MSH	SP/SR	CLAY WITH REMNANT SCHIST FRAGMENTS	WEATHERED ANAKIE MM	B1	M/W	-	15	-	<30	
STRC045	0.00	6.00	DBN	SL	WO	BLACK SOIL - PRECOLLAR	NO SAMPLE	O5	D	-	-	-	120	
STRC045	6.00	28.00	LBN	BS	WO	PERVASIVELY OXIDISED BASALT	CLAYS ABUNDANT	O3	D	-	-	-	100	
STRC045	28.00	38.00	GYBL	BS	FR	FINE GRAINED BS	WEATHERING ON FRACTURES	O3	D/W	-	-	-	650	
STRC045	38.00	66.00	BL	BS	FR	FINE GRAINED BS	CARBONATE & SMECTITE ON FRACTURES	O3	W	-	-	-	250	
STRC045	66.00	82.00	BLBU	BS	FR	FINE GRAINED BS	CARBONATE AMYGDALES & ON FRACTURES	O3	W	-	-	-	750	
STRC045	82.00	88.00	BNYL	CY	SP	MICACEOUS CLAYS	RESID SURFACE ANAAKIE MM PROVENANCE	O1?	W	-	5	-	<30	
STRC045	88.00	114.00	GY	MSH	SR	CHLORITE AND GRAPHITIC SCHISTS	ANAKIE MM	B1	W	-	20	-	<30	

HOLE No.	FROM (DEPTH)	TO	COLOUR	CODE	OXID	DESCRIPTION	COMMENTS	DEPTHCODE	WATER	M/ALOGY	Qz	S2	MAG SUS	D TO B
STRC053	0.00	6.00	DBN	SL	WO	BLACK SOIL - PRECOLLAR	NO SAMPLE	O5	D	-	-	-	200	
STRC053	6.00	34.00	BNBL	BS	WO	PERVASIVELY OXIDISED FG BS	CARB & SMECTITES ON FRACTURES	O3	D	-	-	-	450	
STRC053	34.00	52.00	BLGY	BS	FR	FG BS-WEAKLY AMYGDALOIDAL	CARB & SMECTITE AMYGDALES & FRACT.	O3	D/M	-	-	-	550	
STRC053	52.00	96.00	REBN	CY	WO	CLAYS -AFTER BS PYROCLASTICS?		O3	D/M	-	-	-	130	
STRC053	96.00	112.00	GNBL	BS	FR	FINE GRAINED BS	CARB & SMECTITES ON FRACTURES	O3	W	-	-	-	600	
STRC053	112.00	118.00	REBL	BS	FR	FINE GRAINED BS	PALEOSOL ON UPPER SURFACE	O3	W	-	-	-	200	
STRC053	118.00	120.00	BLGY	BS/SC	FR	MIXED CARBONACEOUS SHALE & BASALT		O3	W	-	-	-	150	
STRC053	120.00	140.00	BLGY	BS	FR	FINE GRAINED BS	SMECTITES ON FRACTURES	O3	W	-	-	-	110	
STRC053	140.00	150.00	CR	SC	WO	MICACEOUS SANDY CLAY	ANAKIE MM PROVENANCE	O4	W	-	15	-	<30	
STRC054	0.00	6.00	DBN	SL	- WO	BLACK SOIL - PRECOLLAR	NO SAMPLE	O5	D	-	-	-	350	
STRC054	6.00	14.00	LBN	BS	- WO	PERVASIVE OXIDISED BS	CLAY & CARBONATE ON FRACTURES	03	D	-	-	-	190	
STRC054	14.00	26.00	DGN	BS	- FR	FINE GRAINED BS	SMECTITE ON FRACTURES	03	D	-	-	-	480	
STRC054	26.00	54.00	DGNBL	BS	- FR	FINE GRAINED BS	CARB & SMECTITE AMYGDALES, FRACTURES	03	D/M	-	-	-	550	
STRC054	54.00	58.00	BL	BS	- FR	MIXED BS AND CARBONACEOUS SHALES		03	M	-	-	-	2100	
STRC054	58.00	70.00	BLBU	BS	- FR	FINE GRAINED BASALT	CARB & SMECTITE ON FRACTURES	03	D/M	-	-	-	550	
STRC054	70.00	72.00	DBN	CY	- WO	CLAY AFTER BS PYROCLASTICS?		03?	D	-	-	-	120	
STRC054	72.00	78.00	DGN	CY	- WO	CLAY AFTER BS PYROCLASTICS?		03?	D	-	-	-	80	
STRC054	78.00	94.00	BLDBN	BS	- FR	FINE GRAINED BASALT	OXIDES, CARBONATE & SMECTITES ON FRACT	03	D/W	-	-	-	700	
STRC054	94.00	110.00	BLBU	BS	- WO/FR	FINE GRAINED BASALT	OXIDES, CARBONATE & SMECTITES ON FRACT	03	D/W	-	-	-	380	
STRC054	110.00	114.00	GN	CY	- WO	CLAY AFTER BASALTIC PYROCLASTICS?		03?	W	-	-	-	160	
STRC054	114.00	126.00	DBN	CY	- WO	CLAY AFTER BASALTIC PYROCLASTICS?		03?	D	-	-	-	120	
STRC054	126.00	138.00	CR	MSH	- SP	FINE MICACEOUS SANDSTONE	ANAKIE MM PROVENANCE	B1	D/W	-	20	-	<30	
STRC054	138.00	150.00	LGR	MSH	SP/SR	BIOTITE HORNBLENDE GRANODIORITE	WEATHERED TO FRESH ABRUPT	B1	D/W	-	35	-	750	
STRC059	0.00	6.00	DBN	SL	- WO	BLACK SOIL - PRECOLLAR	NO SAMPLE	O5	D	-	-	-	-	
STRC059	6.00	16.00	BN	CL	- WO	OXIDES/CLAYS-AFTER BS	PALEOSOL	03?	D	-	-	-	-	
STRC059	16.00	22.00	LBN	CL	- WO	CLAYS WITH REMNANT BS CLASTS	PALEOSOL	03	D	-	-	-	-	
STRC059	22.00	40.00	GYBL	BS	- FR	FINE GRAINED BS	WEATHERING ON FRACTURES	03	D	-	-	-	-	
STRC059	40.00	44.00	GNGY	BS	- WO/FR	FINE GRAINED BS	WEATHERING ON UPPER SURFACE & FRACT.	03	D	-	-	-	-	
STRC059	44.00	70.00	BL	BS	- FR	FINE GRAINED BS		03	D	-	-	-	-	
STRC059	70.00	86.00	BLGY	BS	- FR	FINE GRAINED BS	CLAYS ON FRACTURES	03	W	-	-	-	-	
STRC059	86.00	94.00	REBN	CL	- WO	OXIDES/CLAYS AFTER BS PYROCLASTICS?		03?	W	-	-	-	-	
STRC059	94.00	98.00	LGN	CL	- WO	CLAYS AFTER BS	PALEOSOL?	03	W	-	-	-	-	
STRC059	98.00	120.00	BLGY	BS	- FR	FINE GRAINED BS	CARBONATE & SMECTITE ON FRACTURES	03	W	-	-	-		
STRC059	120.00	126.00	GYGN	BS	- WO	FINE GRAINED BS	ABUNDANT CLAYS, CARBONATE & SMECTITE	03	W	-	-	-	-	
STRC059	126.00	134.00	GYBL	MSH	- SP	GRAPHITIC SCHIST & VEIN QTZ	ANAKIE METAMORPHICS	B1	W	MARC	15	Tr	-	
STRC059	134.00	138.00	BNGY	MSH	- SR	SCHIST & PSAMMITE	ANAKIE METAMORPHICS	B1	W	MARC	15	Tr	-	